Alma Mater Studiorum · Università di Bologna

Scuola di Scienze
Corso di Laurea Magistrale in Fisica

Systematic investigation of automated plan generation for breast cancer including beam angle and isocenter selection

Relatore:
Dott. Nico Lanconelli

Presentata da:
Sara Spadola

Correlatore:
Prof. Ben Heijmen
Dott. Joan Penninkhof

Sessione I
Anno Accademico 2012/2013

Abstract

Il tumore al seno è il più comune tra le donne nel mondo. La radioterapia è comunemente usata dopo la chirurgia per distruggere eventuali cellule maligne rimaste nel volume del seno. Nei trattamenti di radioterapia bisogna cercare di irradiare il volume da curare limitando contemporaneamente la tossicità nei tessuti sani. In clinica i parametri che definiscono il piano di trattamento radioterapeutico sono selezionati manualmente utilizzando un software di simulazione per trattamenti. Questo processo, detto di $trial-and-error$, in cui i differenti parametri vengono modificati e il trattamento viene simulato nuovamente e valutato, può richiedere molte iterazioni rendendolo dispendioso in termini di tempo. Lo studio presentato in questa tesi si concentra sulla generazione automatica di piani di trattamento per irradiare l'intero volume del seno utilizzando due fasci approssimativamente opposti e tangenti al paziente. In particolare ci siamo concentrati sulla selezione delle direzioni dei fasci e la posizione dell'isocentro. A questo scopo, è stato investigata l'efficacia di un approccio combinatorio, nel quale sono stati generati un elevato numero di possibili piani di trattamento utilizzando differenti combinazioni delle direzioni dei due fasci. L'intensità del profilo dei fasci viene ottimizzata automaticamente da un algoritmo, chiamato $iCycle$, sviluppato nel ospedale Erasmus MC di Rotterdam. Inizialmente tra tutti i possibili piani di trattamento generati solo un sottogruppo viene selezionato, avente buone caratteristiche per quel che riguarda l'irraggiamento del volume del seno malato. Dopo di che i piani che mostrano caratteristiche ottimali per la salvaguardia degli organi a rischio (cuore, polmoni e seno controlaterale) vengono considerati. Questi piani di trattamento sono matematicamente equivalenti quindi per selezionare tra questi il piano migliore è stata utilizzata una somma pesata dove i pesi sono stati regolati per ottenere in media piani che abbiano caratteristiche simili ai piani di trattamento approvati in clinica. Questo metodo in confronto al processo manuale oltre a ridurre considerevol-mente il tempo di generazione di un piano di trattamento garantisce anche i piani selezionati abbiano caratteristiche ottimali nel preservare gli organi a rischio. Inizialmente è stato utilizzato l'isocentro scelto in clinica dal tecnico. Nella parte finale dello studio l'importanza dell'isocentro è stata valutata; ne è risultato che almeno per un sottogruppo di pazienti la posizione dell'isocentro può dare un importante contributo alla qualità del piano di trattamento e quindi potrebbe essere un ulteriore parametro da ottimizzare.

Contents

Summary

Breast cancer is the most common cancer in women worldwide. Radiation therapy is frequently used after surgery to destroy residual cancer cells inside the breast volume.

A constant challenge in radiotherapy treatment is to ensure delivery of a curative dose to the target volume while simultaneously limiting normal tissue toxicity. Such tradeoffs in radiotherapy treatment planning are solved by manual tuning of treatment parameters in a treatment simulation software application, called treatment planning system. This often requires many re-optimization steps, making the process time-consuming. The difficulty of knowing when to terminate the search for better plans, and the lack of overview of the possible plans also implies that no guarantee can be given that the best alternative among all possibilities is found.

This study focuses on the automated generation of treatment plans for whole breast irradiation including beam angle and isocenter selection. To this aim, a combinatorial approach is investigated, consisting of the generation of a large number of candidate plans with different combinations of (near-)opposite beam directions for which beam intensity profiles are automatically optimized by an in-house algorithm. Among these candidate plans, a sub-set of feasible plans is considered. Selection of the final plan is made by means of a weighted sum, score function; the weights are tuned to obtain plans which on average resemble the tradeoff between organs at risk sparing and target irradiation in clinical practice. Initially all candidate plans were generated for the clinical isocenter. In the final stage of the study, isocenter variation was investigated as well.

Chapter 1 In the first chapter, a brief description of the radiotherapy background is presented. It starts with sections on biological and medical aspects of cancer, with a particular focus on breast cancer. Then it continues providing details on physics in radiotherapy and treatment techniques and equipment for breast cancer treatments.

Chapter 2 This chapter provides a description of the optimizer used for beam intensity profile optimization, called *iCycle*, with details on the applied multi-criteria approach. It ends with the definition of the aim of the study.

Chapter 3 In this chapter, the materials and methods for the investigations are described. It includes a description of a method used for selection of the best treatment plan.

Chapter 4 This chapter discusses the results of the investigations.

Chapter 5 This chapter concludes and gives directions for further research.

Chapter 1

Introduction to the study

1.1 Cancer

Cancer, medically known as *malignant neoplasm*, is a class of diseases characterized by unregulated cell growth. Different factors can cause this disease, from genetic predisposition to environmental factors that can directly damage genes or combine with existing genetic faults within cells. In humans over 200 different cancers are known. Tumors are classified by the type of cell that is initially affected.

Normal cells in the body follow a preordained path of growth, division, and death. The programmed cell death is called *apoptosis*. Unlike regular cells, tumor cells do not experience programmatic death and instead continue to grow and divide. This leads to a mass of abnormal cells that grows out of control. Figure 1.1 shows the reproductive process for normal and tumor cells. When a cell is mutated, the mutation can be transmitted to the daughter cells, which in turn continue to mutate and duplicate in an uncontrolled way. The uncontrolled proliferation of cells can lead to benign or malignant disease; if not treated in time both may harm the patient and could lead to death.

Benign tumors do not invade neighboring tissues or spread throughout the body; therefore, the patients may be cured with only local treatment with a high rate of survival.

Malignant tumors, on the other hand, can invade the organs near its primary site and may also spread to more distant parts of the body through the lymphatic system or blood stream. When cancer cells break away from the primary (original) tumor and travel to other places in the body, another tumor may form. The new occurrences of disease thus generated are referred to as *metastases*. The secondary tumor is of the same type as the primary tumor. Metastatic tumors are very common in the late stages of cancer and are

more difficult to treat.

Cancer is classified in five broad groups by the type of cell it originates from. *Carcinomas* originate from cells covering internal and external part of the body, such as lung, breast and colon cancer. *Sarcomas* are characterized by cells located in bone, cartilage, fat, connective tissue, muscle and other supportive tissue. *Lymphomas* are tumors that originate from the lymph nodes and immune system tissue while *leukemias* begin in the bone marrow and often accumulate in the blood stream. *Adenomas* are cancers arising in the thyroid, the pituitary gland, the adrenal gland and other glandular tissue.

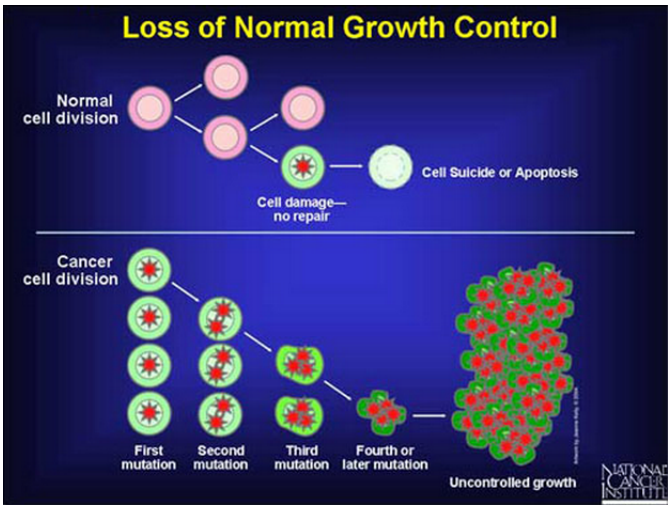

Figure 1.1: *Cell growth in normal cells (top) and cancer cells (bottom).*

1.2 Breast cancer

Breast cancer is the most common cancer in women worldwide, with more than 1 million new diagnoses each year [1]. More than 1 in 8 women receive a diagnosis of breast cancer at some time during their lifetime [2]. Men as well can suffer for this disease; although this is 100 times less common than in women, men tend to have poorer outcomes due to delays in diagnosis. Nowadays, the median age at diagnosis for breast cancer is 61 years of age while diagnosis for women younger than 34 is rare.

Prognosis and survival rates for breast cancer greatly depend on the cancer type, stage, treatment, and geographical location of the patient. In the western world, the overall 5-year relative survival, which measures the survival of the cancer patients in comparison to the general population to estimate the effect of cancer, is 89.0% [2].

1.2.1 Breast anatomy

In women, the breasts overlay the pectoralis major muscles and usually cover much of the chest (see Fig. 1.2). At the front of the chest, the breast tissue can extend from the clavicle (collarbone) to the middle of the sternum (breastbone). At the sides of the chest, the breast tissue can extend into the axilla (armpit), and can reach as far to the back as the latissimus dorsi muscle, extending from the lower back to the humerus bone (the longest bone of the upper arm).

As a mammary gland, the breast is an inhomogeneous anatomic structure composed of layers of different types of tissue, among which two types predominate: adipose tissue and glandular tissue. The glandular tissue effects the lactation functions of the breasts. The adult breast contains 14–18 irregular lactiferous lobes that converge to the nipple, to ducts; the milk ducts are immediately surrounded with dense connective tissue that functions as a support framework. The glandular tissue of the breast is biochemically supported with *estrogen*, therefore, breast structure and shape change with age. The dimensions and weight of the breast vary among women, ranging from approximately 400 *cc* to 3000 *cc*.

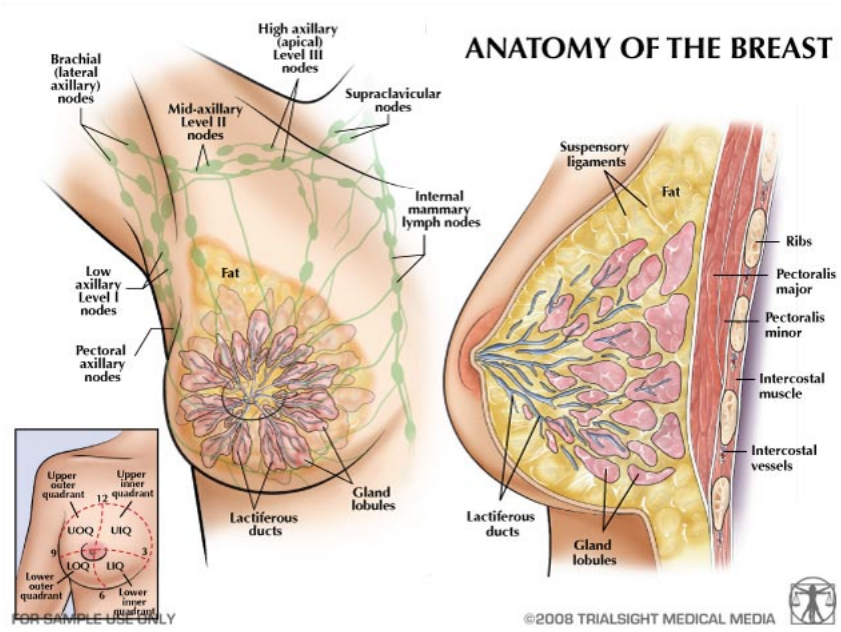

Figure 1.2: *Breast anatomy.*

Figure 1.2 shows the breast anatomy together with the schematic representation of the lymphatic system. Approximately 75% of the lymph fluid from the breast travels to the ipsilateral axillary lymph nodes. The other 25% of the lymph fluid travels to the parasternal nodes (adjacent the sternum bone), to the other breast, and to the abdominal lymph nodes.

The axillary lymph nodes include the pectoral (chest), subscapular (under the scapula), and humeral (humerus-bone area) lymph-node groups, which drain to the central axillary lymph nodes and to the apical axillary lymph nodes.

1.2.2 Breast cancer staging

Diagnosis of breast cancer usually involves mammography. The results of noninvasive examination with mammography and additional tests, such as ultrasound or MR imaging, are sufficient to warrant excisional biopsy to examine the tissue of interest. Most types of breast cancer are easy to diagnose by microscopic analysis of the biopsy. After breast cancer has been diagnosed, during the *staging* process, tests are done to find out whether cancer cells have spread throughout the body.

The dense network of lymphatics in the skin may facilitate widespread cutaneous permeation by tumor. The most common sites of regional lymph node involvement in breast cancer are the axillary, internal mammary and supraclavicular regions. As most of the lymph fluid passes from the breast to the axillary nodes, these nodes are the major site of regional metastases from breast carcinoma. Besides sentinel lymph node biopsy, additional examinations during staging may include chest X-ray, CT scan, bone scan and PET scan (Positron Emission Tomography).

A well-known and commonly used classification for cancer staging is the TNM system, which classifies tumors based on size (T), involvement of lymph nodes (N), and whether the tumor has metastasized (M) (spread to a more distant part of the body). Larger size, nodal spread, and metastases have a worse prognosis. The main stages are:

- **Stage 0 (carcinoma in situ)** is divided in three classes.
  - *Ductal carcinoma in situ* (DCIS) is a noninvasive condition in which abnormal cells are found in the lining of a breast duct. The abnormal cells have not spread outside the ducts to other tissues in the breast.
  - *Lobular carcinoma in situ* (LCIS) is a condition in which abnormal cells are found in the lobules of the breast. This condition seldom becomes invasive cancer.
  - *Paget disease of the nipple* is a condition in which abnormal cells are found in the nipple only.
- **Stage I** cancer is divided in two stages:
  - *stage IA* the tumor is 2 cm or smaller and has not spread outside the breast.
  - *stage IB* small clusters of breast cancer cells (larger than 0.2 mm but not larger than 2 mm) are found in the lymph nodes.

- **Stage II to III** tumor cells are within the breast or regional lymph nodes. The stages (subdivided in IIA, IIB, IIIA, IIIB and IIIC) differ by location and dimension of the tumor.
- **Stage VI** cancer has spread to other organs of the body, most often to distant lymph nodes, bones, lungs, liver and brain.

Infiltrating or invasive ductal cancer is the most common histologic type of breast cancer and comprises 70% to 80% of all cases.

1.2.3 Treatment modalities

The staging system reported in the previous section was created to provide a strategy for grouping patients with respect to prognosis. Therapeutic decisions are formulated partly according to TNM classification but primarily depend on tumor size, lymph node status, estrogen-receptor and progesterone-receptor levels in the tumor tissue, human epidermal growth factor receptor status, menopausal status, and the general health of the patient. The treatment may include surgery, radiotherapy and adjuvant therapy (drugs-based) such as hormone blocking therapy and chemotherapy or a combination thereof.

- **Surgery** involves the physical removal of the tumor, typically along with some of the surrounding tissue. Frequently, a sentinel lymph node biopsy is done as well. Standard surgery includes: mastectomy (removal of the whole breast), quadrantectomy (removal of one quarter of the breast), lumpectomy (remove of a small part of the breast) and oncoplastic surgery (breast reconstruction surgery).
- **Radiotherapy** All histologic types of invasive breast cancer may be treated with breast-conserving surgery plus whole breast radiation therapy. Radiotherapy is conventionally given, as *adjuvant* therapy after surgery to the whole breast and the region of the tumor bed and regional lymph nodes, to destroy microscopic tumor cells that may have escaped surgery. The addition of radiotherapy minimizes the local recurrence at the primary site (curative setting). Radiotherapy is also used in a palliative setting where cure is not possible. The treatment aim is then local disease control or symptomatic relief (e.g. pain).
- **Hormone blocking therapy** Some breast cancers require estrogen to continue growing, identified by the presence of estrogen receptors and progesterone receptors on the tumor cell surface. These ER+ cancers can be treated with drugs that either block the receptors or alternatively block the production of estrogen.

- **Chemotherapy** is particularly beneficial in estrogen receptor-negative (ER-) disease. Most chemotherapy medications work by destroying fast-growing and/or fast-replicating cancer cells usually by causing DNA damage upon replication.

1.3 Biological mechanism of radiotherapy

In radiotherapy, ionizing radiation is used to induce damage to the DNA in the cells. Normal cells have mechanisms for repairing $single-strand$ DNA damage. $Double-stranded$ DNA breaks are more difficult to repair and contribute most to cell death.

Cancer cells are generally less differentiated and more reproductive than healthy differentiated cells. In addition, they have a diminished ability to repair sub-lethal damage. Single-strand DNA damage is then passed on through cell division; damage to the cancer cells' DNA accumulates, causing them to die or reproduce more slowly. This distinction between normal cell and tumor cell sensitivity to ionizing radiation is the main characteristic that makes radiotherapy a successful treatment for cancer.

The DNA can be damaged by photons or charged particles by direct or indirect ionization of the atoms which make up the DNA chain. In photon therapy most of the radiation effect is through indirect ionization by free radicals. Free radicals are atoms, molecules or ions that have an unpaired valence electron or an open electron shell, and are therefore highly chemically reactive. Human tissues mainly constitute of water. When water molecules are ionized hydroxyl radicals are created ($HO^{\bullet}$); the hydroxyl radical reacts with neighboring molecules, usually by stealing hydrogen atoms, and regains the lost electron forming a water molecule. If the hydroxyl radical steals the hydrogen from a piece of DNA, a genetic mutation may occur resulting in a cancer gene being switched on.

Oxygen is a potent radiosensitizer, increasing the effectiveness of a given dose of radiation by forming DNA-damaging free radicals. Solid tumors can outgrow their blood supply, causing a low-oxygen state known as hypoxia. Tumor cells in a hypoxic environment may be as much as 2 to 3 times more resistant to radiation damage than those in a normal oxygen environment, limiting the efficiency of the photon radiation treatment.

The effect of radiation on the survival of cells can be investigated by in vitro or in vivo techniques. Figure 1.3 shows the cell survival as a function of radiation dose by plotting the surviving fraction on a logarithmic scale on the y-axis and absorbed dose on a linear scale on the x-axis. The shape of the curve is influenced by the type of radiation. Depending on the type of radiation, the cell survival curve exhibits an exponential function of dose (shown by black lines), sometimes with an initial shoulder region for low dose administration. Several factors can make cells less radiosensitive such as removal of oxygen to create a hypoxic state, the use of low dose rates or multi-fraction irradiation.

The red curves in Figure 1.3 show the cell survival curves a multi-fraction treatment. Fractionation of the total dose is frequently used in radiotherapy to allow normal cells to recover (and repair DNA damage). As tumor cells are less efficient in repair, and replicate faster, DNA damage will accumulate over time. Moreover, tumor cells that were chronically or acutely hypoxic (and therefore more radio-resistant) may re-oxygenate between fractions, improving the tumor cell kill.

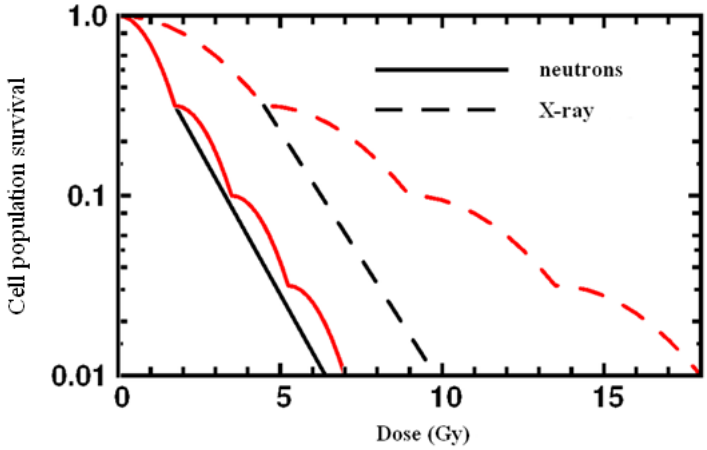

Figure 1.3: *Typical dose-survival curves for mammalian cells exposed to X-rays and fast neutrons. Black lines: single fraction treatment, red lines: multi-fraction treatment.*

1.4 Interaction of radiation with matter

Radiation is classified in two main categories, ionizing or non-ionizing radiation, depending on its capability of ionizing matter (see Fig. 1.4). Radiotherapy uses ionizing radiation, such as X-ray photons, electrons, protons and ions, to treat cancer. The particle interaction with the surrounding tissues depends on the mass and charge. Charged particles directly ionize the matter and deliver dose. Photons and neutrons (non-charged particles) can deliver dose but indirectly.

When an X-ray beam passes through matter, high energy charged particles are produced along the way by interactions of photons with atoms. These particles produce secondary ionizations along their track, depositing energy in the matter.

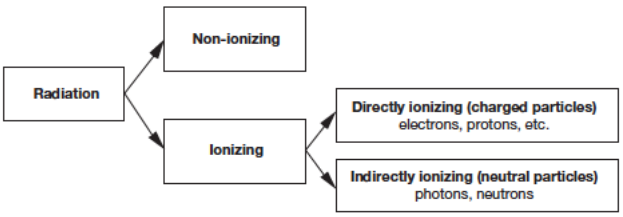

Figure 1.4: *Classification of radiation; radiotherapy uses ionizing radiation.*

1.4.1 X-ray photons

1.4.1.1 Photon beam production and spectrum

X-ray photons are produced by the interaction of fast electrons with nuclei (*bremsstrahlung*) or electrons (*characteristic* photons) of target atoms, usually a high-Z material such as tungsten in a linear accelerator (linac). The photon spectrum consists of a continuous distribution in energy (due to contribution of bremsstrahlung) and discrete energy peaks originating from the characteristic photons, as shown in Figure 1.5. The total bremsstrahlung spectrum, for a target of atomic number Z, is given by the Kramer's equation:

$$I(h\nu) = CZ(E_m - h\nu) \tag{1.4.1}$$

where $I(h\nu)$ is the beam intensity of photons with energy $h\nu$, C is a proportionality constant and E_m is the maximum energy. E_m is equal to the energy of the incident electrons, which is generally between 4 and 25 MeV in radiotherapy. The mean photon energy is approximately one third of the maximum energy.

In radiotherapy, beam quality is globally indicated by the maximum photon energy in the spectrum, as determined by the energy of the electrons used to generate the X-rays. For example, a beam with a maximum photon energy of 6 MeV is a called a 6MV photon beam.

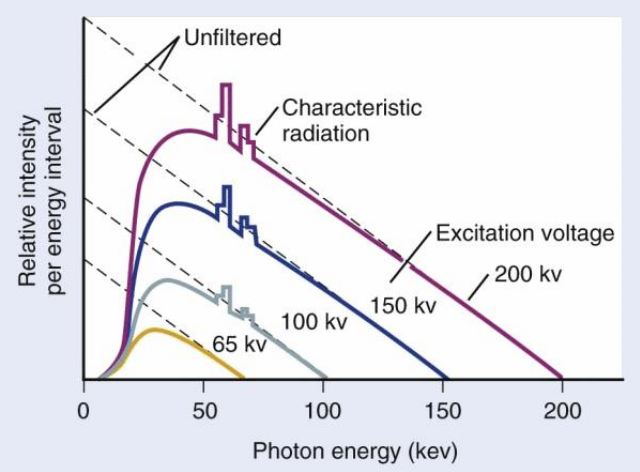

Figure 1.5: *Spectral distribution of diagnostic X-rays calculated for a thick tungsten target. Dotted curves are the spectral distributions without filtration and and the solid curves are for a filtration of 1 mm aluminum. The peaks on top of the continuous bremsstrahlung spectra are related to characteristic radiation for the target material.*

1.4.1.2 Modalities of photon interaction

X-rays interact with matter in different ways; the strengths of these interactions depend on the energy $h\nu$ of the X-rays and the atomic number Z of the material, but not much on chemical properties since the X-ray photon energy is much higher than chemical binding energies. X-ray photons may interact either with orbital electrons or with the nucleus of the atoms. The diagnostic energy range, the interactions are always with orbital electrons. The energy of interacting photons may be fully used for generating fast charged particles such as electrons and positrons. A photon interaction may also generate a fast charged particle plus a scattered photon. The generated charged particles gradually loose their energy in the material and on their path ionizing atoms may be produced. In photon beam radiotherapy the main interactions occurring are photoelectric effect, Compton scattering and pair production.

Photoelectric effect The photoelectric effect is a mechanism by which photons can be absorbed by matter. If a photon with a slightly higher energy than the binding energy of the orbital electrons of the attenuator collides with one of them, the photoelectric effect can

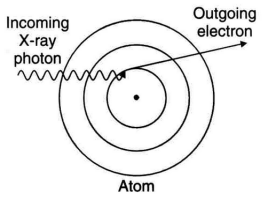

Figure 1.6: *Schematic representation of the photoelectric effect.*

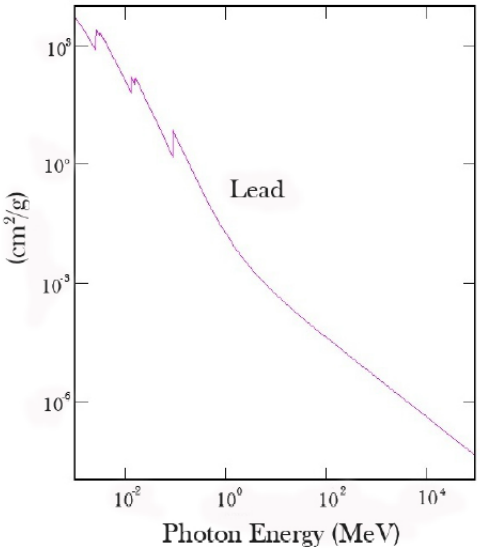

Figure 1.7: *Photoelectric cross section for lead. Peaks in the cross section correspond to electron binding energies.*

take place. The photon disappears, giving the electron sufficient energy to be emitted and ejected from the atom with a kinetic energy E_k (Fig. 1.6) given by:

$$E_k = h\nu - E_b \tag{1.4.2}$$

where $h\nu$ is the energy of the incident photon and E_b is the binding energy of the electron. Interaction probability decreases with increasing photon energy, roughly described by:

$$\sigma_{ph} \propto Z^4 (h\nu)^{-3.5} \tag{1.4.3}$$

The photoelectric cross section σ_{ph} of lead is shown in Figure 1.7 as a function of photon energy. Different peaks are visible, corresponding to the binding energies of the lead's orbital electron. These peaks, called absorption edges, reflect the fact that for $h\nu$ smaller than the binding energy, it is not possible for photons to interact through the photoelectric effect

with electrons in a certain shell, while they can interact for $h\nu$ equal to or greater than the binding energy.

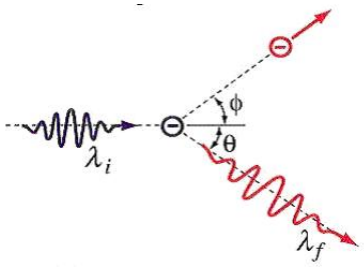

Figure 1.8: *Schematic representation of the Compton effect.*

Compton effect The Compton effect (incoherent scattering) represents a photon interaction with a loosely bound electron. The incident photon energy $h\nu$ is much larger than the binding energy of the orbital electron. The photon transmits part of its energy to the recoil electron and is scattered as photon with energy $h\nu'$ through a scattering angle θ, as shown schematically in Figure 1.8. The angle ϕ represents the angle between the incident photon direction and the direction of the recoil electron.

To satisfy the conservation of momentum and energy, the scattered photon is emitted with energy (considering the electron as free):

$$h\nu' = \frac{h\nu_0}{1 + \frac{h\nu_0}{mc^2}(1 - cos\theta)} \tag{1.4.4}$$

where $h\nu_0$ is the energy of the incident photon, m is the electron mass.

The probability that a photon interacts with a free electron by the Compton effect is given by the Klein-Nishina equation. The cross section of the Compton effect, σ_c depends linearly on the atomic number Z of the attenuator. As example, the cross section of the Compton effect for the lead as a function of photon energy is shown in Figure 1.9.

Pair production In pair production the interacting photon disappears and an electron-positron pair with a combined kinetic energy equal to $h\nu - 2m_ec^2$ is produced in the nuclear Coulomb field (see Fig. 1.10). Pair production has an energy threshold of $2m_ec^2 = 1.02MeV$, equal to the sum of the rest masses of the generated electron and positron. When the positron's kinetic energy becomes close to zero, it will annihilate and create two photons. The probability for pair production is zero for photon energies below the threshold energy and increases rapidly with photon energy above 1.02 MeV. The cross section σ_{pp} varies approximately as Z^2, where Z is the atomic number of the attenuator.

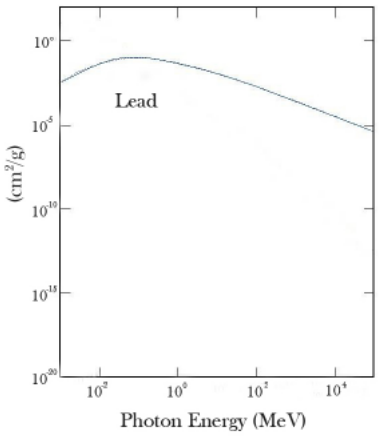

Figure 1.9: *Cross section of Compton effect in lead attenuator.*

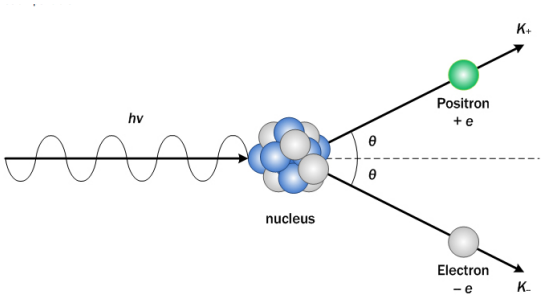

Figure 1.10: *Pair production.*

1.4.1.3 Photon attenuation and absorption

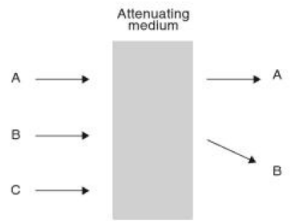

Figure 1.11: *Photon interaction: process of attenuation. A. Transmission; B. Scattering; C. Absorption.*

When an X-ray beam passes through matter the beam intensity is reduced due to the *attenuation* by the medium. Apart from absorption of photon, radiation is scattered (Fig. 1.11). The intensity is defined as the rate of flow of photon energy through a unit area

perpendicular to the beam direction.

The intensity $I(x)$ of a mono energetic photon beam, attenuated by an attenuator of thickness x (expressed in $[W/cm^2]$), is given as:

$$I(x) = I_0 e^{-\mu(h\nu,Z)x} \tag{1.4.5}$$

where I_0 is the original intensity of the unattenuated beam and $\mu(h\nu, Z)$ is the linear attenuation coefficient, which depends on photon energy $h\nu$ and attenuator atomic number Z.

The linear attenuation coefficient (expressed in $[cm^{-1}]$) is related to the total cross section for attenuation, σ, (expressed in $[cm^2/g]$)

$$\sigma = \frac{\mu}{\rho} \tag{1.4.6}$$

with ρ the density of the attenuator (in $[g/cm^3]$). The total attenuation coefficient is given by the sum of the coefficients for the individual photon interactions:

$$\sigma = \frac{\mu_{ph}}{\rho} + \frac{\mu_c}{\rho} + \frac{\mu_{pp}}{\rho} \tag{1.4.7}$$

that represent the photoelectric effect, Compton effect and pair production, respectively. The mass attenuation coefficient for soft tissues is reported in Figure 1.12. This graph shows that the predominance of one effect over the others depends on the energy of the beam.

In radiotherapy, beams energies range from 4 to 23 megavolt (MeV), so the predominant effect is the Compton effect (see Fig. 1.12).

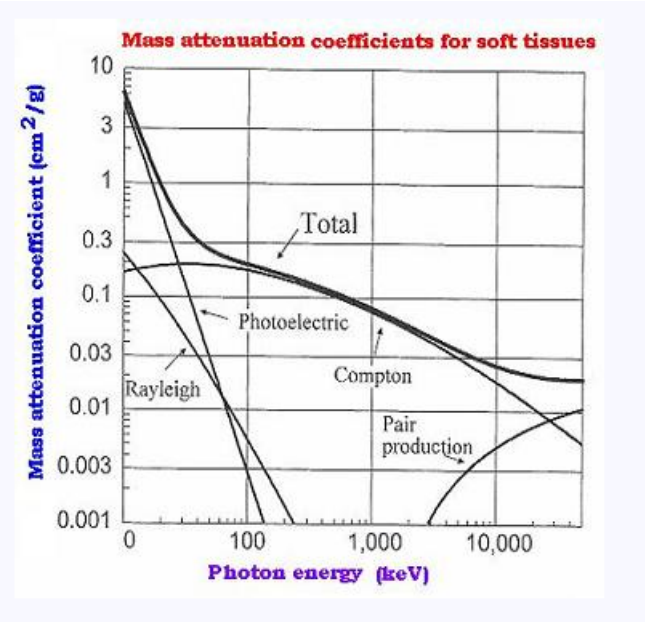

Figure 1.12: *Contribution of the photoelectric effect, Compton effect, pair production and Rayleigh scattering to the mass attenuation coefficient μ/ρ as function of photon energy.*

1.4.1.4 Dose delivery

When a photon beam enters the patient, it interacts with the body. **Adsorbed Dose (D)** is defined as the energy deposited by ionizing radiation per unit of mass of the material, so the mean energy $d\bar{\epsilon}$ deposited in the element of mass dm

$$D = \frac{d\bar{\epsilon}}{dm} \tag{1.4.8}$$

The unit of the absorbed dose is joule per kilogram (J/kg) but in radiation therapy the unit Gray is more often used, $1\ Gy = 1\ J/kg$.

Figure 1.13 shows dose deposition of a photon beam inside a patient. Beneath the surface the dose first rises rapidly, reaches a maximum value at depth z_{max} and then decreases almost exponentially until it reaches a minimum value at the patient's exit point.

The dose region between the surface and depth z_{max} is called dose $build-up\ region$ and results from the relatively long range of energetic secondary charged particles (electrons and positrons) that first are released in the patient by photon interactions and then deposit their kinetic energy in the patient. High-energy photons produce high-speed electrons with a high momentum component in the forward direction and the dose build-up region is larger than for low-energy photons. The delivered dose as a function of depth in a medium depends

on beam energy, field size, and the distance from the source. The percentage depth dose (PDD) is given by

$$PDD(z) = \frac{D_z}{D_{z_0}} \times 100 \tag{1.4.9}$$

where D_z is the absorbed dose at any depth z, and D_{z_0} is the absorbed dose at a fixed reference point, defined by the highest dose (Fig. 1.13).

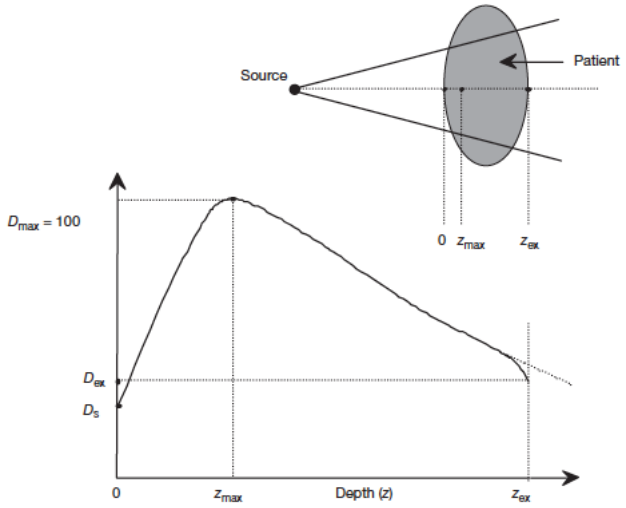

Figure 1.13: *Dose deposition from a megavoltage photon beam in a patient. D_s is the surface dose at the beam entrance side, D_{ex} in the surface dose at the beam exit. D_{max} is the dose maximum often normalized to 100, resulting in a depth dose curve referred to as the percentage depth dose (PDD) distribution. The region between $z = 0$ and $z = z_{max}$ is called the dose build-up region [3].*

1.4.2 Electrons

Megavoltage electron beams are used for radiotherapy of superficial tumors, e.g. in the skin. As electrons travel through a medium they interact with atoms by Coulomb force interactions with atomic orbital electrons and atomic nuclei. Through these collisions, electrons loose their kinetic energy (collision and radiative losses) or change their traveling direction (scattering). The rate of energy loss by collisional interactions depends on the electron energy and on the electron density of the medium. More precisely the rate of energy loss increases with the energy of the electron and the atomic number of the medium. Figure 1.14 shows depth doses for various electron beam energies; the general shape of the depth dose curve for electron beams differs from that of photon beams (Fig. 1.13). Typically, electron beams deliver high surface dose (compared to photon beams). After the dose maximum, the

dose falls off rapidly and levels off at small low level dose component.

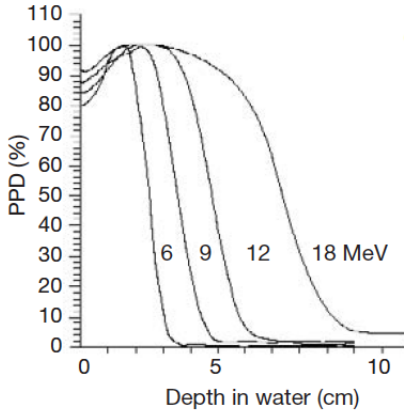

Figure 1.14: *PDD curves in water for electron beams with energies of 6, 9, 12 and 18 MeV [3].*

1.4.3 Protons and ions

Radiation therapy with protons and ions have gained attention, because of the specific depth dose curves for these particles. Figure 1.15 compares a proton depth dose curve with curves for electrons and X-ray photons of 2 different energies. With protons, dose is delivered to a very localized region at the end of the particle's range.

When a fast charged particle moves through matter, it ionizes atoms of the material and deposits dose along its path. Because the interaction cross section increases as the charged particle's energy decreases a peak occurs over the last few millimeters of the particle's range; this maximum is called the Bragg peak. Proton range and therefore the Bragg Peak depth in the tissue depends on proton energy, as shown in Figure 1.16.

Due to their relatively large mass, protons have little lateral scatter in tissue and the beam stays focused, delivering only low-dose to surrounding tissue and maximum dose to the tissue at the location of the Bragg peak.

In most treatments, protons of different energies with Bragg peaks at different depths are applied to treat the entire tumor. The contributions of the individual beams (with different energies) are shown as thin blue lines in Figure 1.17 and the total radiation dose of the protons, called the Spread-Out Bragg Peak (SOBP), is shown as a heavy dashed blue line. While tissues behind or deeper than the tumor receive no radiation from proton therapy, the tissue in front of or shallower than the tumor still receives a considerable dose. As can be seen in Figure 1.17, the proton beam PDD is still highly favorable compared to X-ray photons.

For heavy ions, the Bragg peak dose is higher than for protons offering an improved dose conformation as compared to photon or proton beams. Heavy ions also exhibit potential radiobiological advantages; very heavy ions (above oxygen) have the disadvantage that beyond the Bragg peak, the dose does not decrease to zero, since nuclear reactions between the heavy ions and the atoms of the tissue lead to production of lighter ions which have a higher range. Currently the availability of heavy ion radiotherapy is limited to the use of carbon.

Radiotherapy equipment for photon beam treatments can (in general) be used for electron beam treatments, while for protons and ion therapy large investments are required.

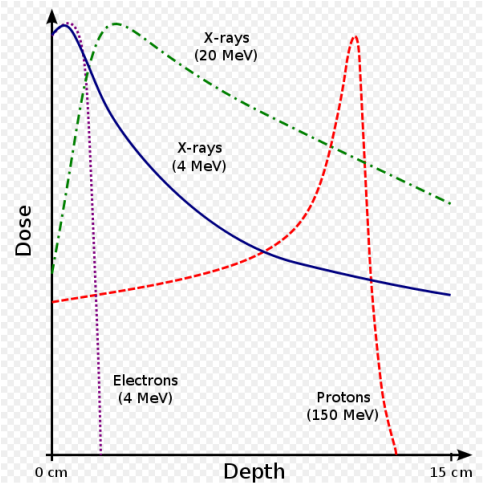

Figure 1.15: *Dose depth profiles for X-rays (4 MeV: blue, 20 MeV: green), an electron beam (4 MeV: purple) and protons (150 MeV, red).*

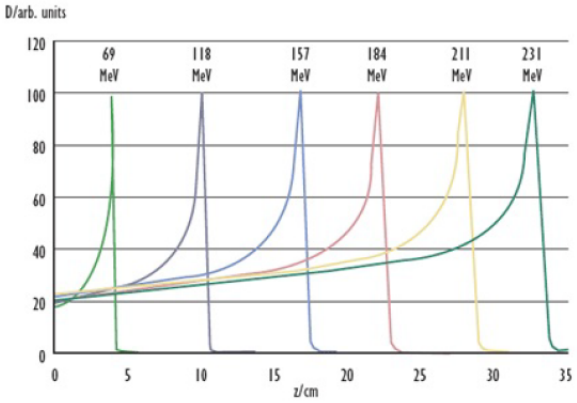

Figure 1.16: *The in-depth position of the Bragg peak depends on energy of the proton particles. Typically, the range of 180 MeV protons is approximately 23 cm.*

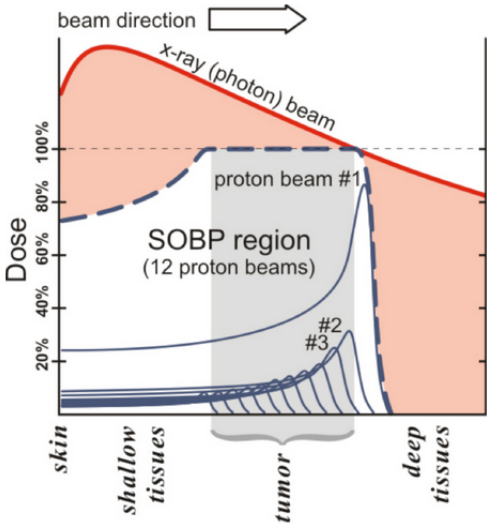

Figure 1.17: *Spread Out Bragg Peak (SOBP, dashed blue line) of a proton beam, compared to a photon beam PDD (red line). The SOBP is the sum of several individual Bragg peaks (thin blue lines) at staggered depths, generated with protons with variable energies. The red area represents the additional dose delivered by x-ray radiotherapy which can be the source of damage to normal tissues and of secondary cancers.*

1.5 Radiotherapy treatment

In radiotherapy, dose can be delivered in two different ways; using radioactive sources implanted in the patient, within or close to the tumor (**brachytherapy**) or with beams of ionizing radiation produced outside the patient and directed towards the tumor in so-called **teletherapy** or **external beam radiotherapy** (EBRT). EBRT is more often used since it is less invasive and not every kind of tumor can be treated with brachytherapy. Generally, photons or electrons beams are used.

1.5.1 Brachytherapy

Brachytherapy, also known as internal radiotherapy, involves placement of short-range radiation sources (radioisotopes) directly at the site of the tumor or next to the area requiring treatment. With this technique, the dose is concentrated in the delivery area and falls off very rapidly. Therefore, surrounding normal tissues receive substantially lower doses than the tumor. Most common brachytherapy sources emit low energy photons, however, in a few specialized situations β or neutron emitting sources are used. An advantage of brachytherapy is the accurate localization and immobilization of the somas relative to the tumor, which removes the problem of organ movement and set-up errors present in fractionated external beam radiotherapy. Brachytherapy is considered whenever possible to treat accessible localized tumors of relatively small volume. It is used as a radical single modality treatment or in combination with EBRT to deliver boost dose.

The three main types of brachytherapy treatment in terms of the placement of the radioactive source are *interstitial*, *intracavity* and *contact*.

- In interstitial brachytherapy, sources are placed directly in the target tissue. For breast cancer, e.g as *boost* after EBRT, it involves the temporary placement in breast tissue, of several flexible plastic catheters. Each catheter is subsequently loaded with the radiation source to deliver the planned radiation dose to the treatment area.

- With intracavity brachytherapy, an applicator loaded with radioactive sources is placed inside a body cavity such as the vagina or anal canal. It may also be used after lumpectomy for (accelerated) partial breast irradiation (APBI), where a single soft catheter with a balloon at the tip is placed in the cavity. the balloon is then inflated with a saline solution and a radiation source is inserted into the inflated balloon for several minutes to deliver the dose of radiation (see Fig. 1.18).

- Superficial brachytherapy can be used for very superficial lesions less than 1 mm thick.

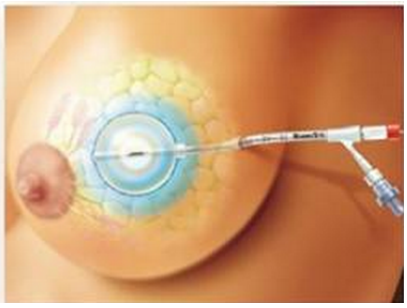

Figure 1.18: *Brachytherapy for breast cancer using a catheter with a balloon at the tip, placed in the lumpectomy cavity.*

1.5.2 External beam equipment

Since the discovery of X-rays in 1895, the technology to produce photon beams has been greatly developed. In the early days, kV tubes were used to produce treatment beams. Nowadays, a linear accelerator is used to produce high energy (MeV) electron beams. Most common treatment units are **gantry-based** linear accelerators (linacs). A linac in a gantry based treatment unit is shown in Figure 1.19; the gantry can rotate 360° around the patient, lying on the couch. Gantry based systems are mostly suitable for delivery of coplanar treatments (all beam directions lying in the plane perpendicular to the patient axis). If a non-coplanar delivery has to be performed the couch must be rotated. This extends the treatment time since the radiographers have to enter the treatment room each time the couch has to be rotated and the patient has to be aligned again.

Medical linacs accelerate electrons to a kinetic energy from 4 to 25 MeV, using radio frequency fields in the range from 10^3 MHz to 10^4 MHz; these electrons are produced by a diode or triode electron gun. They contain a heated filament cathode and a perforated anode. Electrons are emitted thermionically and focused with a potential difference between cathode and anode. The electrons are then accelerated to the desired kinetic energy inside a waveguide, a linear path in vacuum in which electrons are several times affected by a potential difference, generated by the RF-field.

Figure 1.20 shows a schematic representation of the treatment head. For the production of a photon beam, the electrons hit a X-ray target at the exit of the waveguide. After primary collimation, the photon beam strikes a flattening filter made of high-Z material. If the accelerator is designed to deliver X-ray beams produced by electrons of more than one energy, a second flattening filter, optimized for that energy, will be rotated into position using the carrousel. After the flattening filter the beam encounters the transmission ion chamber used to monitor the beam intensity. In modern linacs, a multi-leaf collimator is part of the secondary collimator to shape the treatment fields in accordance with the tumor

shape. A typical multi-leaf collimator (MLC), shown in Figure 1.21, consists of 40-80 pairs of opposing leaves, each around 5 mm to 10 mm wide and around 10 cm thick to attenuate the X-rays. Each leaf in the MLC can be moved independently to block part of the field. An MLC can also be used for intensity modulation within a field.

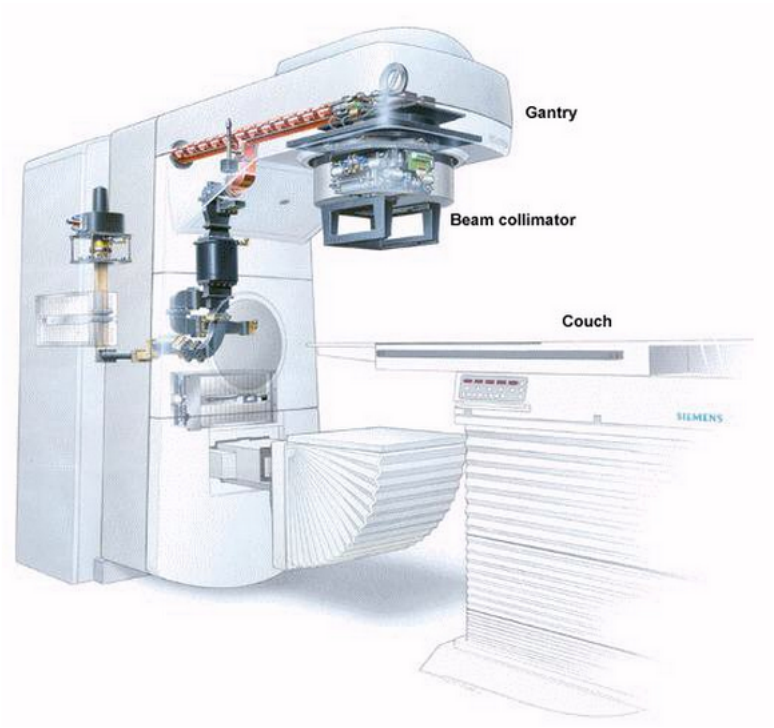

Figure 1.19: *Gantry-based treatment unit.*

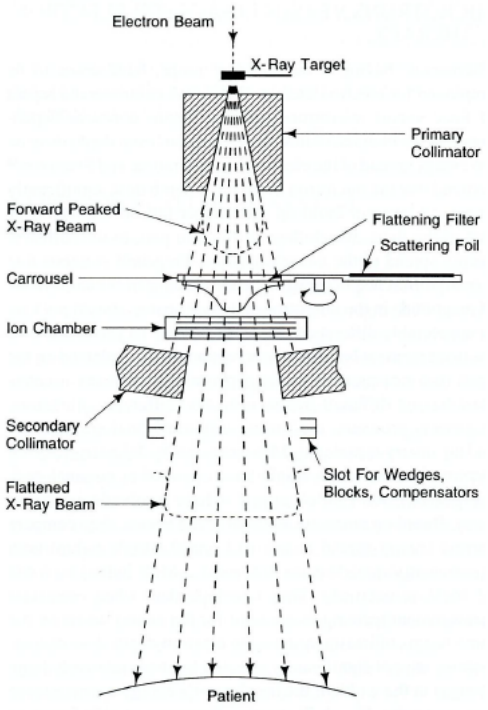

Figure 1.20: *Schematic diagram showing the basic components of the treatment head of a linac [4].*

Figure 1.21: *Multi-leaf collimator.*

1.6 Radiotherapy treatment planning for breast cancer

Breast-conserving surgery in combination with external beam radiotherapy has become the standard treatment for early stage breast cancer since the survival rates proved to be similar to that with radical surgery. For many years, breast radiotherapy field borders were based on the visible or palpable anatomy and/or fluoroscopy, while 2D dose planning was performed on the basis of one or more single-density body-outline contours. Currently, breast cancer radiotherapy has gradually shifted towards computed tomography (CT) guided treatment planning. This enables the application of techniques such as three-dimensional-conformal radiotherapy (3D-CRT) and intensity modulated radiotherapy (IMRT). In highly conformal techniques such as 3D-CRT and IMRT, accurate target volume delineation is critical because its size and shape directly affect the applied field sizes.

1.6.1 Target volume definition

Gross tumor volume (GTV), clinical target volume (CTV), internal target volume (ITV) and planning target volume (PTV), see Fig. 1.22, can be defined to generate treatment plans [5].

- **GTV** is the primary tumor or other tumor mass shown by clinical examination e.g. medical imaging; this volume always contains the highest tumor cell density and may be absent in case of complete surgical resection.
- **CTV** contains the GTV when present and/or subclinical microscopic disease that has to be eradicated to cure the tumor. The required GTV-CTV margin is derived from histological examination of tumor cell spreading around GTV and biological characteristics of the tumor.
- **PTV** is the volume generated by adding a margin to the CTV to account for the potential inter- and intra-fraction variation in tumor position and shape. The CTV to PTV margin is used to ensure an homogeneous dose to the CTV.
- **ITV** may be as an intermediate volume for generating the PTV, describing internal tumor motion, e.g. respiratory tumor motion in lung cancer.

Selection of unnecessary large margins will result in excessive dose delivery to organs at risk (OAR). On the other hand, too small margins will lead to unacceptable risk of partially under-dosing the tumor. The planning target volume is used in treatment planning to select appropriate beams to ensure that the prescribed dose is actually delivered to the CTV.

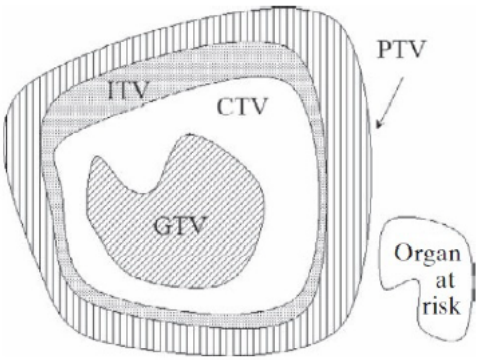

Figure 1.22: *Graphical representation of volume of interest in radiotherapy.*

1.6.2 Target delineation for breast cancer treatment

After palpation, the breast and surgical breast scar are marked with radio-opaque wires. A CT scan is then acquired starting superior to the shoulder and including all of the ipsilateral lung and 5 cm below breast tissue.

When breast target volume delineation on the CT slices is performed by the physician, various references and landmarks are used: radiopaque wires visible on CT, glandular breast tissue and bony structures. In practice, the breast CTV, including glandular breast tissue, is delineated within the extent of the radiopaque wires marking the palpable breast. The breast CTV is not extended into the pectoralis major or the ribs and does not include the skin. The breast PTV is generated by adding a 3D-margin of 5 to 8 mm around the breast CTV; in patients treated with the breath-hold technique the margin is currently 8 mm.

For boost GTV delineation surgical clips are used as well as hematoma (and seroma if present), as visible on CT images. The boost CTV is generated by adding a 3D-margin of 10 mm around the lumpectomy cavity. The CTV to PTV margin (generally 5 mm) is then added to account for respiration, inter- and intra-fraction variation in patient position and breast swelling. Both breast and boost PTV are retracted to 5 mm within the skin surface to exclude the build-up area from the planning treatment volume.

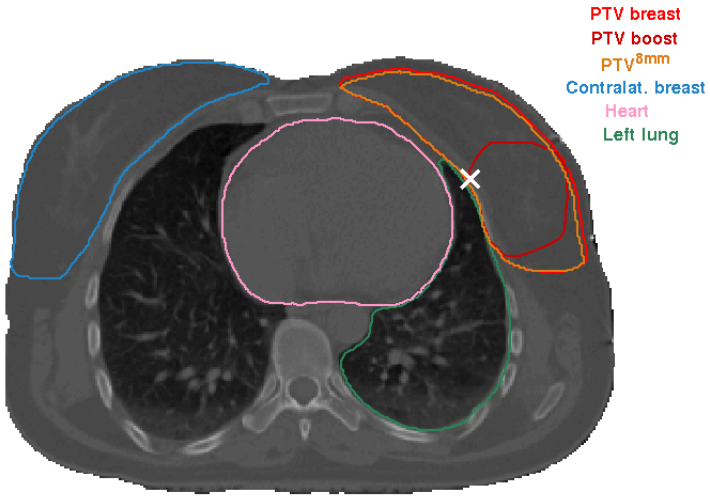

Figure 1.23: *Structures of interest for left-sided patient Le04.*

1.6.3 Organs at risk and radiotherapy-induced complications

In breast cancer radiotherapy treatment, the heart, ipsilateral lung and contralateral breast are considered as organs at risk (OAR). Irradiation of these OARs can lead to complications after breast cancer radiotherapy. Figure 1.23 shows delineations of these structures, in one CT slice. The heart is contoured (only in left-sided breast treatments) to the level of the pulmonary trunk superiorly, including the pericardium, excluding the major vessels. Both lungs are contoured in their entirety; the contralateral breast was contoured using an automated, atlas-based, contouring system (ABAS).

- **Heart** Exposure of the heart increases the subsequent rate of ischemic heart disease. In a population-based case-control study [6] the overall average of mean dose to the heart was estimated to be 6.6 Gy for women with tumor in the left breast, versus 2.9 Gy for those with tumors in the right breast. According to this study, the rate of major coronary events increased linearly with mean dose to the heart with no apparent threshold.

- **Ipsilateral lung** Pulmonary complications following radiotherapy are quite common. In a study, on short-term pulmonary complication following breast cancer radiotherapy [7], the mean dose resulted as a robust parameter correlated with the risk of pneumonitis. Mean dose to the ipsilateral lung ranged from 2.5 to 18 Gy (median 12 Gy).

- **Contralateral Breast** In patients treated for breast cancer, the most common secondary cancer is contralateral breast cancer, accounting for approximately 50% of all

second cancers [8]. For patients treated with 25 fractions of 2 Gy (50 Gy of total dose) to the regional lymph nodes and chest wall (using different techniques) the mean dose to contralateral breast was in a range from 1.3 to 4.3 Gy [9]. Sachs and colleagues introduced a model that predicts no increase of cancer risk with increasing dose over the approximate dose range from 3 to 40 Gy [10]. For low doses of ionizing radiation, non-linear dose-risk models are needed to describe the development of secondary tumor following exposure to radiation [11].

Figures 1.23 and 1.24 show for 3 patients the position of the OARs relative to the target volume. The individual anatomic characteristics vary greatly. Heart dimension and distance from the PTV, chest wall curvature as well as target breast and contralateral breast sizes and shapes have a significative influence on the final dose in these OARs.

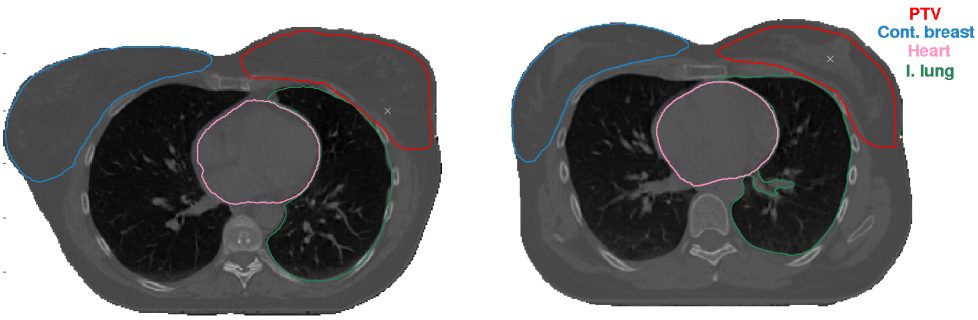

Figure 1.24: *CT slices of two left-sided breast cancer patients (left panel: Le15, right panel: Le01) with delineation of PTV, contralateral breast, heart and ipsilateral lung. Among these patients a large variation exists in terms of chest wall curvature, heart-to-target distance and breast dimension and shape.*

1.6.4 3D Conformal radiotherapy (3DCRT) treatment planning for breast cancer

The total dose prescribed to the whole breast is 50 Gy, delivered in 25 fractions of 2 Gy. Thereafter, an additional boost to the high risk area with prescribed total dose of 10 to 20 Gy, can be delivered in 5 to 10 fractions of 2 or 2.5 Gy.

Two opposite tangential beams are selected to create a dose distribution conformal to the breast PTV. Gantry angles are determined to achieve maximum avoidance of the heart, ipsilateral lung and contralateral breast. Shielding is adapted with use of the multi-leaf collimator (MLC). Wedges and a maximum of three MLC segments per beam may be used to obtain a homogenous dose distribution. Figure 1.25 shows a dose distribution generated by a technician using a commercial treatment planning system (TPS), the wedges and the two tangential beams are visible as well. For most patients, 6 MV (range 4-8 MV) photons are chosen as optimal. However, for large breast volume and separation, 6 MV energy may be used in combination with higher energies (commonly 10 MV) to produce better dose homogeneity.

If additional dose is necessary to the tumor bed, a boost plan can be created conformal to the boost PTV. It generally consist of 3 beams coming from the patient front. Wedges and MLC shielding are applied in such a way that the 95%-isodose line closely encompasses the boost PTV in three dimensions.

Beam's-eye-view projections are used to define gantry angles, isocenter position, MLC shapes and other parameters. In treatment plan generation all these parameters are tuned by a technician, using a commercial treatment planning system (TPS), in an iterative *trial* and *error* process. The 3D dose calculation algorithm, implemented in the TPS, generates the resulting dose distribution. If the dose distribution is not satisfactory, the operator changes some parameters, based on experience, for a new run of the dose calculation algorithm.

The iterative process, schematically shown in Fig. 1.26, continues until the dose distribution is satisfactory according to the planner; the plan then has to be reviewed and approved by the treating physician. This process is time consuming and can lead to sub-optimal plan quality depending on the skills of the operator and the physician and the time available for the trial-and-error process.

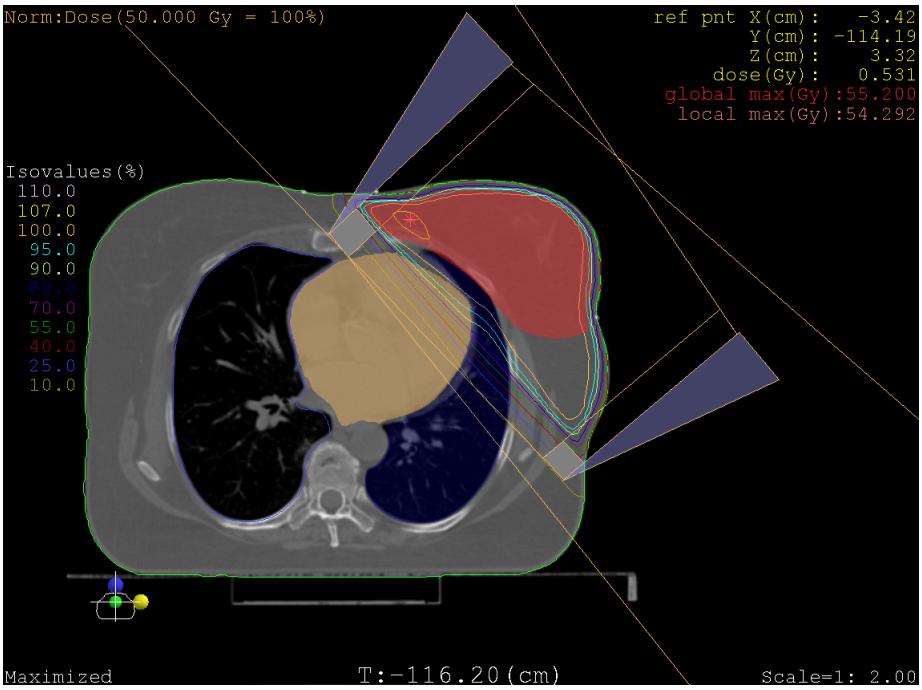

Figure 1.25: *Dose distribution generated with a commercial treatment planning system (TPS) for 3D-CRT. The volumes of interest are highlighted by different colors (e.g. the PTV in red); the beam directions and openings are represented with orange lines while the wedges in front of each beam are depicted as grey triangles. Isodose lines of different colors give a representation of the dose distribution.*

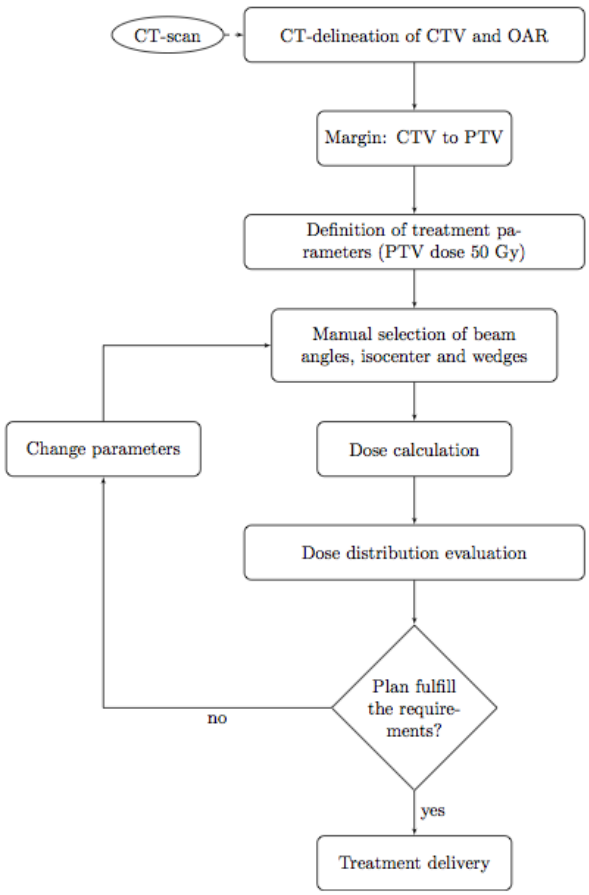

Figure 1.26: *Diagram that describes the steps taken in the generation of a 3D-CRT treatment plan with a commercial treatment planning system. The iterative loop represents the manual (trial and error) adjustment of the angles, isocenter position, collimator opening, wedge factors, beam energies and weights.*

1.6.5 Intensity modulated radiation therapy

In intensity modulated radiation therapy (IMRT), beam intensity profiles are modulated by dividing each treatment beam into subfields, each with a different shape, intensity, and position. The subfields are shaped using the MLC (see Fig. 1.27). Two methods can be used to deliver IMRT fields with an MLC:

- **static** or **step-and-shoot**: dose delivery is switched off between changes in MLC position from one subfield to the next subfield.
- **dynamic**: dose is continuously delivered while the leaves move with varying speeds.

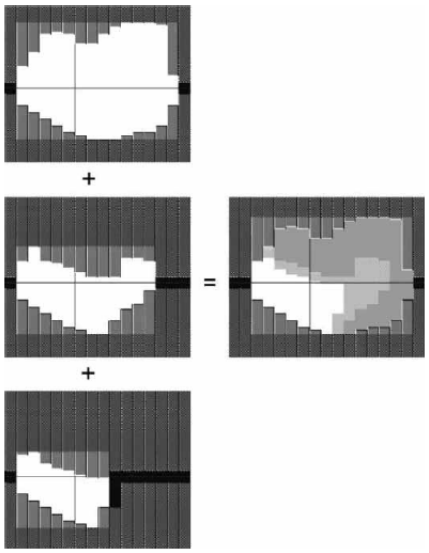

Figure 1.27: *Schematic representation of IMRT delivery by using several (3) subfileds.*

Treatment parameters for IMRT can be tuned by means of forward or inverse planning.

- **Forward planning** is an extension of conventional treatment planning since the selection of the subfields is performed manually similar to conventional trial-and-error 3DCRT planning (see Sect. 1.6.4 and Fig. 1.26). More than one subfield may be used for each beam direction. Manual definition of the subfields relies on the intuitive choices of MLC segment shapes based on the beam's eye view of the PTV or structure created from isodose lines. The weights of the segments can be optimized using a computer optimization algorithm to achieve the desired dose distribution.
- **Inverse planning** or computer optimization of intensity profiles. The idea is to first define the desired dose distribution and then try to obtain it by optimizing intensity

profiles. In inverse planning, the radiation oncologist and physicist decide the prescribed target volume dose coverage *objectives* and *constraints* together with the ones for normal tissue sparing. In this method the optimization of the fluence profiles from each beam direction made by minimization of an *objective* function. Subsequently, sequencing transforms each optimization profile into a series of segments, which can be delivered with a multi-leaf collimator.

Data in literature suggest an advantage of IMRT over conventional (non-optimized) treatment of the breast with regard to a reduction in breast and skin toxicity. It is therefore expected that the use of IMRT will increase over the coming years to improve dose homogeneity in the breast and to standardize treatment planning procedures.

Chapter 2

Multi-criteria optimization and aim of the study

2.1 Pareto-optimal plans

In radiotherapy treatment planning the aim is to eradicate the tumor cells by delivering a sufficient high dose to the target volume while trying to keep the dose to surrounding healthy tissues as low as possible. The treatment planning problem is defined by constraints and objectives for the PTV and the OARs. This typically results in a optimization problem with multiple criteria. In multi-criteria optimization, multiple objectives are in competition with each other, so that reaching one objective can lead to not fully fulfilling the others.

Typically, no single optimal solution exists that simultaneously optimizes each objective. A solution is called $non-dominated$ or $Pareto-optimal$ if none of the objective functions can be improved without deteriorating other objective values. Without additional preference information, all Pareto optimal solutions can be considered mathematically equally good. Therefore, user-defined preferences are necessary to differentiate and choose between solutions.

An example is given in Figure 2.1. It shows for one right-sided patient, mean lung and contralateral breast doses for IMRT plans generated with various sets of beam angles. Among all plans generated, only a subset are Pareto-optimal for contralateral breast and lung mean dose. The Patero-optimal plans, shown in cyan, lie in the lower left corner of the graph, where the lower values for contralateral breast and/or lung mean dose can be found.

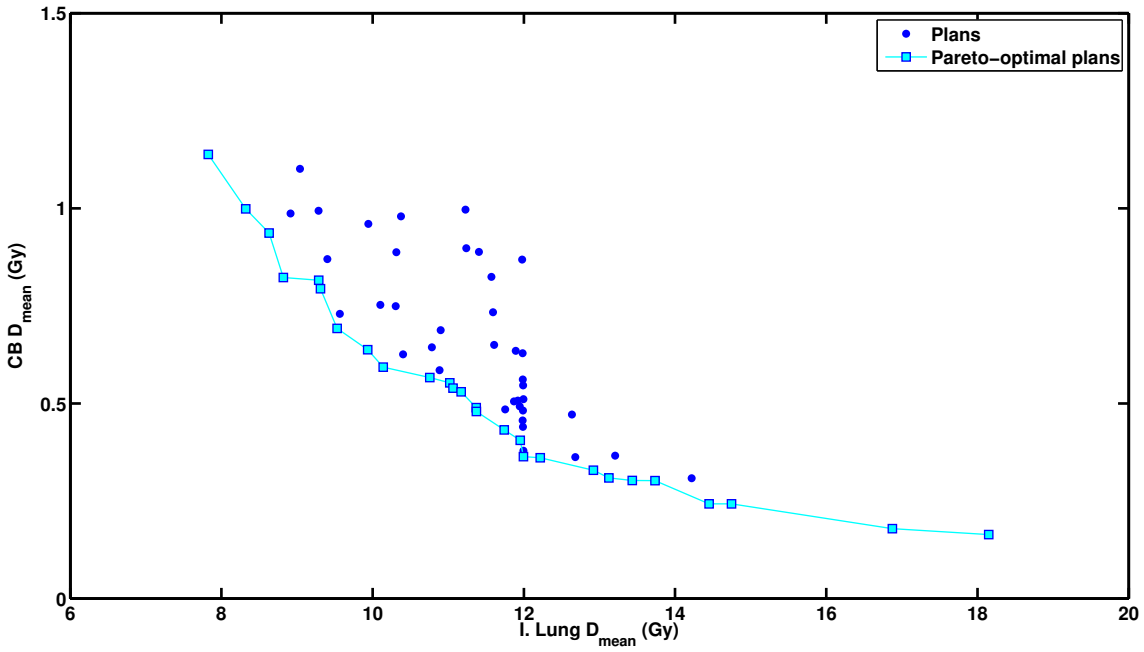

Figure 2.1: *The Pareto-optimal plans, represented in cyan squares, for contralateral breast (CB) and ipsilateral lung mean doses.*

2.2 iCycle for treatment planning

iCycle is a novel in-house developed algorithm for automated, multi-criteria optimization of beam angles and IMRT fluence profiles. In iCycle, both selection of optimal beam orientations and optimization of beam profiles are based on a user-defined $wish - list$, containing hard constraints and objectives with ascribed priorities (Breedveld *et al* 2007 [12]).

- **Constraints** must be strictly met, otherwise the plan is considered invalid. Too strict constraints may limit possibilities to generate attractive plans.
- **Objectives** are wishes, goals to be met as much as possible (within the imposed constraints).

Priorities are used for having a relative importance ranking of the objectives; the higher an objective priority is, the higher the probability that the corresponding objective will be approached closely, reached or even exceeded. Both size and shape of the breast as well as the size and location of the OAR (heart, lungs and contralateral breast) vary significantly between patients (see Fig. 1.23 and 1.24). Including multiple levels in the wish-list gradually reduces dose in the OARs. In this way, large initial dose reduction in some OARs is

prevented, leaving space for dose reduction in other OARs. In the first step, objectives have relatively easy goal value to achieve while in the later steps the goal values are set to more demanding values (i.e. greater dose reduction in OARs).

The wish-list construction is made in collaboration with physicians and technicians to ensure the generation of plans clinically acceptable and of good quality. If the wish-list (constraints, objectives and priorities) is well-defined, it will produce a class solution, which can be used for a group of patients.

Furthermore, a list of candidate beam orientations has to be given in input; it can be restricted to a coplanar beam arrangement, or extended for generation of non-conplanar plans. Directions can be excluded from the candidate set, e.g., to eliminate beam directions that may cause collisions between the treatment couch (or the patient) and the gantry.

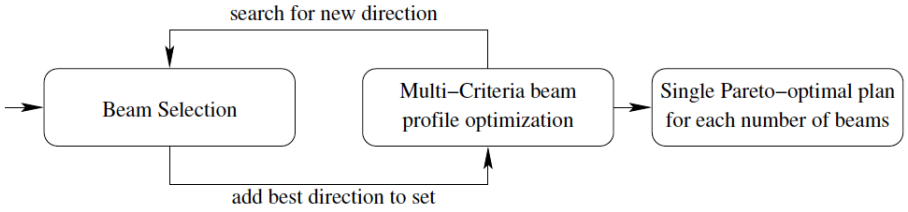

Figure 2.2: *iCycle routine for beam angle selection and IMRT fluence profile optimization: the optimal beam is selected and added to the previously optimized plan. A multi-criteria optimization is done with the plan composed by the previously selected beams plus the candidate beam to generate a Pareto-optimal IMRT plan. The output from the latter optimization is used to define the problem to be solved in the next iteration. Picture from [12]* .

2.2.1 Plan generation

Generation of a treatment plan is performed in an iterative procedure, schematically represented in Figure 2.2. The generation of the plan for a patients starts with an empty plan, i.e., no beams selected. Sequentially, optimal beam orientations are selected from the candidate beams and added to the plan till a maximum number of beams (user-defined) is reached.

Iteration i starts with selection of the ith beam orientation to be added to the plan. To select this new optimal direction all the not yet selected candidate beams have to be evaluated one-by-one by solving for each of them an IMRT optimization problem for a beam arrangement consisting of the previous $i-1$ beams plus the candidate beam. The selected candidate will be the one obtaining the most favorable score. Finally iCycle generates a Pareto-optimal IMRT plan including the beam directions selected so far using the $2p\epsilon c$

method (see Sect. 2.2.2). The output of this 2$p\epsilon c$ optimization is used to define the IMRT optimization problem to be solved in the orientation selection of the $i+1$ optimal beam.

Consequently, plan generation for a patient always results in a series of plans with an increasing number of beams all of them Pareto-optimal for beam intensity profiles. It was shown that beam addition in iCycle always results in improved plan quality regarding the highest prioritized objective that can still be improved on (Breedveld *et al* 2012 [13]).

2.2.2 2pϵc optimization

Given the wish-list and a set of chosen beams, the beam profile optimization in iCycle is made with the 2pϵc algorithm. This algorithm is based on the ϵ-constraint method (Haimes *et al*. [14]), in which each objective is optimized separately, and then constrainted during the optimization of the other (lower prioritized) objectives. This method is extended to a 2-phase ϵ-constraint optimization (2pϵc), where a goal value can be assigned to each objective used in the first phase of the optimization. In the second phase a full optimization of the objectives is pursued (Breedveld *et al*. [12]).

All constraints and prioritized objectives are given in a prioritized list, i.e. the wish-list which leads the optimization. The basic idea behind this method is that when is possible to minimize the dose below a certain threshold (i.e. its goal) for one objective, it is often more desired to minimize the dose for the other (lower priority) objectives first than to directly minimize the dose for the higher objectives to its fullest extent.

During the first iteration of the first phase, the objective having highest priority is being optimized:

$$\begin{aligned} \text{minimize} \quad & f_1(x) \\ \text{subject to} \quad & g(x) \leq 0 \end{aligned} \tag{2.2.1}$$

where $f_1(x)$ is the objective function with priority 1, associated with goal b_1, while $g(x)$ represents the (hard) constraints, summarized in a vector.
This optimization results in x^*, and gives a bound for the optimized objective (eq. 2.2.2) which is set as constraint during the optimization of the following objective. The new bound is chosen according to the following rule:

$$\epsilon_i = \begin{cases} b_i, & f_i(x^*)\delta < b_i \\ f_i(x^*)\delta, & f_i(x^*)\delta \geq b_i \end{cases} \tag{2.2.2}$$

where b_i and ϵ_i are the goal and new bound of the objective i, $f_i(x^*)$ is the obtained value for the objective f_i and δ is a slight relaxation to create some space for subsequent

optimizations (usually set to 1.03, i.e. 3%). The next optimization optimizes f_2 keeping f_1 constrained:

$$\begin{aligned} \text{minimize} \quad & f_2(x) \\ \text{subject to} \quad & g(x) \leq 0 \\ & f_1(x) \leq \epsilon_1. \end{aligned} \tag{2.2.3}$$

This is repeated for all the n objectives.
In the second phase of multi-criteria optimization, all objectives which met their goals are minimized to their fullest while keeping all others constrained starting, with the highest priority objective.

2.3 Aim of the study

This study investigates automated generation of an IMRT treatment plan for whole breast irradiation with two tangential beams with automated beam angle and isocenter selection. Beam angle selection was not performed by iCycle (see Sect. 2.2). Instead, for each patient a set of candidate plans was generated using different beam arrangements (combinatorial approach). For each beam arrangement the intensity beam profiles were automatically optimized using iCycle, based on a wish-list with a description of plan constraints and objectives. Among all these plans, plans were identified that were Pareto-optimal with respect to beam arrangement (and isocenter position). To identify the single 'best' plan, a score function was used that on average resulted in the clinically selected beam configuration.

Clinical questions investigated in this study were:

- What wish-list results in high quality IMRT plans for whole breast treatment with tangential fields?
- How sensitive are PTV coverage and OAR dose distributions for beam configuration and isocenter selection?
- Is it possible to automatically select for each patient the beam configuration and isocenter for at least a plan quality as obtained clinically by technicians?
- How critical is the isocenter positioning for plan quality?

Chapter 3

Materials and methods

3.1 Patient data

For this study, 30 patient data sets were randomly selected from the database of patients treated with surgery plus breast conserving therapy in the Erasmus MC between October 2012 and April 2013 (15 left-sided and 15 right-sided breast cancer patients). For 7 left-sided patients, the CT-scan was acquired in deep inspiration breath-hold (BH). These patients have an unfavorable position of the heart with respect to the breast. With the breath-hold technique a larger spacing between the thoracic wall and heart is created, compared with normal breathing, resulting in a lower dose to the heart.
The resolution of all CT-scans was 0.98 x 0.98 x 2.5 mm^3. Clinical treatment plans were made using commercial treatment planning software XiO (Elekta). Clinical plans consisted of two opposing tangential beams encompassing the whole breast, and if applicable, 2 or 3 additional beams to deliver an extra dose to the tumor bed. Wedges were used to modulate the beam profiles.

For all patients, the whole breast (CTV) as well as the organs at risk were delineated. A planning target volume (PTV) was generated by first adding a margin of 5 mm to the CTV and then retracting it by 5 mm from the skin. For breath-hold patients, a margin of 8 mm was used. For evaluation purposes, PTV^{8mm} was considered as well; this structure was generated by retracting the PTV 8 mm from the skin to exclude the region of the build-up area (see Sect. 1.4.1.4). Radiotherapy for breast cancer often involves incidental exposure of the nearby healthy organs. Lungs and contralateral breast were delineated as OAR for all patients. Heart was delineated for left-breast treatment only, as for the right-breast treatment, dose to the heart is generally low because of the large separation between heart and PTV. Contralateral breast was delineated by an atlas-based contouring program (ABAS, Elekta).

3.2 Treatment plan generation

Clinically, the directions of the 2 nearly opposing tangential beams are selected by a dosimetrist. Beam orientations are chosen from partial arcs of typically 40 degrees at the lateral and medial side of the patients (see Fig. 3.1). Because of the limited set of candidate beam configurations, a combinatorial approach was used to investigate automated beam angle selection, instead of using the multi-criterial beam-angle optimization procedure in iCycle (Sect. 2.2). The combinatorial approach consists of the automatic generation of a plan for each possible combination of beam angle candidates, using iCycle for optimization of the beam profiles. Therefore, for each patient, from n medial candidate beams and m lateral candidate beams, nxm plans are generated.

The central beams in the two arcs were matched to the beam angles chosen by the technician for the clinical treatment plan. The width of the arcs was set to 20° and beams within the arcs were defined with a separation of 2°, as illustrated in Figure 3.2. In this way, 11 beams are defined on both the medial and the lateral side, resulting in 121 possible combinations of beams, for which an IMRT plan was generated. All patients were treated clinically with 6 MV beams and for most of them also higher energy beams were added to obtain a more homogenous dose distribution. For patients clinically treated with two energies, IMRT plans were generated using beams of 6 and 10 MV.

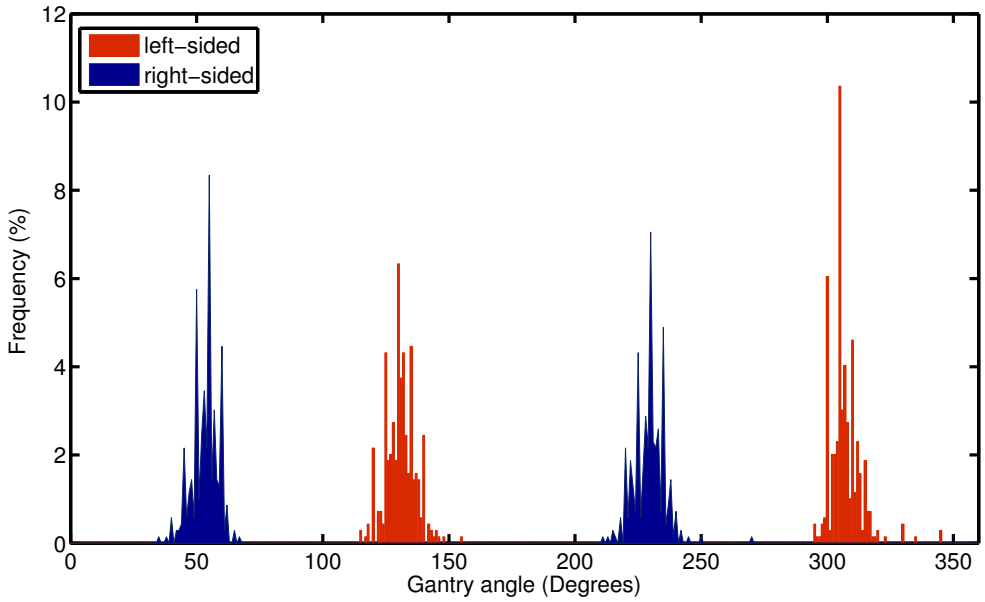

Figure 3.1: *Frequency of use of medial and lateral gantry angles in clinical treatment planning (Erasmus MC 2012), for left and right breast treatments.*

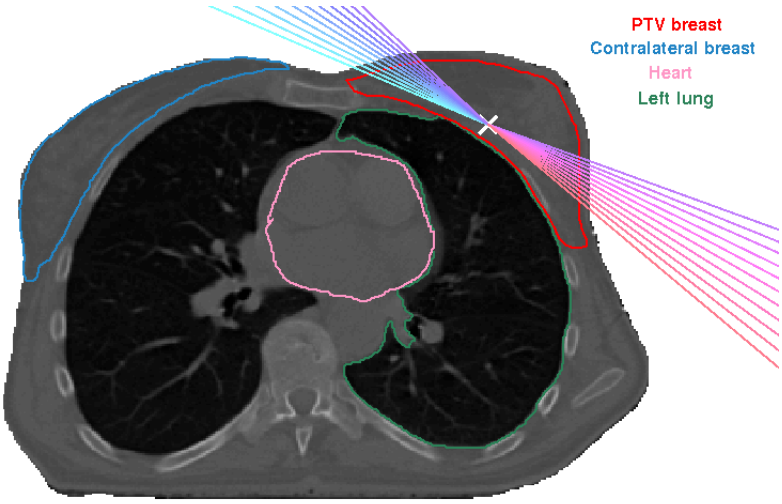

Figure 3.2: *Definition of the candidate beams in the combinatorial approach.*

3.2.1 iCycle for IMRT plan generation

The wish-list was made in collaboration with physicians and technicians. The clinical 3D conformal plans were used as reference dose distribution for the selection of the objectives in the wish-list. As the beam models implemented in iCycle and the clinical TPS are not exactly the same, no high accuracy direct comparison can be made between the dose distributions. Therefore, in the rest of the study, comparisons were made only between plans generated with iCycle.

Table 3.1 shows the final wish-list used in the study. Objectives concerning the heart are only present in the wish-list for left breast treatments. The objectives will be discussed in Sections 3.2.1.1 and 3.2.1.2.

Table 3.1: *Wish-list for left and right side breast. D^p = prescribed dose, α = parameter related to cell survival, S = sufficient parameter.*

Constraints

	Volume	Type	Limit	
	PTV	Maximum	53.5 Gy	(=107% of D^p for PTV)
	Patient	Maximum	53.5 Gy	

Objectives

Priority		Volume	Type	Goal	Parameter
left	right				
1	1	PTV	LTCP	1	$D^p = 50\ Gy$, $\alpha = 0.8$, S = 0.5
2	2	Contralateral breast	Mean	1 Gy	
3	3	Ipsilateral lung	Mean	12 Gy	
4	-	Heart	Mean	7 Gy	
5	-	Heart	Maximum	50 Gy	
6	4	PTV	Variance	1.5	
7	5	Contralateral breast	Maximum	10 Gy	
8	6	Patient	Maximum	50 Gy	
9	-	Heart	Mean	4 Gy	
10	-	Heart	Maximum	42.5 Gy	
11	7	Ipsilateral Lung	Mean	6 Gy	
12	8	Patient ring 3 cm	Maximum	42.5 Gy	

3.2.1.1 PTV coverage and dose homogeneity

The highest priority in radiotherapy treatment is generally the irradiation of the whole volume enclosed in the PTV, i.e. breast glandular tissue plus a safety margin to a high dose. Even though the PTV dose in clinical plans can range from 95% to 112% of the prescribed dose (D^p), homogeneous dose is highly desirable. In clinical practice, small volumes receiving 112% are accepted if a complex patient anatomy requires it. For optimizing the dose distribution, iCycle uses only a sub-set of voxels, randomly sampled in the structures of interest, and a small degree of freedom is left to the achievement of goals (see Sect. 2.2.2). Therefore the PTV dose was constrained to 107% of D^p to ensure that even the dose inside a single voxel of PTV was always below the 112%. Choosing this maximum dose constraint

for the PTV also helped to avoid hot spots in the normal tissue outside the PTV.

The highest priority is given to the objective that optimizes the PTV dose distribution using a LTCP (Logarithmic Tumor Control Probability, Alber and Reemtsen 2007 [15]), cost function:

$$LTCP = \frac{1}{m}\sum_{j=1}^{m} e^{-\alpha(d_j - D^p)}$$

where m is the number of voxel in the target structure, D^p the prescribed dose, d_j the dose in voxel j and α the cell sensitivity parameter. The LTCP will penalize underdosage, but still allows partial underdosage. For a homogeneous dose equal to D^p, the value of LTCP approaches 1.

A higher value for α results in larger penalty for voxels with low dose. Therefore a higher percentage of the PTV will receive at least 95% of the prescribed dose. Setting the α value goal to 0.8 always allows to achieve a high PTV coverage. The 'Sufficient' (S) parameter value is used to stop the minimization of this objective at the defined S value in the first phase of the optimization, to leave room for minimization of lower prioritized objectives (Sect. 2.2.2).

To obtain a more homogeneous dose in the PTV, the variance objective was introduced, in the lower level of the wish-list; this parameter was defined as:

$$Var = \frac{1}{n}\left\|Ax - d\right\|^2$$

where d is the current mean dose and Ax is the dose in the individual n voxels belonging to the PTV. Minimizing this parameter (in conjunction with the LTCP) allows squeezing the dose in a small interval around D^p. During the optimization of the wish-list, the influence of the variance on the dose distribution was studied.

3.2.1.2 Organs at risk objectives

Sparing of OARs was obtained in two steps by using a so-called two-level wish-list (Table 3.1). In the first level (objectives with priority 2 to 5) dose is reduced with a high priority but to a relatively modest level. In the second level (priority 7 to 11), doses are reduces to a lower level. In this way the optimizer will gradually reduce the dose delivery in the OARs, preventing that large initial reduction in one of the organs compromises sparing of the others.

Due to high risk of secondary tumor induction, the contralateral breast received the highest priority among the OARs in both levels of the wish-list. The request for a mean dose reduction below 1 Gy is just after the objective for PTV coverage while in the second level, according to the clinical practice, the request is to confine the 10 Gy isodose line outside the contralateral breast.

Heart was the second OAR to be considered since the risk of ischemic disease increases linearly with the dose with no apparent threshold [6]. In the majority of patients with a left breast tumor the heart is not directly adjacent to the PTV and the ipsilateral lung fills the space between heart and target volume. Therefore, giving a higher priority to the ipsilateral lung, instead of the heart itself, helped to create a steeper dose gradient in the region of the chest wall resulting in sparing both lung and heart. In the second level of the wish-list the priorities of heart and lung are reversed.

The goals for mean dose reduction in ipsilateral lung and heart in the first level were chosen considering the more difficult cases for which even a high dose of 11 Gy for lung and 7 Gy for heart can still be accepted by the physicians. The goals for these organs in the second level have been tuned considering the best possible sparing achieved in clinics. For the heart, an additional objective for minimization of maximum dose was introduced to induce a steeper gradient between PTV and this structure.

In whole breast treatments with tangential beams, high dose regions outside the PTV ($\geq$107% of the prescribed dose) may appear on the patient side especially for patients with pendulous breast or high body mass index. To avoid these hot spots, a restriction to 50 Gy is given to the patient volume outside the PTV. In addition, at a later stage during the optimization (priority 12 in Table 3.1), the dose to a volume at the lateral side of the patient, 2 cm from the PTV and 3 cm under the skin (orange structure in Fig. 3.3), is minimized to the 85% of D^p.

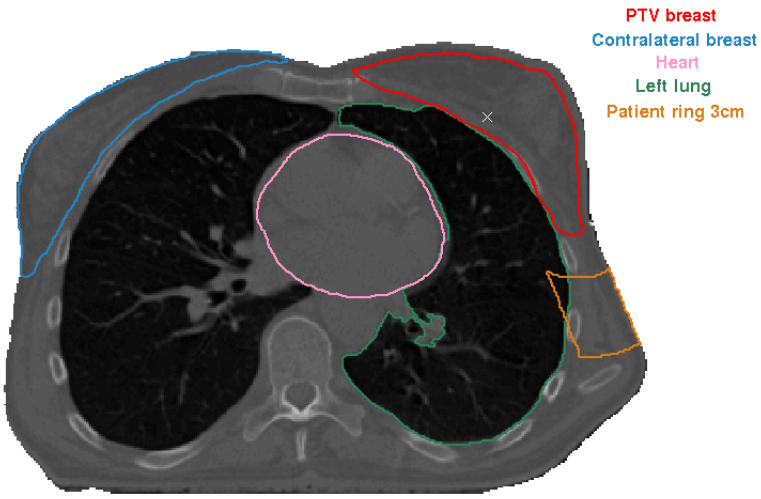

Figure 3.3: *Contours of the structures use in the wish-list.*

3.2.2 Treatment plan evaluation

Evaluation of dose distributions was based on the following parameters:

- PTV coverage, PTV $V_{95\%}$, defined as the percentage of volume receiving at least 95% of the prescribed dose,
- $\mathbf{D_{xcc}}$, representing the minimum dose received by x cubic centimeter of the target,
- $\mathbf{D_{x\%}}$, representing the minimum dose received by x% of the target volume,
- Heterogeneity index (HI) for PTV, estimated as

$$HI = \frac{D_{5\%}}{D_{95\%}} \tag{3.2.1}$$

- Mean dose for PTV and OARs

To exclude underdosage in the build-up region from the analyses, D_{xcc} and $D_{x\%}$ were evaluated for PTV^{8mm}.

3.2.3 Feasible plans

For each patient, a subset of the 121 generated plans was selected as feasible. These feasible plans were characterized by a high PTV coverage in order to guarantee the effectiveness of the radiotherapy treatment. Therefore, the starting point of each plan selection consisted of detecting feasible plans and leave aside plans with a sub-optimal PTV dose distribution.

Feasible plans were selected considering only the $V_{95\%}$ of PTV^{5mm} and the near-minimum dose D_{V-2cc} of PTV^{8mm}. The effectiveness of radiotherapy could be compromised when the minimum request on PTV $V_{95\%}$ and D_{V-2cc} are not achieved.

Thresholds for PTV V_{95} (th_V) and D_{V-2cc} (th_D) were assigned, patient per patient, by

$$th_V = \begin{cases} 99\%, & V_{95}^{med} \geq 99\% \\ V_{95}^{med}, & V_{95}^{med} < 99\% \end{cases} \tag{3.2.2}$$

$$th_D = \begin{cases} 46.5Gy, & D_{V-2cc}^{med} \geq 46.5Gy \\ D_{V-2cc}^{med}, & D_{V-2cc}^{med} < 46.5Gy \end{cases} \tag{3.2.3}$$

where V_{95}^{med} and D_{V-2cc}^{med} are the median values of PTV coverage and near-minimum dose in the 121 plans for each patient respectively. Only plans for which both the PTV parameters were equal or higher than the sufficient values were taken into consideration.

3.2.4 Score function for selecting favorable Pareto-optimal plans

Breast-only tangential radiotherapy is associated with a low, but real risk of pneumonitis and cardiac disease, as well as secondary tumor induction. Therefore, the quality of the dose distributions of all feasible plans was discriminated based on OARs sparing.

For right-sided patients, the only OARs are ipsilateral lung and contralateral breast, so Pareto-optimal plans can be represented on a frontier in the plane of lung and contralateral breast mean dose. For left-sided patient the heart was considered as well, therefore Pareto-optimal plans are distributed on a surface in the space of the OAR mean doses.

To select among the feasible plans only the favorable Pareto-optimal plans, a weighted sum score function was used. Given a set of solutions a weighted sum can only select a special class of Pareto-optimal solutions, as demonstrated by Gass and Saaty [16]. Multiple criteria are combined into a single criterium by multiplying each objective with a positive weight and summing up the weighted objectives. A solution to the resulting single criterium problem is a solution with special performance characteristics. By varying the individual weights, the weighted sum can be tuned to generate special optimal solutions.

To select favorable plans for a patient considering the relative sparing of OARs, the mean doses in the organs at risk were used as objectives. Performance values s_{ij} were evaluated comparing the mean dose in OAR j for plan i (D_j^i) with the average value of the mean dose of organ j considering all feasible plans, $\overline{D_j}$:

$$s_{ij} = D_j^i - \overline{D_j} \quad for \quad j = 1, 2 \dots N \tag{3.2.4}$$

For right-sided patients the objectives are only two (N = 2) while for left-sided patient the heart was considered as well (N = 3). The total score of plan i is then given by the sum of all the performance values multiplied by the relative weights w_j and divided by a normalization factor, as follows

$$Score_i = \sum_j^N w_j \frac{s_{ij}}{\frac{\sqrt{\sum_i (s_{ij})^2}}{M}} \quad for \quad i = 1, 2 \dots M \tag{3.2.5}$$

where M is the number of feasible plans and the coefficients w_j were defined as the relative weight of the objective O_j. Since low mean doses in organs at risk are desired, the best plan for OARs sparing, given a set of relative weights, is obtained by minimizing the total score. The use of the standard deviation as a normalization factor is necessary to not be sensible to particular anatomic characteristics of the patient.

3.2.5 Selection of weights

By tuning the weights it is possible to give more importance to sparing of one organ instead of an other. In the attempt to find weights for selection of the Pareto-optimal plan that matches best with the clinical practice, the plans generated with the clinically used angles were considered as reference plan. However, it turned out that the clinically used angles did not produce a Pareto-optimal plan for all patients.

To better understand how different sets of weights affect plan selection, 9 different sets of weights were systematically evaluated for all 30 patients. The sum of the weights was set equal to 1.

For right side breast, only two objectives were considered, one for contralateral breast and one for ipsilateral lung; the 9 sets of weights were defined starting from 0.9 for the contralateral breast and 0.1 for the lung and continued increasing ipsilateral lung weight by steps of 0.1 while consequently decreasing the contralateral breast weight. For left side breast, three objectives were used, for heart, lung and contralateral breast; considering the linear relation between heart and lung mean dose for those two organs the same weights were used. Therefore, the 9 sets of weights were generated starting from a weight of 0.05 for both heart and ipsilateral lung and a weight of 0.9 for contralateral breast and then heart and lung weights were increased of 0.05 in each step while the contralateral breast weight was decreased by consequence. For each set of weights, the feasible plan with the lowest score is selected as the best Pareto-optimal plan. This resulted in the selection, for each patient, of 9 best plans starting with the extreme case of selecting the plan with best contralateral breast sparing characteristics (at the expense of a higher exposure of ipsilateral lung and heart) passing from an equal importance for all the OARs (equal weights) and going to the extreme opposite case of a plan with low dose in lung (at the cost of higher dose in contralateral breast).

The 9 plans selected with different sets of weights were compared, one by one, to the the plan generated with clinical angles. For this purpose the euclidean distance between these plans and the clinical plan in the OAR mean dose space was calculated. The plan with smallest distance has the more similar characteristics in OAR sparing to the plan with the clinical beams. Since one plan can be selected by different sets of weights, the frequency with which a set of weights selected the plan closest to the clinical angles plan was evaluated and analyzed. The more frequent sets of weights were used in the weighted sum for best plan selection.

3.3 Sensitivity to isocenter position

The generation of treatment plans requires the selection of the position of the beam isocenter. In clinical practice, this parameter is chosen by the technician who makes the plan. The guideline for positioning the isocenter is to place it inside the PTV volume, in the slice where the breast has the biggest volume, within a distance from the lung surface of approximately 2 *cm*. Each patient is a separate case to be considered by the planner. For the 30 patients in this study, the distance of the isocenter from the ipsilateral lung contouring was measured.

The combinatorial optimization was repeated for different isocenter positions, resulting in 121 plans per patient per isocenter position. The isocenter was moved in the z direction (same x and y in the axial slice) 1 *cm* cranially (up) and 1 *cm* caudally (down) with respect to the slice containing the clinical isocenter. In addition, 4 isocenter positions were defined at a distance of 0.5, 1, 2 and 3 *cm* from the ipsilateral lung contour in the axial slice of the clinical isocenter. The direction of movement across the PTV was set to be perpendicular to the line connecting the two points generated from the lead wire positioned around the palpable breast. Figure 3.4 illustrates the 4 isocenter positions used (colored stars) and the clinical isocenter (yellow point), in the slice of the clinical isocenter. For three patients the breast size was too small to consider the isocenter at 3 *cm* from the lung.

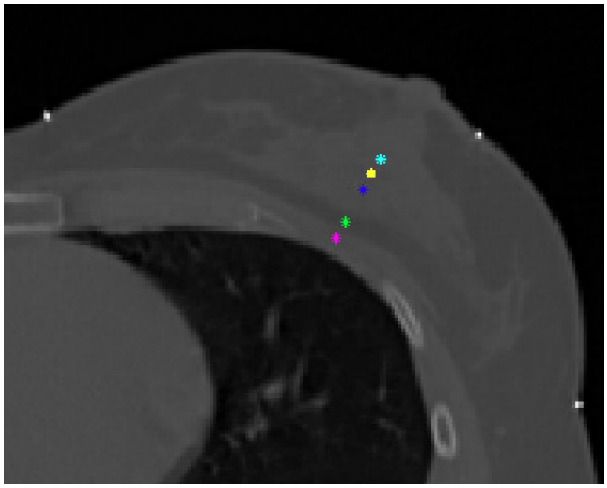

Figure 3.4: *Axial CT slice of a left sided patient. To investigate the sensitivity of isocenter position, 4 isocenters were defined at 5 mm (magenta), 1 cm (green), 2 cm, (blue) and 3 cm (cyan). The clinical isocenter position, in this case 24 mm distant from the ipsilateral lung, is represented by a yellow dot.*

Chapter 4

Results

This chapter starts with the tuning of the variance parameter (Section 4.1) and the evaluation of the PTV dose parameters (Section 4.2). In Section 4.3 the thresholds for the feasible plan selection are discussed. In Section 4.4 the selection of Pareto-optimal plans using the weighted sum is presented. A detailed description of the results for one patient is presented in Section 4.5. Then, the results on the plan selection for 30 patients are summarized, analyzed and discussed in Section 4.6. Finally in Section 4.7 the isocenter positioning analysis is presented, for 10 left and 10 right breast patients.

4.1 Wish-list optimization: variance objective

The variance parameter in the wish-list was varied from 0.5 to 2.5 and plans were generated with clinically used beam angles for 10 patients. Figure 4.1 shows the effect of this parameter on $V_{95\%}$, heterogeneity index (HI) and mean dose in heart and ipsilateral lung. A value of 0.5 results in a good PTV coverage, but also in an increase in mean and significant maximum dose in OARs. In most of patients, relaxing the variance at 1.5 still guarantees a high PTV coverage while at the same time a reduction of mean dose (up to 0.5 Gy) in OAR can be achieved. The intermediate value of 1.5 is superior to 2.5, as only a small or no gain in OAR sparing can be achieved at the cost of lower PTV coverage and a less homogeneous dose.

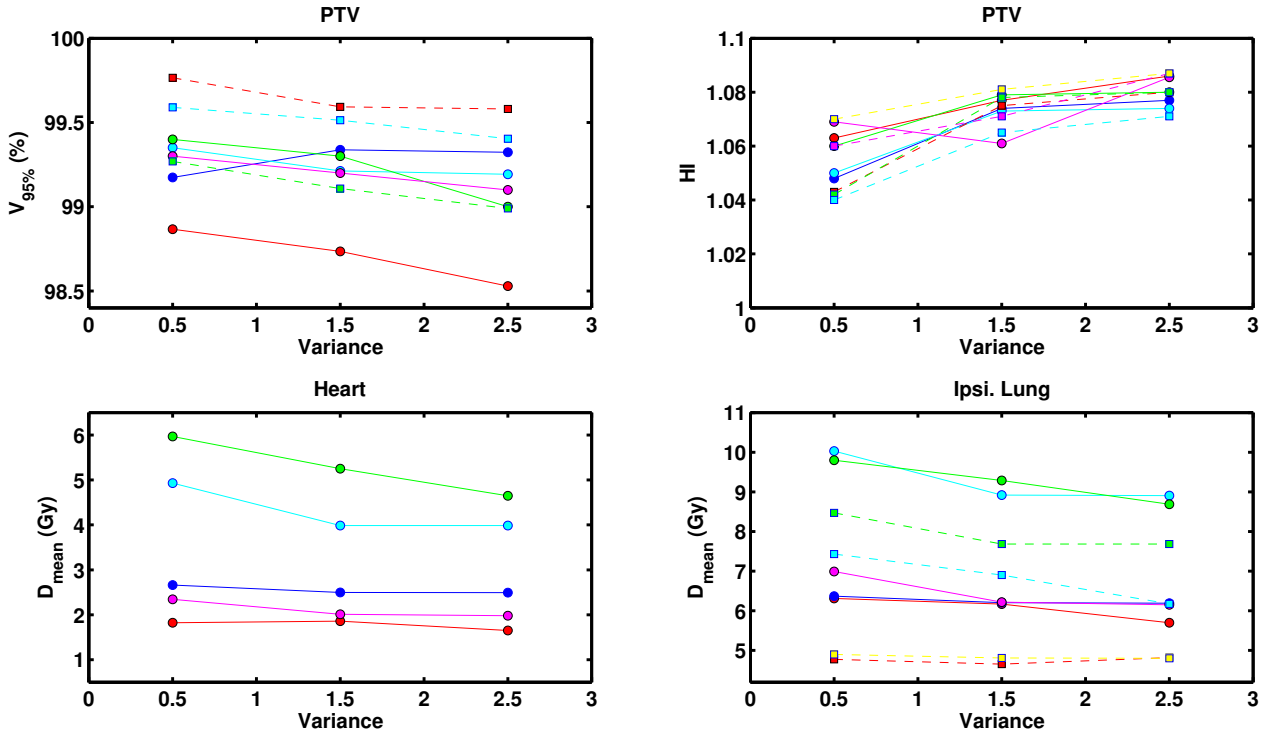

Figure 4.1: *The graphs represent, starting from the upper left and going clock wise, the effect of the variance objective on PTV coverage, heterogeneity index and heart and ipsilateral lung mean dose. Solid lines: 5 left-sided patients, dashed lines: 5 right-sided patients.*

4.2 Evaluation of PTV dose parameters

The near-minimum and near-maximum doses were investigated for 20 patients (121 plans per patient) to find significant parameters to discriminate on in the plan selection. Near-minimum and near-maximum values can be estimated using the dose-volume parameters $D_{x\%}$ and D_{xcc}.

To estimate the near-maximum dose, D_{2cc} and $D_{2\%}$ were calculated in each of the 121 plans, patient by patient (see Fig. A.1 in Appendix A). The D_{2cc} values were in general higher than $D_{2\%}$ (ranging approximately from 8 to 45 cc). No values larger than 53.8 Gy were found. This shows that including constraints at 107% of the prescribed dose (53.5 Gy) guarantees that the maximum PTV dose is indeed always lower than maximum accepted value of 112% (56 Gy).

Also the near-minimum was considered; this value was evaluated for PTV^{8mm}, to exclude underdosage in the build-up region under the skin. The dose received by a percentage x of PTV^{8mm} was investigated with the values $D_{98\%}$ and $D_{95\%}$ (not shown). In all the patients the minimum dose received by 98%, and therefore also 95%, of the volume is always larger than 95% of the D^p, with these parameters no apparent under-dosage is present. A second disadvantage of these parameters is that the volume considered directly relates to the PTV volume, and will change from patient to patient.

Therefore, the minimum dose received by the total volume minus x cc was analyzed (D_{V-xcc}). For 20 patients this parameter was evaluated with x ranging from 0.1 to 5 cc, to evaluate the minimum dose received by the total volume minus x cc. This parameter ensures that the under-dosage is confined to a certain volume x regardless of the dimensions of the target volume.

This data of 121 plans per patient is graphically represented in Figure 4.3 using box and whisker plots for the parameter D_{V-2cc}. In the box and whisker plot, the central mark of each box represents the median value, the edges of the box are the 25th and 75th percentiles, the whiskers extend to the 2nd and 98th percentiles, and outliers are plotted individually. In the graphs a fluctuation of the median values for the different near-minimum parameters among patients is observed. Also the extension of the boxes varies from patient to patient.

Figure 4.2 shows the median value of all plans per patient as a function of the volume x cc (see box and whisker plots A.2 in Appendix A). When the parameter x is changed from 5 cc to 0.1 cc the near-minimum dose decreases for all patients and the variation in near-minimum dose between plans for individual patients becomes larger. These volumes relate to a volume of less than 800 voxels. Discriminating on such a small volume may discard too many (good) plans.

The median values for D_{V-5cc} and D_{V-3cc} for most patients are higher than 47 Gy and higher than 46.5 Gy for all patients. This means that the volume receiving less than 46.5

Gy (93% of prescribed dose) is always smaller than 3 cc in more than 50 % of the plans generated.

In the end the dose to a volume of PTV^{8mm} minus 2 cc was chosen to evaluate the near-minimum dose. For 14 of the 20 patients the median value of this parameter in the 121 plans was higher than 46.5 Gy. In clinical plans, an underdosage of 46.5 Gy is usually accepted if this is not in the volume of PTV boost and occurs in a small volume (smaller than 5 cc).

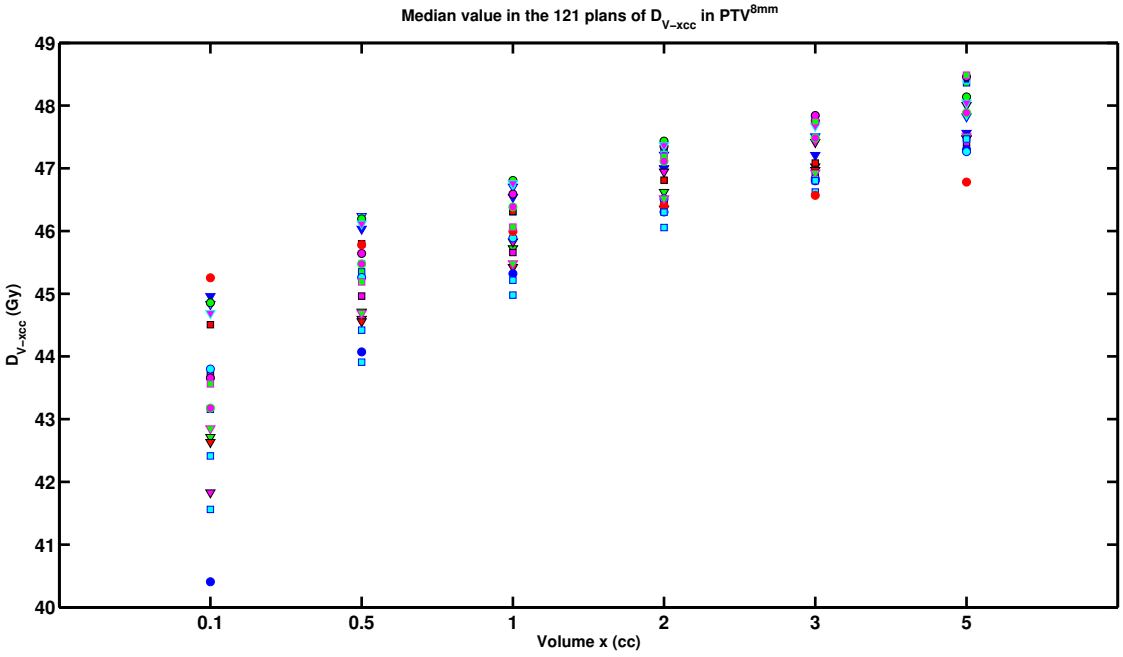

Figure 4.2: *Near-minimum dose as a function of the volume x (cc). Each point represents for a single patient the median of the doses received by a volume (V - x cc) of* PTV^{8mm} *in the 121 plans.*

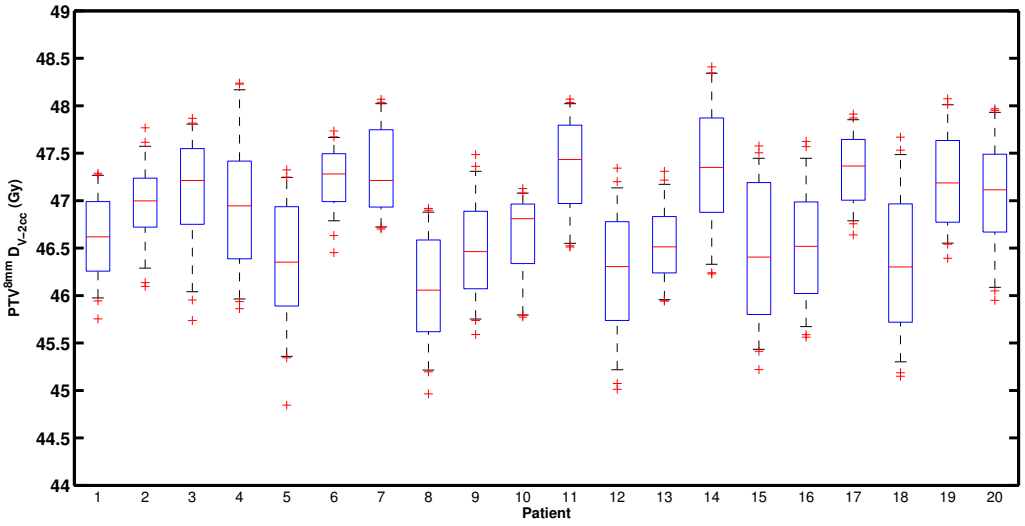

Figure 4.3: *The values of the D_{V-2cc}, in 121 plans, are represented with box and whisker plot for 20 patients.*

4.3 Selection of feasible plans

Once the 121 plans with all the possible combinations of beam directions were generated, plans were selected based on PTV coverage and the near-minimum value in PTV^{8mm}.

A plan having the 99% for PTV $V_{95\%}$ and a value of 46.5 Gy (93% of D^p) for $D_{V_{tot}-2cc}$ is characterized by a high coverage in combination with an acceptable underdosage in a volume as small as 2 cc. There is no need to ask for better values, since this usually comes with increased mean dose in OARs. The 99% for PTV $V_{95\%}$ and 46.5 Gy for $D_{V_{tot}-2cc}$ were considered sufficient values for selecting the feasible plans.

Due to the large variations in breast and chest wall size and shape it was not possible to achieve a median PTV coverage larger than 99% for all patients. As a consequence, the use of predefined thresholds to select the feasible plans for all patients would result in discarding too many initially generated plans. Patient specific sufficient values were defined to select feasible plans.

If, for a patient, the median values ($V^{med}_{95\%}$ and D^{med}_{V-2cc}) for PTV D_{V-2cc} and $V_{95\%}$ (considering all the 121) plans were lower than 99% and 46.5 Gy respectively these median values were used as sufficient values.

Figure 4.4 shows graphically for two patients how the feasible plans are selected with these two thresholds. From these graphs it is clear that it was not possible for all patients

to fulfill the a-priori set sufficient parameters (due to specific anatomy). For the patient represented in the left graph V_{95}^{med} and D_{V-2cc}^{med} were higher than 99% and 46.5 Gy, so the latter were used to choose the feasible plans (blue points); while the other patient (right panel in Fig. 4.4) had lower V_{95}^{med} and D_{V-2cc}^{med} so these two values where used as selection criteria (solid lines).

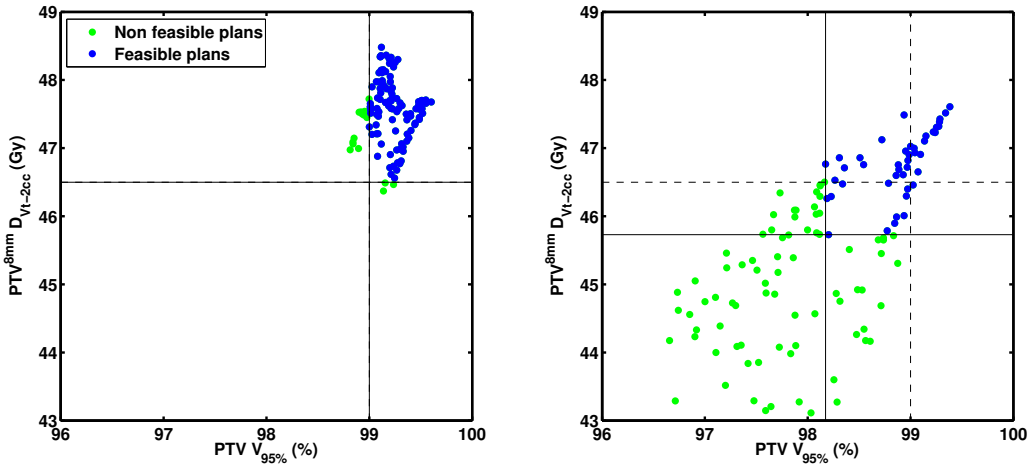

Figure 4.4: *Selection of feasible plans (blue) for two patients. a priori set thresholds and applied (patient-specific) sufficient value are represented by dashed and solid lines respectively. For the patient in the right graph, the application of the a priori thresholds (99% for $V_{95\%}$ and 46.5 for D_{V-2cc}) would result in only 10 feasible plans.*

4.4 Selection of Pareto-optimal plans using a weighted sum score

4.4.1 Relation between heart and lung dose

For left-sided patients the Pareto-optimal plans are distributed on a surface in the space of heart, ipsilateral lung and contralateral breast mean doses. Figure 4.5 shows heart mean dose versus lung mean dose for all Pareto-optimal plans for the 15 left-sided patients. An approximately linear relation exist between those two parameters and the slope and doses values depends on the specific patient anatomy. Therefore in the next sections as well as in Appendix the Pareto-optimal plans for left-sided patients are projected in the ipsilateral lung and contralateral breast mean dose plane.

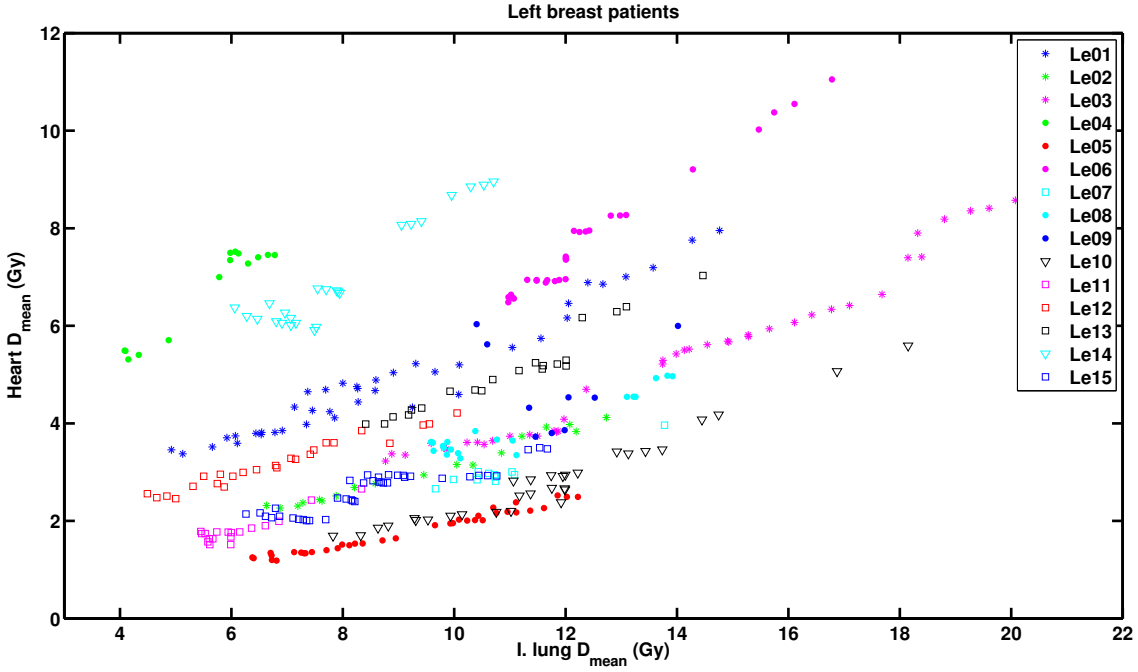

Figure 4.5: *Mean heart dose as a function of the mean dose in the ipsilateral lung for 15 left-sided patients. Each marker represents a Pareto-optimal plan.*

4.4.2 Selection of coefficients for the weighted sum

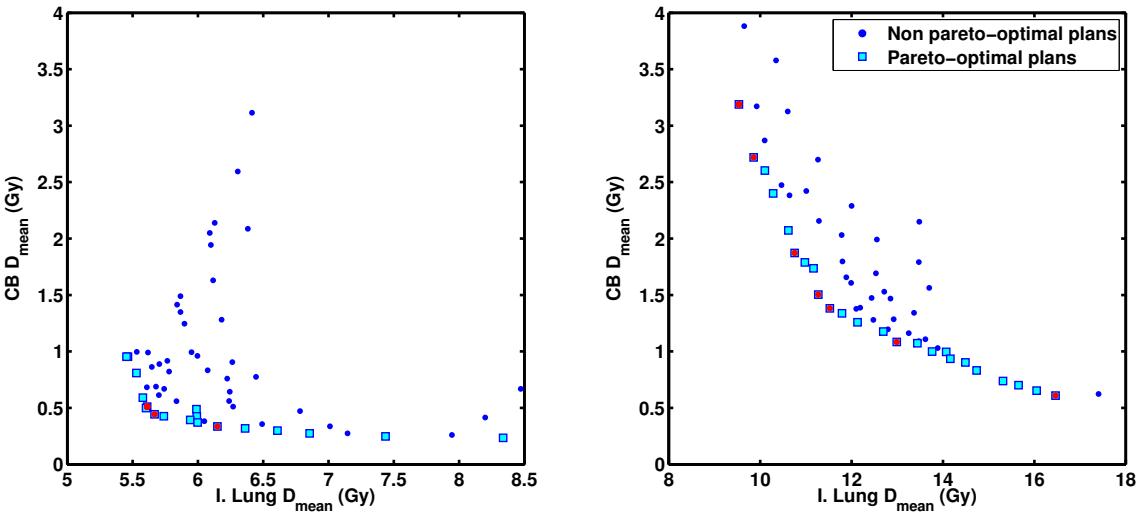

Figure 4.6: *Mean doses for contralateral breast and ipsilateral lung for all feasible plans of two patients are reported (left-sided patient in the left panel and right-sided patient in the right panel). The Pareto-optimal plans for OAR are represented by cyan squares. Among them, the Pareto-optimal solutions that can be selected using the weighted sum used for this study with varied weights (red dots).*

Only a single plan is selected when a set of weights is used (see Section 3.2.5). To analyze the effect of different weights on plan selection, 9 sets of weights were used to select plans on the Pareto-optimal surface. For left-sided tumors, the heart, ipsilateral lung and contralateral breast were considered while in right-sided tumors only two weights were considered (for ipsilateral lung and contralateral breast). The weights were varied between maximum relative importance to the contralateral breast sparing (at cost of high mean dose in lung and heart) to maximum relative importance of lung and heart sparing (with a lower importance to contralateral breast).

Figure 4.6 shows for two patients plans at the Pareto-optimal frontier (cyan squares) and the selected plans by the different sets of weights (red points). Different sets of weights may result in the selection of the same plan (set of beam angles); instead of having 9 plans (red points) per patient on the Pareto frontier only 3 (right panel) and 7 (left panel) were selected because some plans were chosen multiple times by different weights.

For each selected plan (red points), the distance in the graph in the OAR values to the plan with clinically used angles was calculated. Then for each set of weights the frequency with which a set of weights selects the plan more similar to the reference plan was counted. Figure 4.7 displays bar plots of these results.

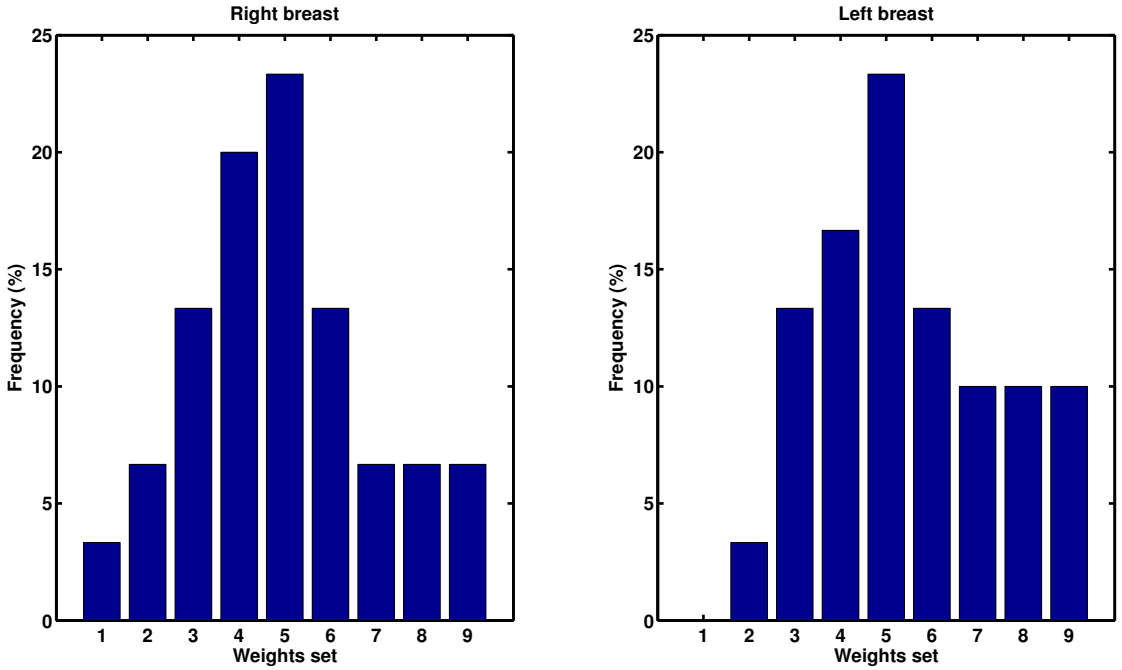

Figure 4.7: *Left and right side patients bar plots representing the number of times that one set of weights had permitted to obtain a best plan as close as possible to the IMRT plan generated with the angles chosen in clinic by the technician. The set number 1 for right-sided correspond to* $w_L = 0.1$ *and* $w_{CB} = 0.9$*, these values are changed with a step of 0.1 so that set 9 is* $w_L = 0.9$ *and* $w_{CB} = 0.1$*. For the left-sided the sets range from* $w_L = w_H = 0.05$ *and* $w_{CB} = 0.9$ *to* $w_L = w_H = 0.45$ *and* $w_{CB} = 0.1$ *with a step of 0.05 for* w_L *and* w_H*.*

For the left-sided patients (right panel in Fig. 4.7), the combination of weight set 5 produces a plan with characteristics similar to the clinical one, for most of the patients. This set consists in equal weighting for heart and lung of 0.25 and a value of 0.5 for contralateral breast.

In right-sided patients (left panel in Fig. 4.7), two sets of weights occur with higher frequency. For two on 15 patients these sets of weights select different plans. The set with contralateral breast weight (w_{CB}) at 0.6 and ipsilateral weights (w_L) at 0.4 gave, for both patients, a plan closer to the clinical angles plan. Therefore, this set was selected, instead of the one with equal weights. A detailed analysis showed that in case of mean dose in ipsilateral lung higher than 10 Gy and mean dose in contralateral breast lower than 1.5 Gy, the best set of weights gave higher priority to ipsilateral lung ($w_L = 0.7$ and $w_{CB} = 0.3$). In case of high dose of contralateral breast and relatively low dose in lung (lower than 10 Gy)

the set of weights with $w_L = 0.3$, $w_{CB} = 0.7$ turned out to be the more suitable. Therefore, three different sets of weights were defined for right-sided patients depending on the median value in contralateral breast and lung mean doses in the feasible plans (D_{CB}^{med} and D_L^{med}). The weights are thus chosen according to the scheme

- $\{D_{CB}^{med} < 1.5Gy\} \wedge \{D_L^{med} < 10Gy\} \quad \rightarrow \quad w_{CB} = 0.6, w_L = 0.4$
- $\{D_{CB}^{med} < 1.5Gy\} \wedge \{D_L^{med} > 10Gy\} \quad \rightarrow \quad w_{CB} = 0.3, w_L = 0.7$
- $\{D_{CB}^{med} > 1.5Gy \wedge D_L^{med} > 10Gy\} \vee \{D_{CB}^{med} > 1.5Gy \wedge D_L^{med} < 10Gy\}$
  $\rightarrow \quad w_{CB} = 0.7, w_L = 0.3$

Figure 4.8 shows the selected plans using these 3 sets of weights for two right-sided patients. With this choice of coefficients for the weighting sum, is possible, on average, to select the best plan with OAR sparing characteristics similar to those chosen for the clinical treatments.

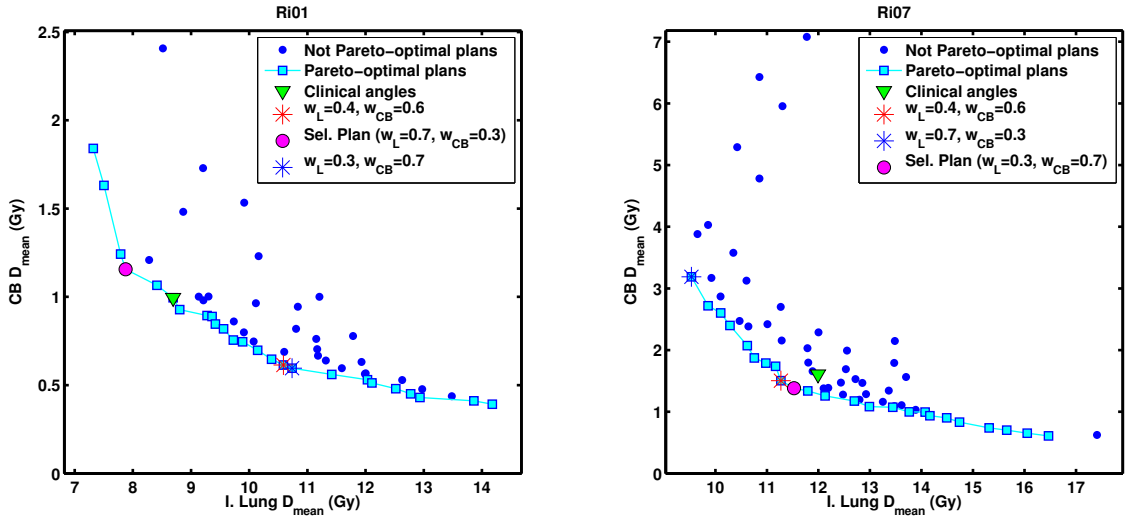

Figure 4.8: *Influence of weight selection for two right-sided patients with high dose in ipsilateral lung. For the patient on the left panel (Ri01)* $D_{CB}^{med} < 1.5$ *Gy while* $D_L^{med} > 10$ *Gy, so the set of weights* $w_{CB} = 0.3, w_L = 0.7$ *was selected. For the patient on the right panel (Ri07)* $D_{CB}^{med} > 1.5$ *Gy and* $D_L^{med} > 10$ *Gy resulting in the set of weights* $w_{CB} = 0.7, w_L = 0.3$. *In both cases the selected plans are closer to the clinical angles plan than the plans selected with the more frequent set of weight* ($w_{CB} = 0.6, w_L = 0.4$).

4.5 Results for one patient

121 IMRT plans were generated using all combinations of the 11 candidate directions on the medial and 11 on the lateral side of the patient; each plan had its intensity profiles automatically optimized with iCycle using the wish-list.

The feasible plans were selected on PTV quality; if the PTV coverage ($V_{95\%}$) and the near minimum value were below the thresholds, defined per patient, the plans were deleted and no more considered. This distinction between plans on PTV dose distribution is graphically represented in Figure 4.9, where the feasible plans (blue dots) are in the upper right region where PTV parameter values are higher. For this patient, the $V_{95\%}$ median value was lower than the 99% (dashed line). Therefore, the threshold for this parameter was set at the median value (98.8 %, represented with solid line); while the threshold for $D_{V_{tot}-2cc}$ in this case was 46.5 Gy.

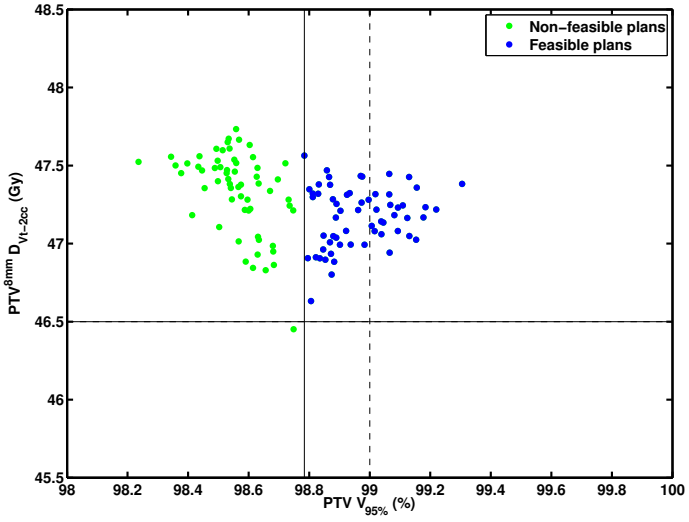

Figure 4.9: *Each of the 121 IMRT plans is represented as a dot according to PTV coverage ($V_{95\%}$) and significant minimum value ($D_{V_{tot}-2cc}$). In this patient the feasible plans (blue points) fulfill the request of 98.7% on PTV coverage and of a maximum under-dosage of 46.5 Gy (solid lines). The green points represent the deleted plans that will be no more considered in the plan selection.*

Figure 4.10 shows mean doses for the heart (left panel) and the left lung (right panel) as function of the contralateral breast mean dose for all feasible plans. The Pareto-optimal plans are selected using a weighting sum score having as objectives the OAR mean doses. It is clear that for this patient the plan generation with the clinically used beam angles (green triangle) is not at the Pareto surface (cyan points in the graph). Even though OAR mean

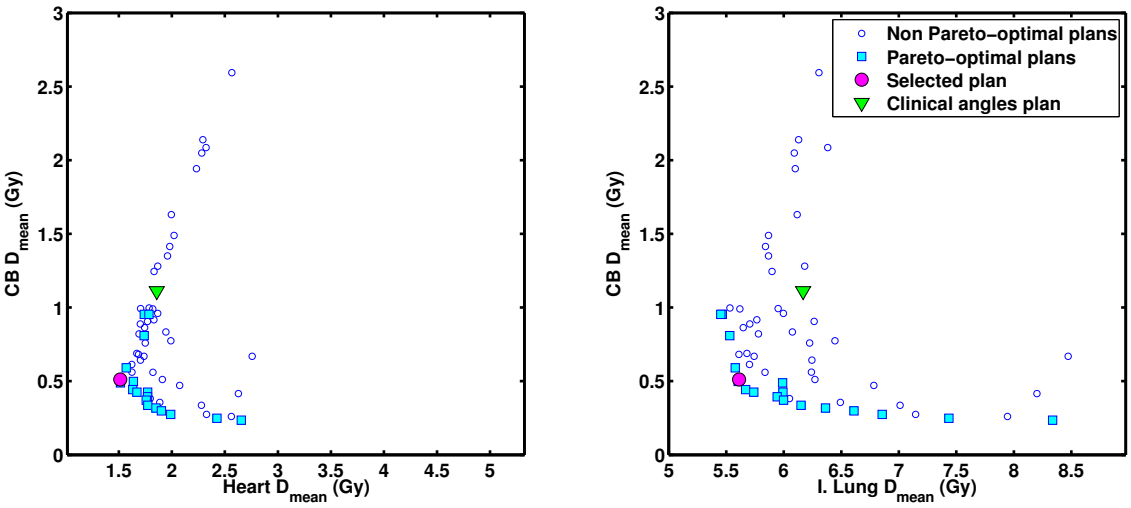

Figure 4.10: *The heart and ipsilateral lung mean doses of feasible plans are plotted versus the mean dose in contralateral breast (CB). Among these Pareto-optimal plans (cyan squares), the red point denotes the plan selected with the weighted sum. The plan generated with the clinical angles is represented by the green triangle.*

doses were already low, a different choice of angles would have resulted in a better sparing.

With the method proposed in this study, the selected plan is a Pareto-optimal plan that is lower both in ipsilateral lung, heart and contralateral breast mean dose by a considerable amount with respect to the clinical plan. Figure 4.11 shows the set of tangential beams in the clinical plan (dashed lines) and in the selected plan (solid violet lines). To achieve a better contralateral breast and lung sparing, the lateral beam was tilted by 8 degrees. The resulting dose distribution for PTV and organs at risk for both plans is also shown in the dose-volume histogram in Figure 4.12. For OARs, the DVH of the plan selected by the weighted summation is always lower than the clinical angles plan meaning that for this patient plan quality could be improved.

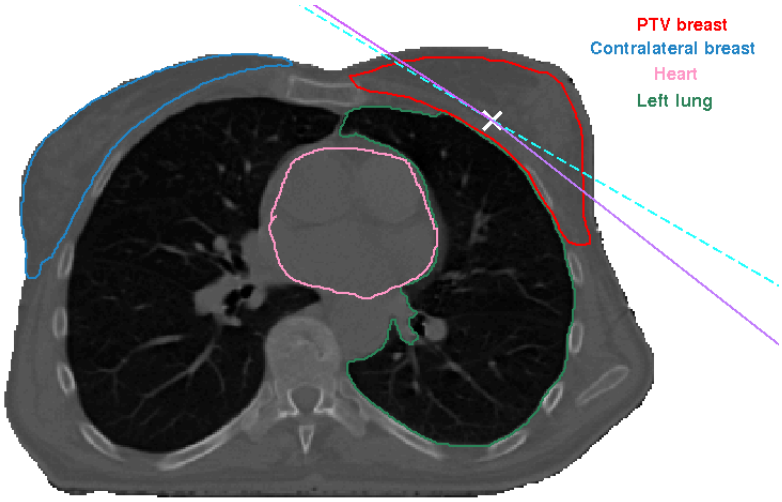

Figure 4.11: *CT slice, where the clinical isocenter is defined (white cross) of a left-sided patient. The beam selected from the technician, at 120 and 303 degrees, are graphically represented with dashed cyan lines. The beams of the Pareto-optimal plan selected with the weighted sum were at 128 and 301 degrees (violet lines).*

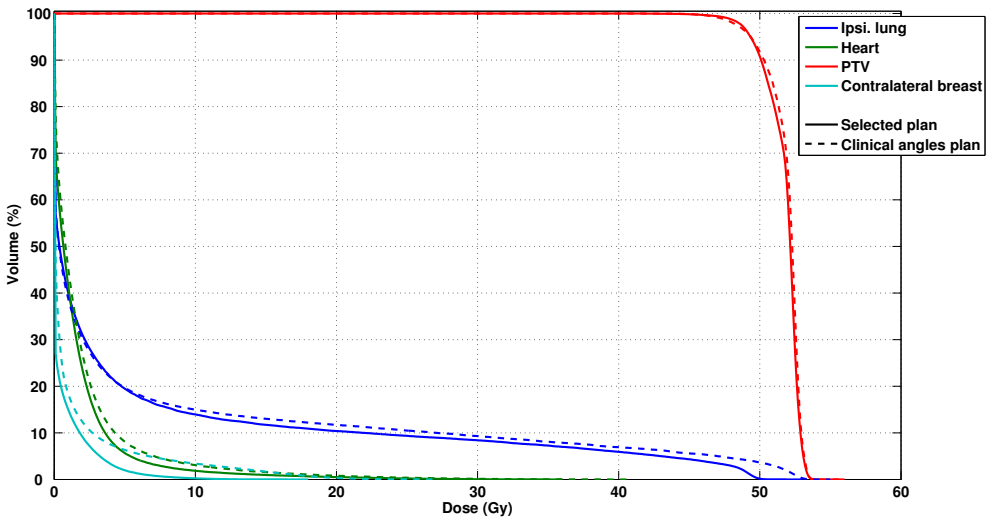

Figure 4.12: *Comparison of the dose volume histograms (DVHs) of two plans generated with different sets of tangential beams for a left side tumor. Dashed lines: IMRT plan with beam directions of the clinical plan (technician defined). Solid lines: the best plan selected among Pareto-optimal plans using a weighted sum score. While dose to the PTV is similar in both plans, dose to organs at risk can be reduced by selecting different sets of tangential beams.*

4.6 Best plan selection

The selection of the best plan among all the plans generated with the combinatorial approach was performed on 30 patients. Results are tabulated in Tables 4.1 and 4.2; plots of the feasible and Pareto-optimal plans with the selected plan for each patient are reported in Appendix B.

For 10 patients the thresholds used for the selection of feasible plans were set to less demanding values than 99% for $V_{95\%}$ and 46.5 for D_{V-2cc} allowing a larger number of remaining plans. For 8 of these patients the best plans selected were selected among the feasible plans with PTV $V_{95\%}$ and/or D_{V-2cc} smaller than 99% and 46.5 meaning that relaxing the requests on PTV coverage was possible to find a better plan for OAR sparing.

Figure 4.13 shows the values of PTV coverage, lung, heart and contralateral breast mean doses obtained for the selected plan versus the clinical beam plans, for all patients. As a result of the required PTV coverage for feasible plans, all selected plans have a PTV $V_{95\%}$ higher than the 98.5%. For left-sided patients, the heart mean dose in the selected plan is always equal or lower than in the clinical plan. For the majority of patients, the mean dose in ipsilateral lung in the selected plans is slightly better or equal to the clinical plan. For only a few patients the mean lung dose increases. The same conclusion can be drawn for the contralateral breast mean dose. Actually, as the mean dose to contralateral breast and lung are conflicting objectives and plans are selected from Pareto-optimal plans, dose to one OAR cannot be lowered without sacrificing the sparing of the other OAR, see also Tables 4.1 and 4.2.

Finally, the near-minimum dose inside the boost volume (retracted 8 mm from the skin) was evaluated on $D_{V_{boost}-0.1cc}$. For 9 of 14 patients, who had a delineated booster volume, the near-minimum dose was higher than 47.5 Gy (95% of D^p). For the other 5 patients the underdosage ranged from 47.4 to 44.7 Gy. Without addition of extra objectives in the wish-list, no guarantee can be given that the small underdosage, allowed at the selection of feasible plans, is not present in the booster volume.

The generation of the 121 plans requires a computational time ranging from 15 to 150 minutes depending on the volumes of the structures optimized and if one of two beam energies were used.

Table 4.1: *Comparison between the PTV coverage and mean dose values of the OARs obtained in the plan with clinical angles and the values obtained in the plan selected with the weighted summation (bold print), patient by patient for the left side breast tumor.*

Patient	PTV $V_{95\%}(\%)$	I. lung $D_{mean}\ (Gy)$	Heart $D_{mean}\ (Gy)$	C. breast $D_{mean}\ (Gy)$
Le01	98,78	12,49	7,86	0,54
	99,16	**12,00**	**7,42**	**0,48**
Le02	98,74	6,17	1,86	1,11
	99,15	**5,61**	**1,51**	**0,51**
Le03	99,09	12,46	4,81	0,58
	99,30	**11,87**	**3,84**	**0,61**
Le04	99,35	4,15	5,31	0,14
	99,37	**4,34**	**5,40**	**0,12**
Le05	99,17	8,36	1,54	0,51
	99,11	**7,45**	**1,36**	**0,56**
Le06	99,24	9,99	2,85	0,51
	99,24	**9,99**	**2,85**	**0,51**
Le07	99,02	9,94	3,46	0,64
	98,84	**10,11**	**3,28**	**0,57**
Le08	99,22	6,82	3,09	1,09
	99,24	**6,21**	**2,99**	**1,18**
Le09	99,33	9,42	4,31	0,56
	99,33	**9,42**	**4,31**	**0,56**
Le10	99,41	7,11	2,06	0,52
	99,20	**7,35**	**2,01**	**0,49**
Le11	99,21	9,31	5,22	0,36
	99,23	**8,58**	**4,67**	**0,40**
Le12	99,09	7,19	2,31	0,21
	99,13	**6,88**	**2,26**	**0,23**
Le13	99,20	6,47	6,14	0,44
	99,17	**7,07**	**6,01**	**0,28**
Le14	97,20	11,31	4,23	0,25
	98,77	**11,46**	**3,73**	**0,22**
Le15	99,49	11,95	2,92	0,41
	99,41	**10,14**	**2,13**	**0,59**

Table 4.2: *Comparison between the PTV coverage and mean dose values of the OARs obtained in the plan with clinical angles and the values obtained in the plan selected with the weighted summation (bold print), patient by patient for the right side breast tumor.*

Patient	PTV $V_{95\%}(\%)$	I. lung $D_{mean}\ (Gy)$	C. breast $D_{mean}\ (Gy)$
Ri01	99,63	5,10	0,28
	99,52	**5,10**	**0,25**
Ri02	98,98	7,44	0,20
	99,14	**7,36**	**0,17**
Ri03	99,02	7,08	0,43
	99,07	**7,06**	**0,33**
Ri04	99,28	11,99	1,61
	99,30	**11,52**	**1,38**
Ri05	98,08	4,72	0,164
	98,61	**4,71**	**0,12**
Ri06	99,41	4,57	0,69
	99,35	**4,64**	**0,56**
Ri07	99,13	6,56	0,39
	99,08	**6,18**	**0,27**
Ri08	99,43	10,22	0,45
	99,29	**10,19**	**0,45**
Ri09	99,33	6,06	0,22
	99,00	**5,99**	**0,17**
Ri10	99,21	9,09	1,79
	99,19	**8,91**	**1,46**
Ri11	99,44	8,69	0,99
	99,40	**7,88**	**1,16**
Ri22	99,60	5,48	0,26
	99,33	**5,05**	**0,32**
Ri13	98,97	7,70	1,00
	99,01	**7,36**	**1,04**
Ri14	99,24	11,25	1,6
	99,32	**11,29**	**1,19**
Ri15	99,16	6,04	0,05
	99,25	**6,05**	**0,04**

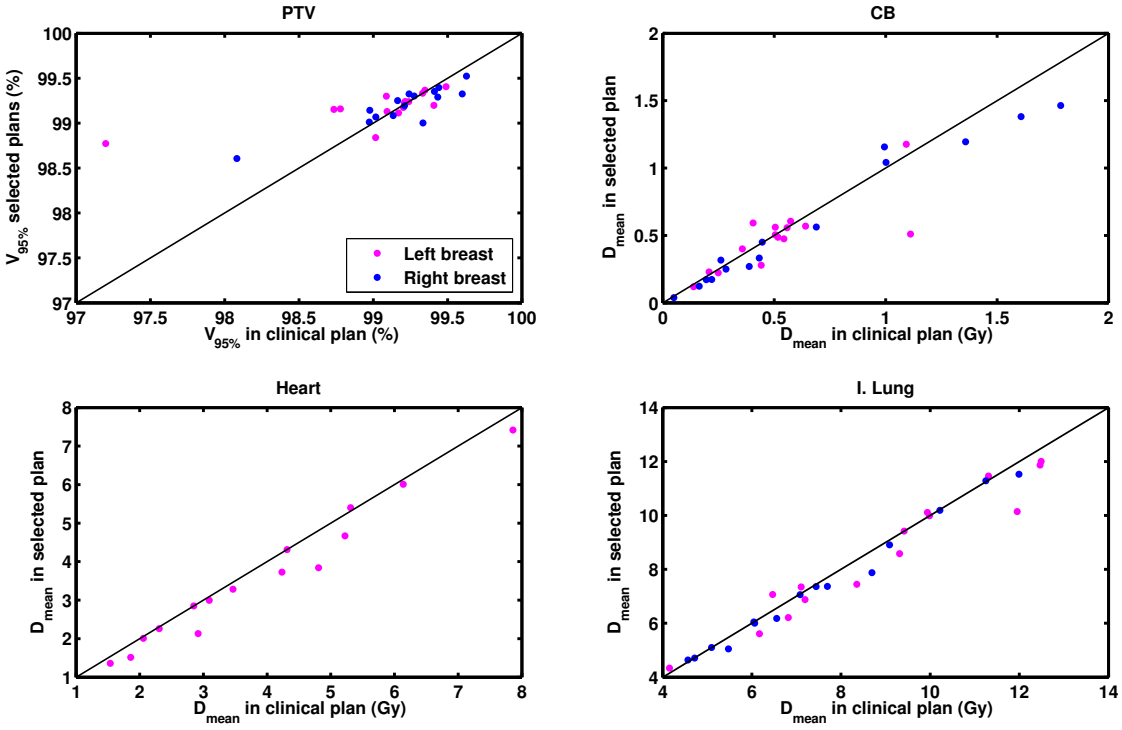

Figure 4.13: *Comparison of the values of PTV $V_{95\%}$ and mean doses in contralateral breast, ipsilateral lung and heart, obtained in plan with clinical angles and in the plan selected. The values for the left-sided patients are reported in magenta while the blue points are the right-sided patients.*

4.7 Isocenter position sensitivity

For 20 patients, 10 for each tumor side, the isocenter was moved along the z direction and within the PTV, so that 6 more isocenter positions were defined. The clinical isocenter distance from the ipsilateral lung is reported for all patients in Table 4.3. For each new beam isocenter 121 plans, with all angle combinations, were generated and analyzed. For every patient, the best plan, per isocenter position was selected with the weighted sum, where the normalization factor was calculated considering all the feasible plans generated with the 7 different isocenter positions. In this way the scores obtained from the best plan, per isocenter position, can be compared among each other.

Table 4.3: *Clinical isocenter position expressed as the distance from the ipsilateral lung in the axial side, for all patients.*

Patient	Isoc. position (mm)	Patient	Isoc. position (mm)
Le01	9	**Ri01**	3
Le02	9	**Ri02**	35
Le03	23	**Ri03**	27
Le04	5	**Ri04**	15
Le05	13	**Ri05**	13
Le06	22	**Ri06**	13
Le07	11	**Ri07**	14
Le08	8	**Ri08**	32
Le09	20	**Ri09**	20
Le10	17	**Ri10**	3

Figure 4.14 shows the Pareto-optimal plans obtained for the 7 different isocenters position for one left-sided patient. Results for the other patients are reported in Appendix C1 and C2. For some patients a large difference in Pareto frontier shape was noted while for other patients the isocenter position does not significantly change plan quality. For all patients only small differences were found between the Pareto-optimal plans obtained after movement of the isocenter in caudal and cranial direction (see left panel in Fig. 4.14).

In Figure 4.15 the best plans scores as function of the isocenter position are represented for all patients, divided in left and right tumors. No isocenter position shows better scores with respect to the others for all patients; the clinical isocenter for most of the patients does

not score the lowest value, meaning that another isocenter could improve the best plan.

The contralateral breast, ipsilateral lung and heart mean doses obtained for the best plan for each isocenter position were investigated. For each of these parameters the differences with the values obtained in the best plan with clinical isocenter were graphically represented (see Appendix C.3). It was not possible to find a general behaviour connecting the plan quality to the position of the isocenter, although for 5 patients an improvement in the sparing of all OARs was possible by moving the isocenter from the clinical position to another position (see Table 4.4). We conclude from this data that it might be beneficial for plan generation to include isocenter position in the optimization as well.

Table 4.4: *Difference in mean dose in OARs (%) between the parameter values in the best plan with the clinical isocenter and the isocenter x cm from the lung in the axial slice. Only plans are shown with an improvement in OAR sparing.*

Patient	Clin. Iso. position (mm)	Isoc. position (mm)	I. lung (%)	C. breast (%)	Heart (%)
Le01	9	5	4	2	5
Le02	8	10	1	2	2
Le06	22	10	6	4	13
Ri01	3	20	6	24	-
		30	7	24	-
Ri03	27	5	2	4	-

To support this finding with statistical data, Wilcoxon signed rank test was used to compare the best plan scores for different isocenter positions. It is a paired difference test comparing the results two by two. A mean difference was considered significant if p-values were smaller than 0.05. The test was performed grouping the patients in 3 ways, only left or right sided patients, or all 30 patients together. No evident correlation between the plan quality and the isocenter position was found in these groups of patients, all p-values were larger than 0.1 (see Tables in Appendix C.3).

In order to have a fully automated treatment generation an initial isocenter has to be given in input as starting point for optimization of isocenter position. This can be done using the CT-scans of the patient and processing the images. Referring to the clinical guidelines, the position on the cranial-caudal direction has to be set at the height of the nipple while in the axial slide usually the isocenter has to be positioned at 2 cm form the ipsilateral lung.

This strategy could be implemented in further studies.

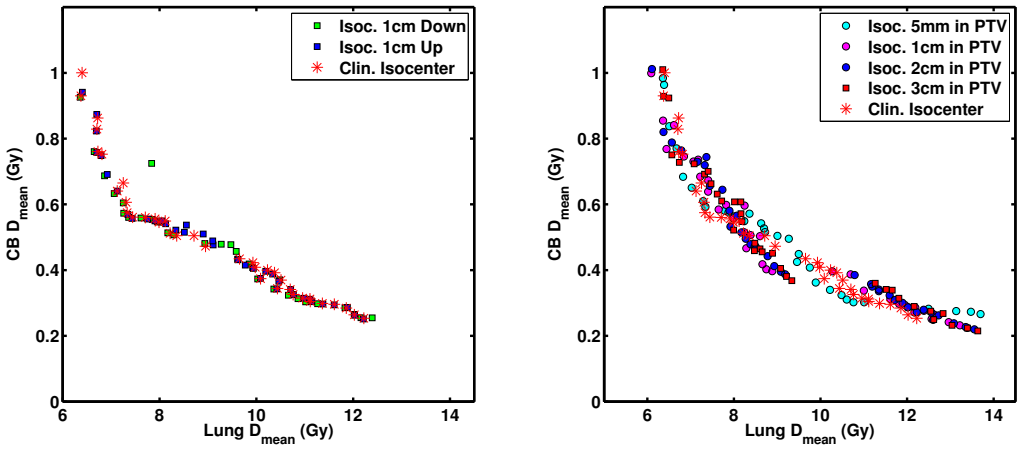

Figure 4.14: *Left breast patient 05 (Le05) for which the clinical isocenter was positioned at 13 mm from ipsilateral lung. Pareto-optimal plans generated with the clinical isocenter (red stars) and other 6 isocenter positions are shown. In the left panel movement of the isocenter in the cranial-caudal direction are considered while in the right panel the isocenter was moved in the axial slice at 4 distances from the ipsilateral lung.*

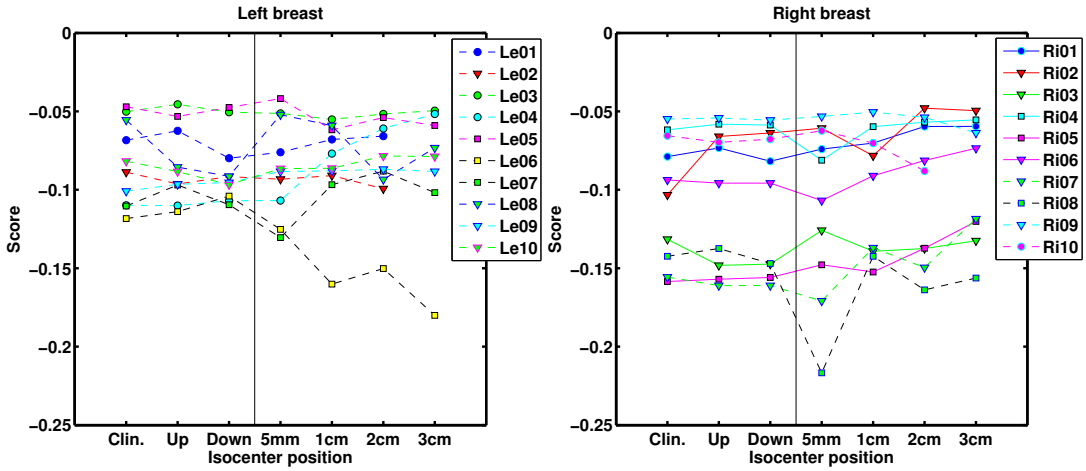

Figure 4.15: *Scores obtained for the best plan for each isocenter position in 10 patients with tumor in left breast and 10 in the right breast. For 3 patients the lack of data for position of the isocenter at 3 cm from the lung was due to small breast size.*

Chapter 5

Conclusions and future research

In this study, an in-house developed beam profile optimizer (iCycle), was used in combination with a combinatorial approach for beam angle selection to generate plans for irradiation of the whole breast with two tangential beams.

A wish-list, describing the desired dose distribution, was produced to steer the iCycle intensity profile optimization algorithm. The multi-objective problem of selecting optimal beam angles was solved by the generation of multiple plans, with different combinations of beam directions belonging to 2 opposite partial arcs. A first selection concerning the PTV coverage and estimation of possible underdosage in the target volume gives feasible plans. Among these solutions Pareto-optimal plans were considered using a weighted sum score function, for OAR sparing. With an appropriate selection of the sum weights it was possible to choose the Pareto-optimal plans with the trade-off between the conflicting dose minimization OARs, as applied in clinical practice.

This method was tested on 30 patients in case of tumors occurring in left or right breast. The beam angles chosen for the clinical treatment did not always lead to Pareto-optimal plans due to the manual selection process (although for many patients it was nearly Pareto-optimal). The beam directions selected with this method always resulted in a Pareto-optimal solution, while for the clinical angles there may be deviations from Pareto-optimality.

The analysis of plan generation with different isocenters from the clinical chosen isocenter showed sensitivity of plan quality to this parameter for some patients; however, no evident correlation between isocenter position and OAR sparing emerged from this analysis. Therefore optimization of isocenter position might be beneficial in terms of plan quality and organs at risk sparing for a (sub) group of patients. A further investigation may aim at finding a connection between patient anatomic characteristics (i.e. chest wall curvature, heart distance to the PTV, breast dimensions) and optimal isocenter position.

In the graphs displaying the results of the feasible plans for contralateral breast and ipsilateral lung mean dose for individual patients, artifacts generated from the wish-list levels can be noted. Especially in some of the patients with a mean dose in ipsilateral lung higher than 10 Gy is possible to detect a stepwise shape of the Pareto-frontier in correspondence of 12 Gy (see patient Le01, in Appendix B). The introduction of an additional level to the actual wish-list may improve the plans by lowering the dose in more steps.

For this study, the candidate beams considered for the combinatorial plan generation were pre-defined by using a fixed arc around the clinically used beam angles. For complete automation of plan generation also the candidate beams have to be defined automatically. Image processing of the patient CT scan provides useful information on breast dimensions and shape together with chest wall curvature. The lead wire marking the breast can be used to define patient specific partial arcs for the plan generation using the combinatorial approach.

Future implementations of the method presented in this study may support physicians and technicians in the generation of treatment plans, finding the most preferred Pareto-optimal solution according to their preferences.

Bibliography

[1] World cancer report. Technical report, International Agency for Research on Cancer, 2008.

[2] M. Krapcho N. Neyman R. Aminou S.F. Altekruse C.L. Kosary J. Ruhl Z. Tatalovich H. Cho A. Mariotto M.P. Eisner D.R. Lewis H.S. Chen E.J. Feuer N. Howlader, A.M. Noone and K.A. Cronin (eds). Seer cancer statistics review, 1975-2009 (vintage 2009 populations). 2012.

[3] *Radiation Oncology Physics: A Handbook for Teachers and Students*. E. B. Podgorsak Technical Editor, 2003.

[4] F. M. Khan. *The physics of radiation therapy*. Lippincott Williams and Wilkins, 2003.

[5] Prescribing, recording, and reporting photon beam therapy. Technical Report 50, International commission on radiation units and measurements (ICRU).

[6] Sarah C. Darby, Marianne Ewertz, Paul McGale, Anna M. Bennet, Ulla Blom-Goldman, Dorthe Brønnum, Candace Correa, David Cutter, Giovanna Gagliardi, Bruna Gigante, Maj-Britt Jensen, Andrew Nisbet, Richard Peto, Kazem Rahimi, Carolyn Taylor, and Per Hall. Risk of ischemic heart disease in women after radiotherapy for breast cancer. *New England Journal of Medicine*, 368(11):987–998, 2013. PMID: 23484825.

[7] Tiziana Rancati, Berit Wennberg, Pehr Lind, Gunilla Svane, and Giovanna Gagliardi. Early clinical and radiological pulmonary complications following breast cancer radiation therapy: {NTCP} fit with four different models. *Radiotherapy and Oncology*, 82(3):308 – 316, 2007.

[8] John D. Boice, Elizabeth B. Harvey, Maria Blettner, Marilyn Stovall, and John T. Flannery. Cancer in the contralateral breast after radiotherapy for breast cancer. *New England Journal of Medicine*, 326(12):781–785, 1992. PMID: 1538720.

[9] Safora Johansen, Luca Cozzi, and Dag Rune Olsen. A planning comparison of dose patterns in organs at risk and predicted risk for radiation induced malignancy in the

contralateral breast following radiation therapy of primary breast using conventional, imrt and volumetric modulated arc treatment techniques. *Acta Oncologica*, 48(4):495–503, 2009. PMID: 19169915.

[10] Rainer K. Sachs and David J. Brenner. Solid tumor risks after high doses of ionizing radiation. *Proceedings of the National Academy of Sciences of the United States of America*, 102(37):13040–13045, 2005.

[11] Safora Johansen, Turi Danielsen, and Dag Rune Olsen. Estimated risk for secondary cancer in the contra-lateral breast following radiation therapy of breast cancer. *Acta Oncologica*, 47(3):391–396, 2008. PMID: 18348001.

[12] M. Keijzer A. W. Heemink Sebastiaan Breedveld, Pascal R. M. Storchi and Ben J. M. Heijmen. A novel approach to multi-criteria inverse planning for imrt. *Phys. Med. Biol.*, 2007.

[13] Peter W. J. Voet Sebastiaan Breedveld, Pascal R. M. Storchi and Ben J. M. Heijmen. icycle: Integrated, multicriterial beam angle, and profile optimization for generation of coplanar and noncoplanar imrt plans. *Medical Physics*, 39(2):951–963, 2012.

[14] Lasdon L. S. Haimes Y. Y. and Wismer D. A. On a bicriterion formulation of the problems of integrated system identification and system optimization. *IEEE Trans. Man Cybern*, 1971.

[15] Reemtsen R. Alber M. Intensity modulated radiotherapy treatment planning by use of a barrier-penalty multiplier method. *Optim. Method Softw.*, 2007.

[16] Gass S. I. and Saaty Thomas L. Parametric objective function (part 2) - generalization. *Journal of the Operations Research Society of America*, 3(4):395–401, 1955.

Appendix A

Evaluation of PTV parameters

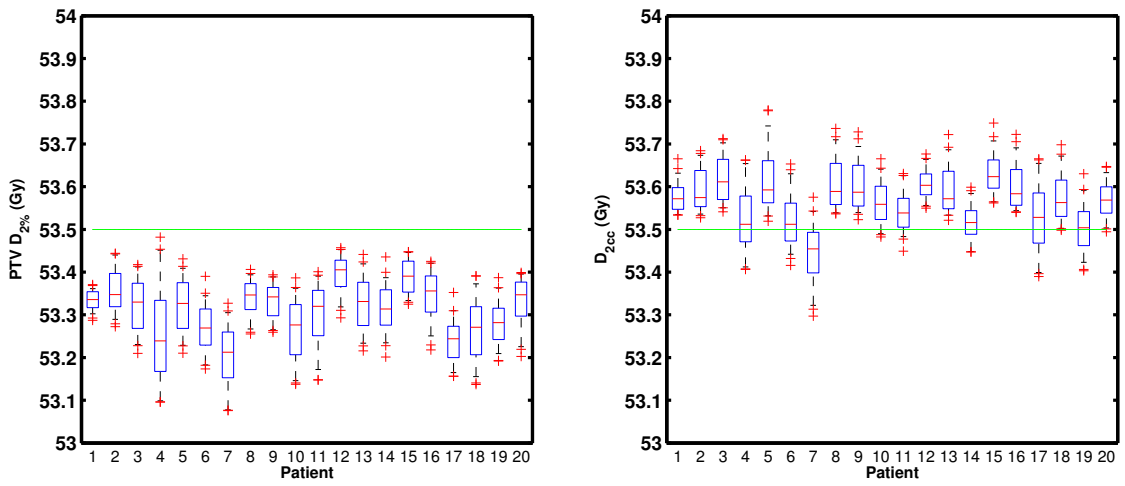

Figure A.1: *Box and whisker plots of near-maximum PTV doses, for 20 patients, $D_{2\%}$ (left) and D_{2cc} (right). On each box, the central mark is the median value, the edges of the boxes are the the 25th and 75th percentiles, the whiskers extend to the 2nd and 98th percentiles; outliers are plotted individually. The green line at 53.5 Gy (107% of D^p) represents the constraint imposed on the maximum dose in the PTV in the wish-list.*

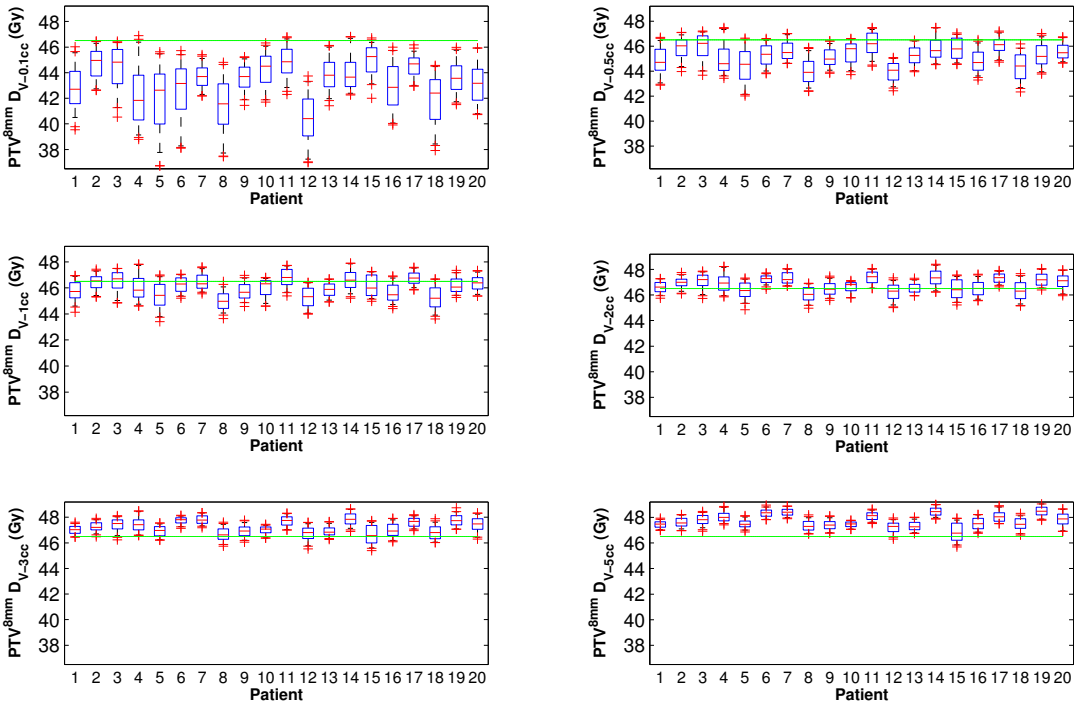

Figure A.2: *Box and whisker plots of the parameters* $D_{V_{tot}-0.1cc}$, $D_{V_{tot}-0.5cc}$, $D_{V_{tot}-1cc}$, $D_{V_{tot}-2cc}$, $D_{V_{tot}-3cc}$ *and* $D_{V_{tot}-5cc}$ *of* PTV^{8mm} *for 20 patients. Patients 1 to 10 had left breast tumor while patients 11 to 20 in right breast. On each box, the central mark is the median value, the edges of the box are the the 25th and 75th percentiles, the whiskers extend to the 2nd and 98th percentiles; outliers are plotted individually. The green line represents the threshold at 46.5 Gy.*

Appendix B

Results per patient: selection of feasible plans and Pareto-optimal plans

B.1 Left-sided patients

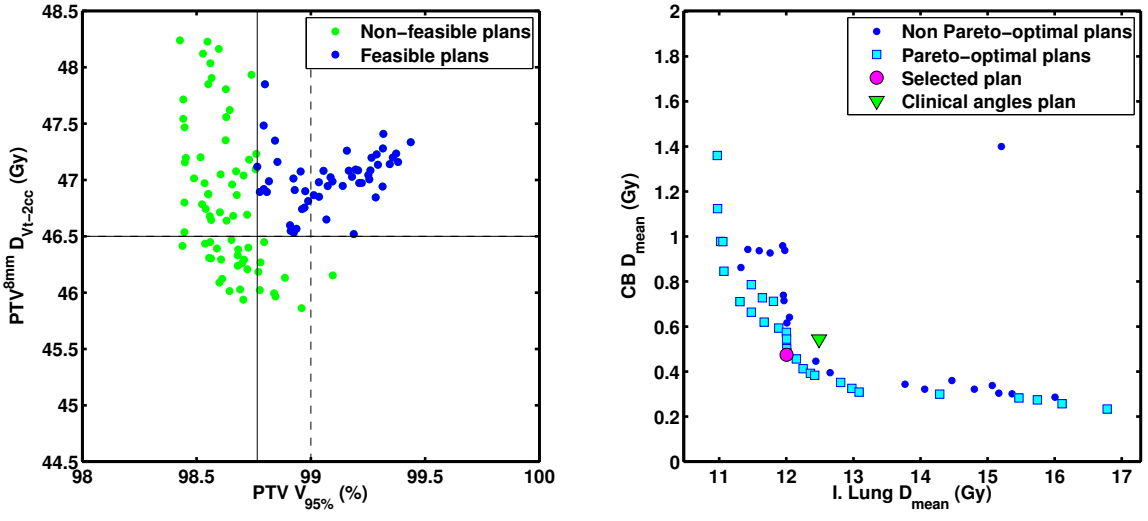

Figure B.1: *Patient left breast 01 (Le01): feasible plans and Pareto-optimal plans.*

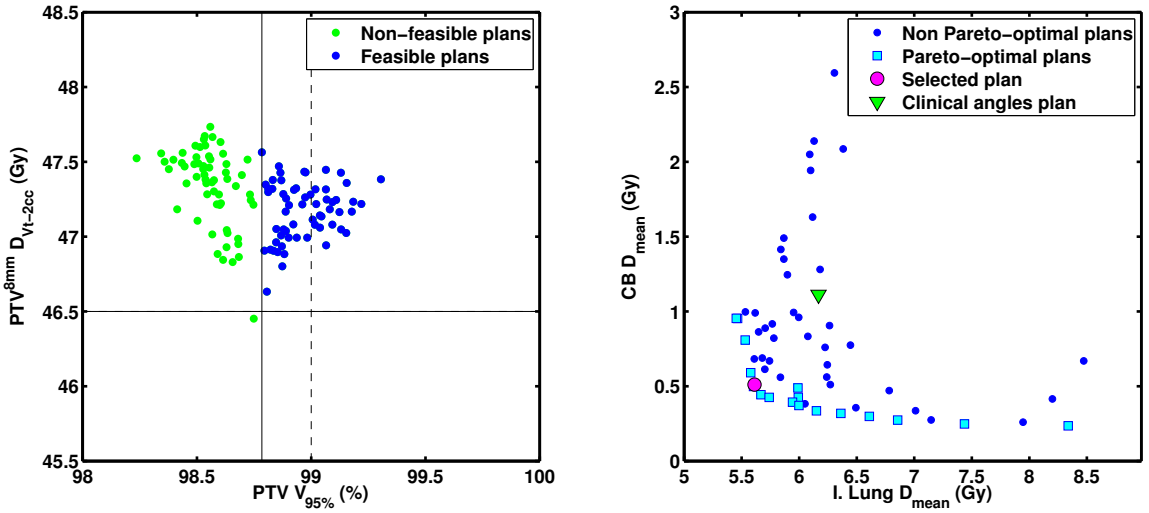

Figure B.2: *Patient left breast 02 (Le02): feasible plans and Pareto-optimal plans.*

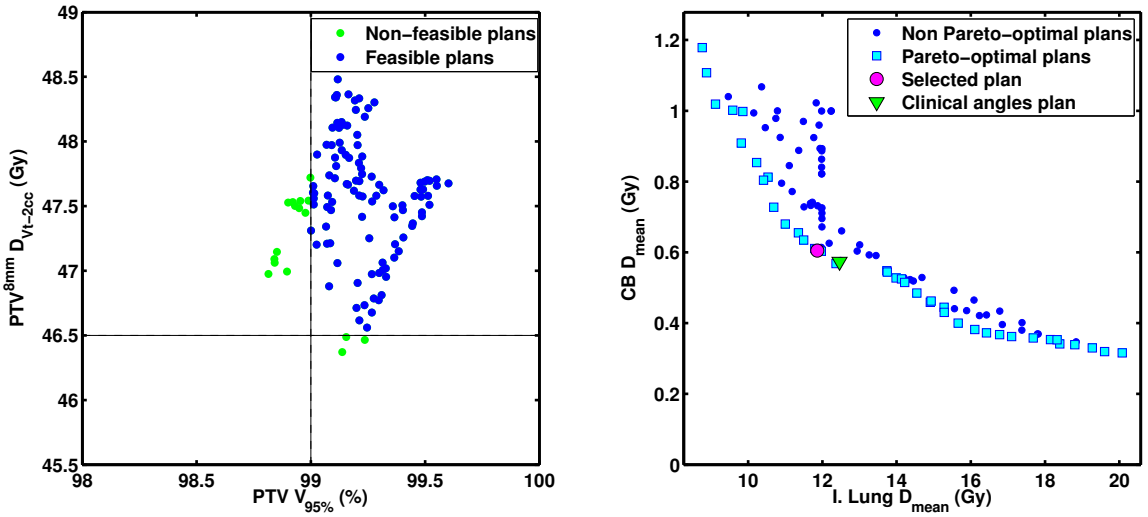

Figure B.3: *Patient left breast 03 (Le03): feasible plans and Pareto-optimal plans.*

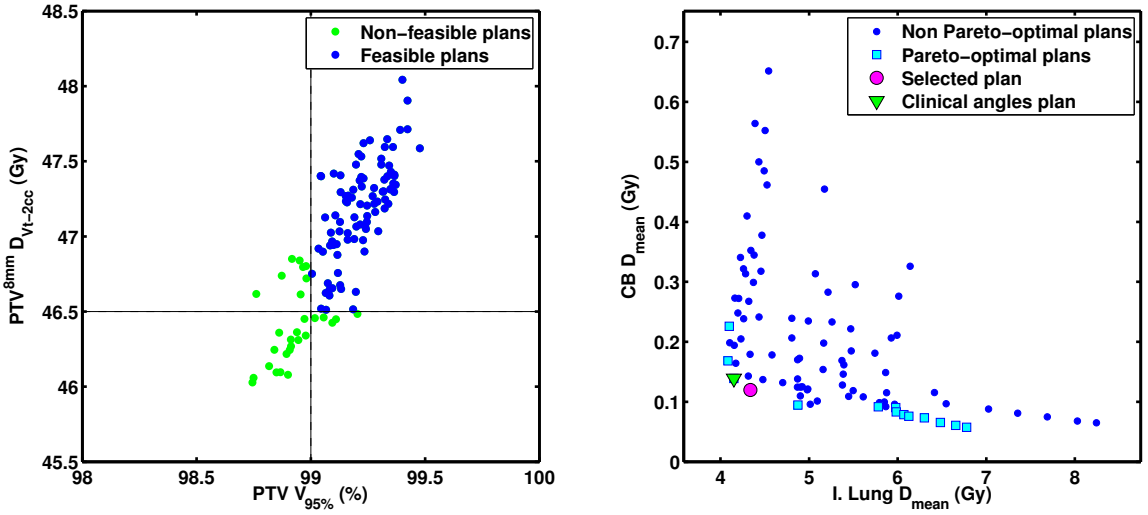

Figure B.4: *Patient left breast 04 (Le04): feasible plans and Pareto-optimal plans.*

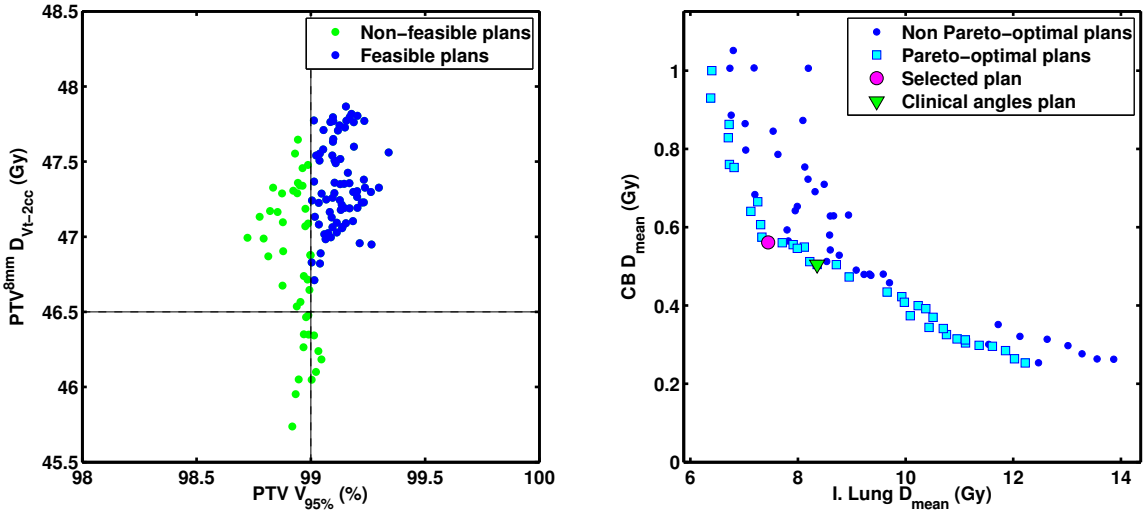

Figure B.5: *Patient left breast 05 (Le05): feasible plans and Pareto-optimal plans.*

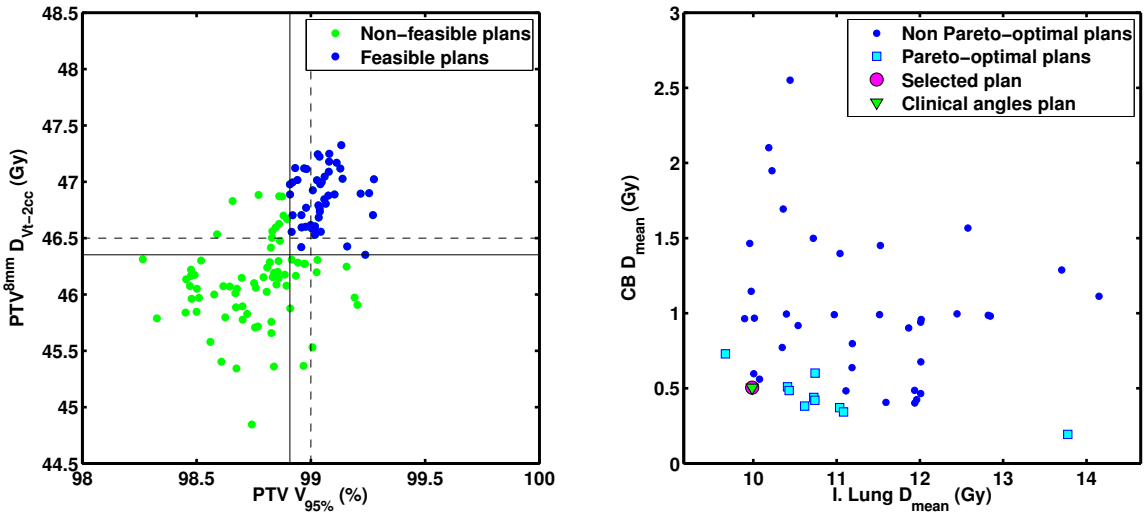

Figure B.6: *Patient left breast 06 (Le06): feasible plans and Pareto-optimal plans.*

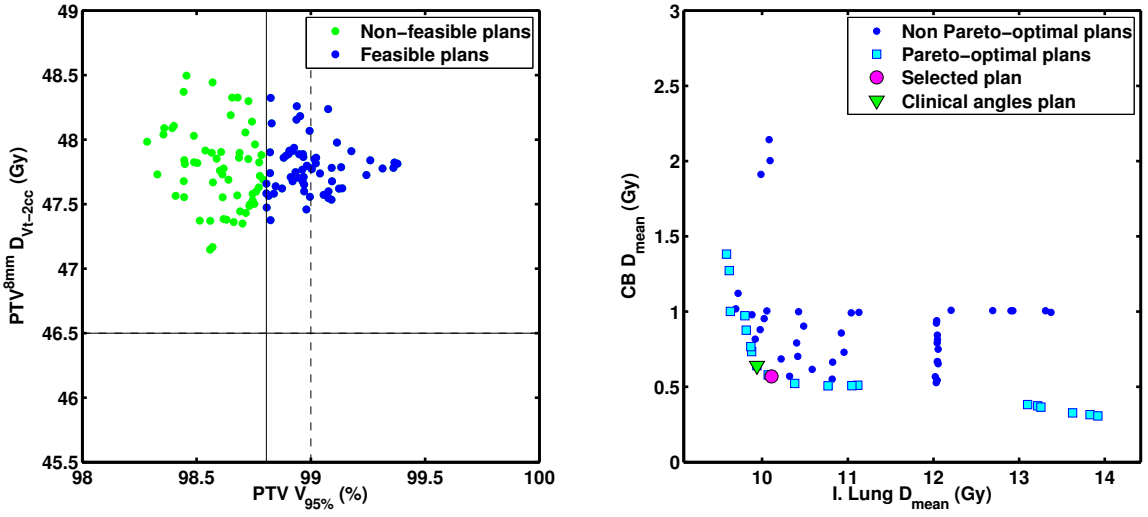

Figure B.7: *Patient left breast 07 (Le07): feasible plans and Pareto-optimal plans.*

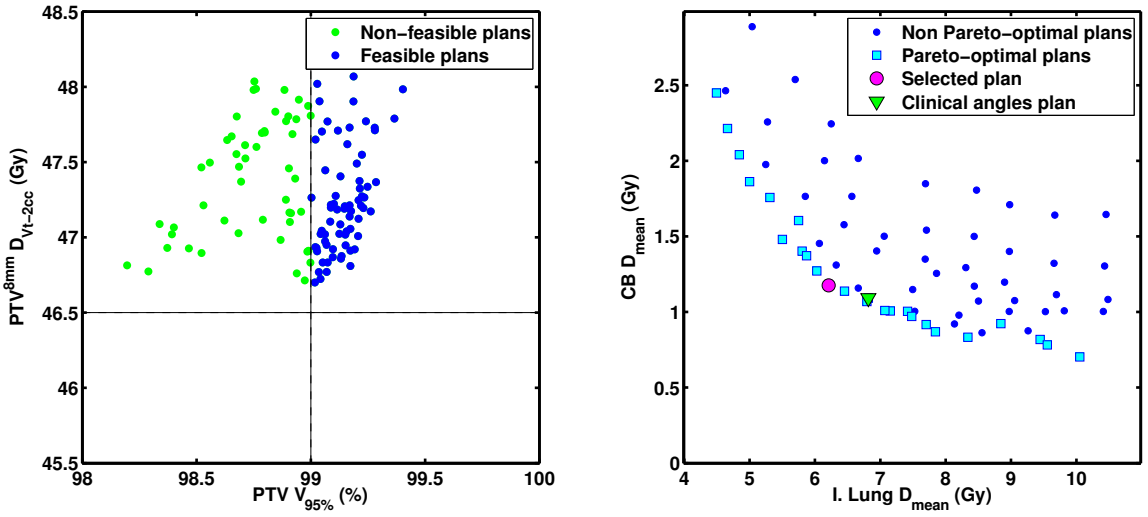

Figure B.8: *Patient left breast 08 (Le08): feasible plans and Pareto-optimal plans.*

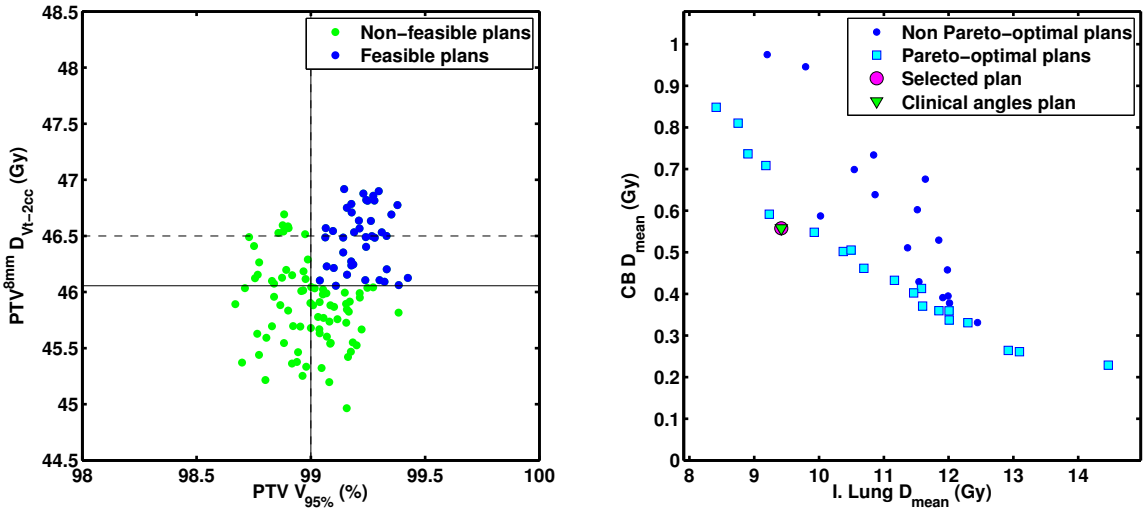

Figure B.9: *Patient left breast 09 (Le09): feasible plans and Pareto-optimal plans.*

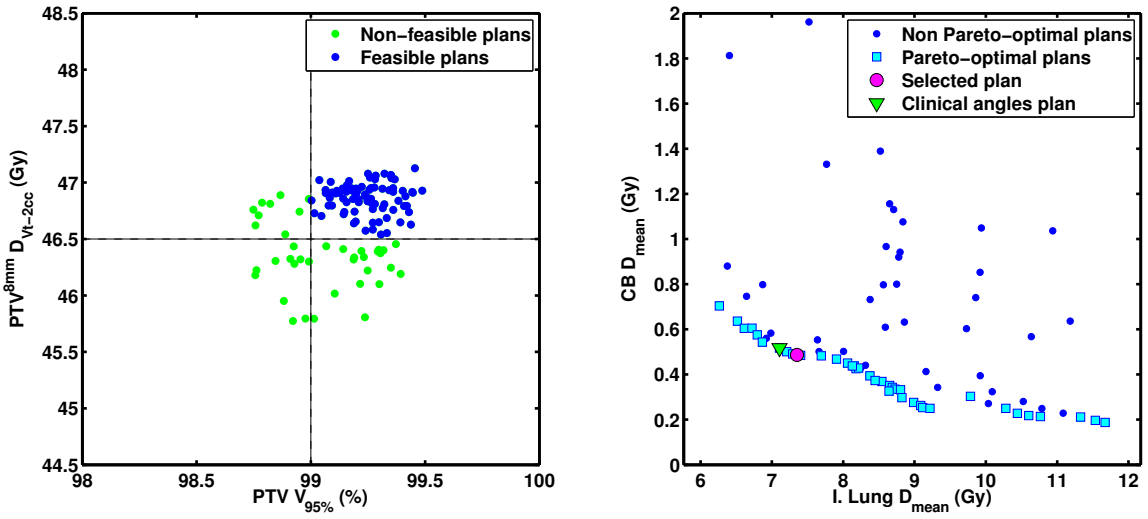

Figure B.10: *Patient left breast 10 (Le10): feasible plans and Pareto-optimal plans.*

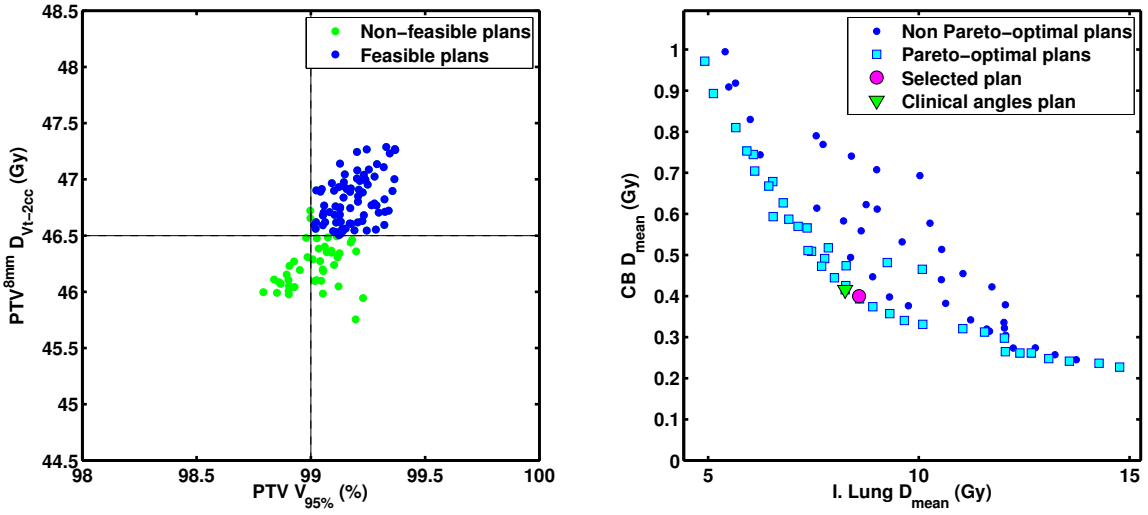

Figure B.11: *Patient left breast 11 (Le11): feasible plans and Pareto-optimal plans.*

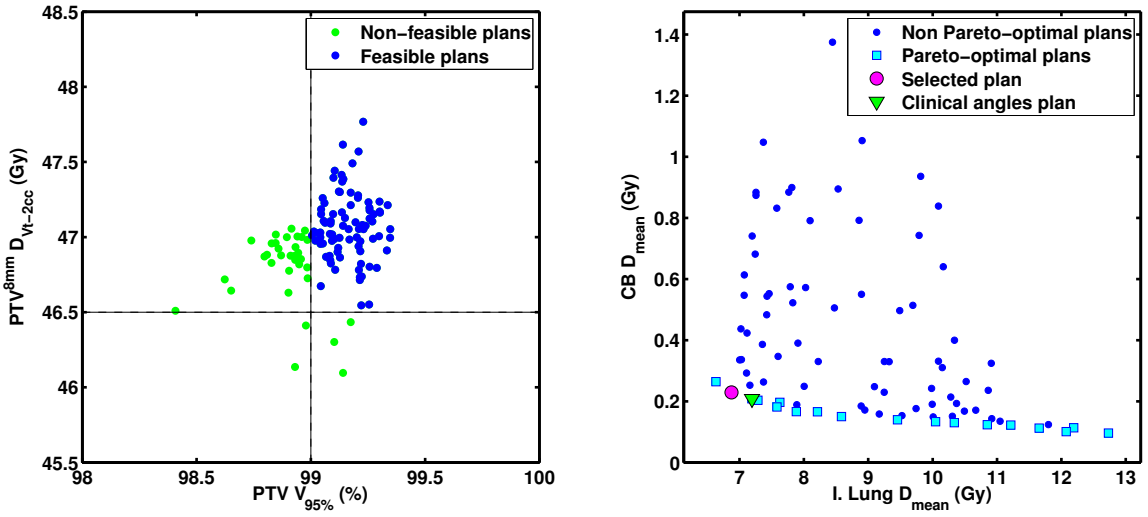

Figure B.12: *Patient left breast 12 (Le12): feasible plans and Pareto-optimal plans.*

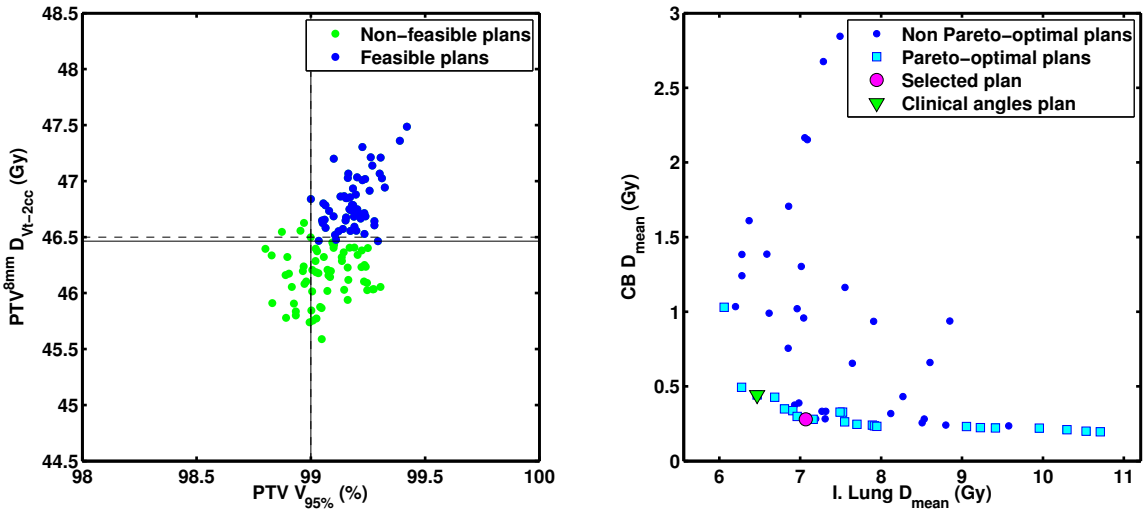

Figure B.13: *Patient left breast 13 (Le13): feasible plans and Pareto-optimal plans.*

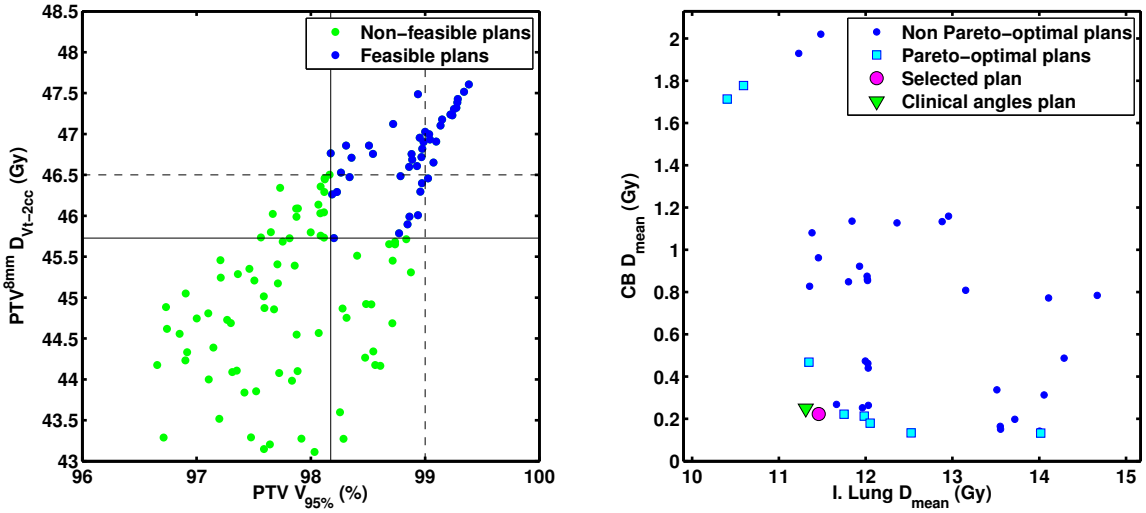

Figure B.14: *Patient left breast 14 (Le14): feasible plans and Pareto-optimal plans.*

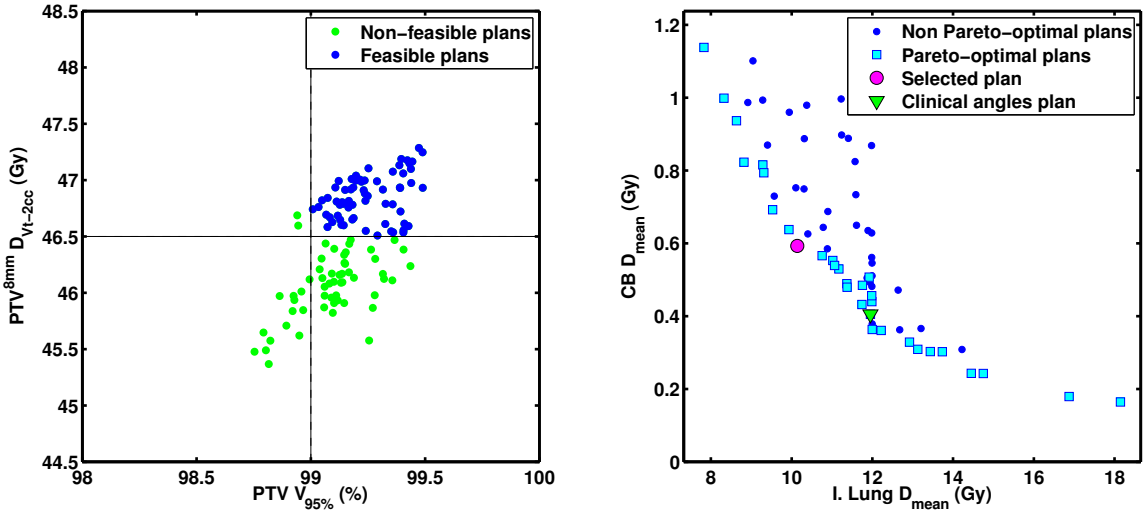

Figure B.15: *Patient left breast 15 (Le15): feasible plans and Pareto-optimal plans.*

B.2 Right-sided patients

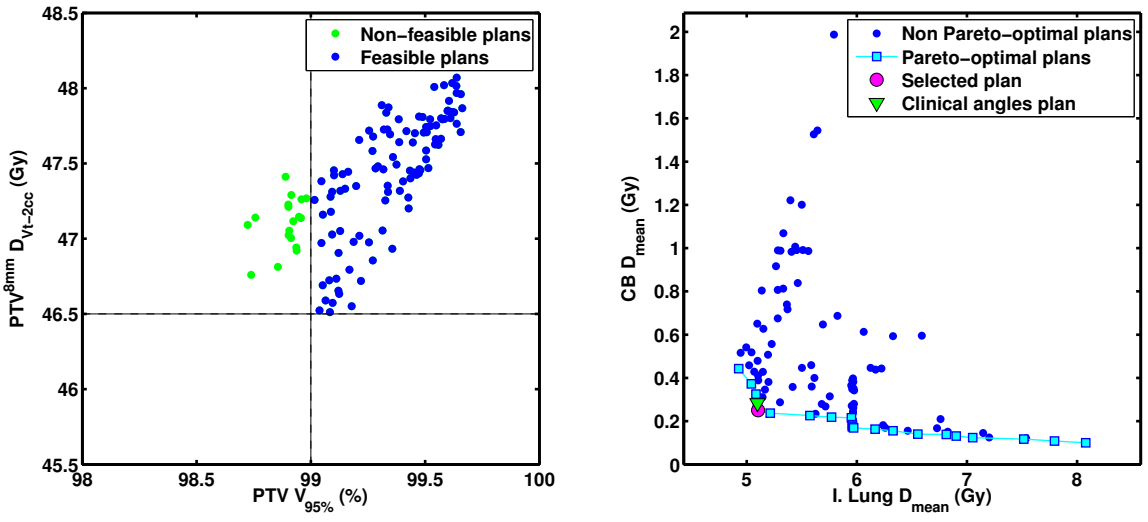

Figure B.16: *Patient right breast 01 (Ri01): feasible plans and Pareto front.*

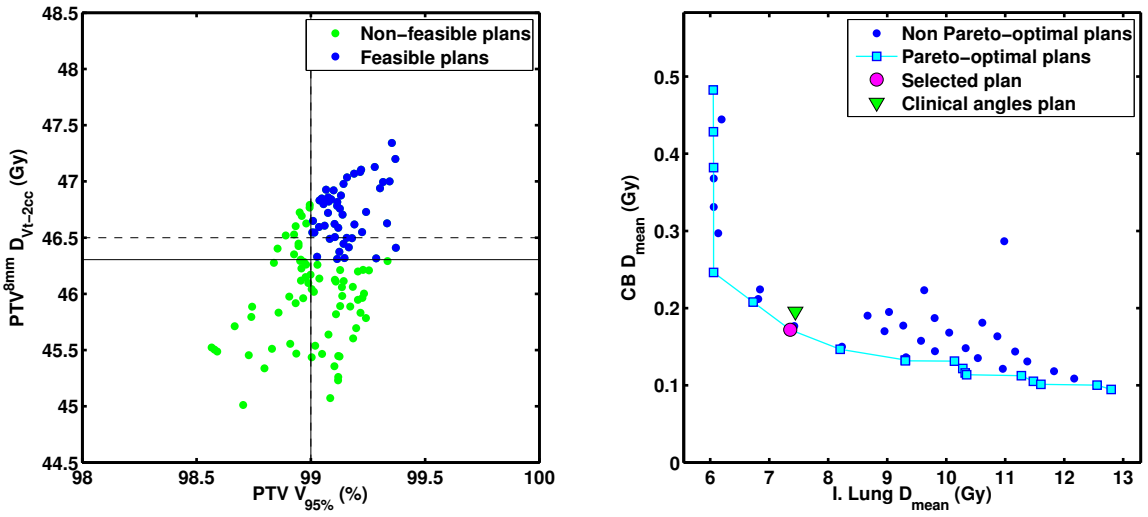

Figure B.17: *Patient right breast 02 (Ri02): feasible plans and Pareto front.*

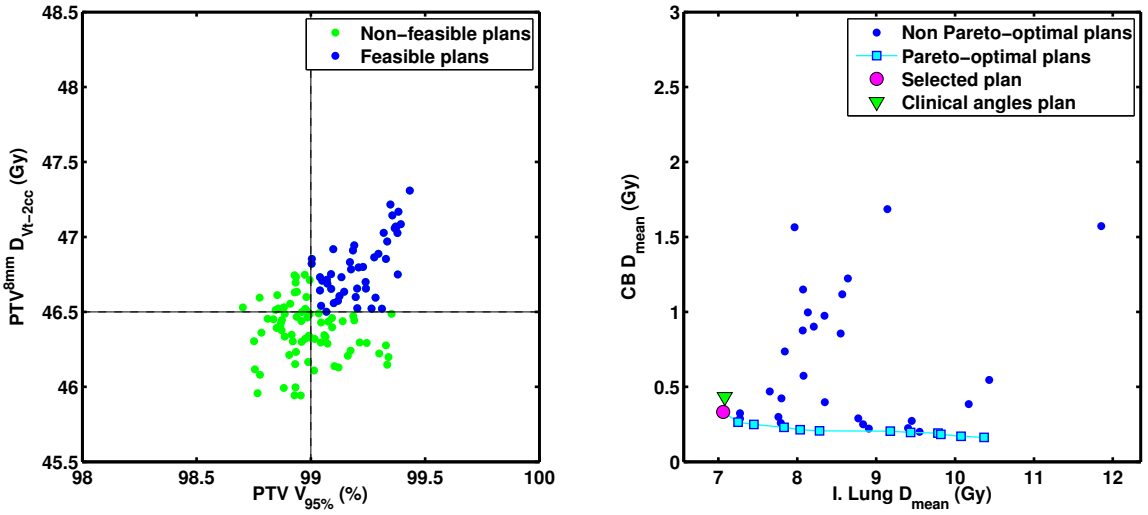

Figure B.18: *Patient right breast 03 (Ri03): feasible plans and Pareto front.*

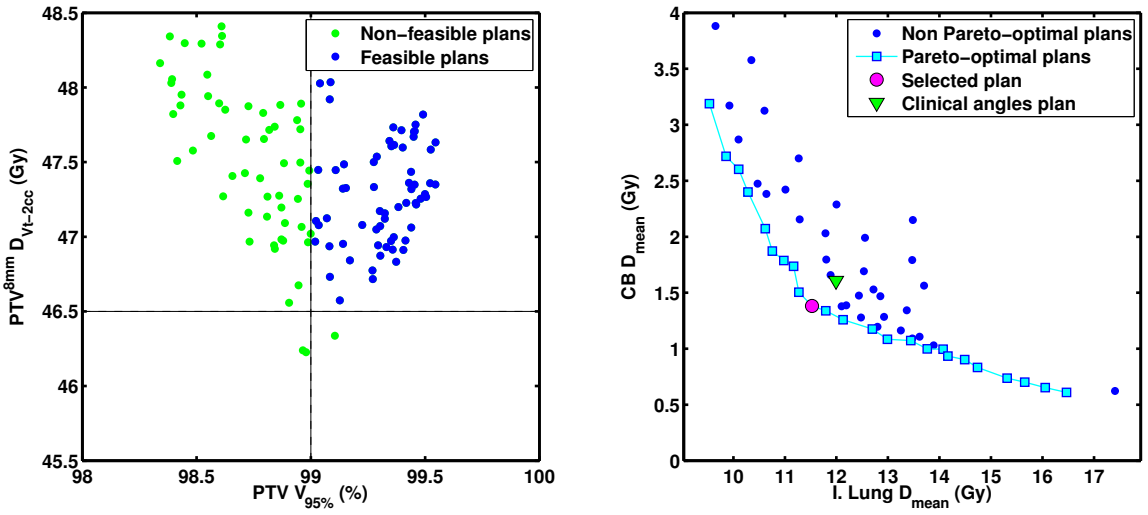

Figure B.19: *Patient right breast 04 (Ri04): feasible plans and Pareto front.*

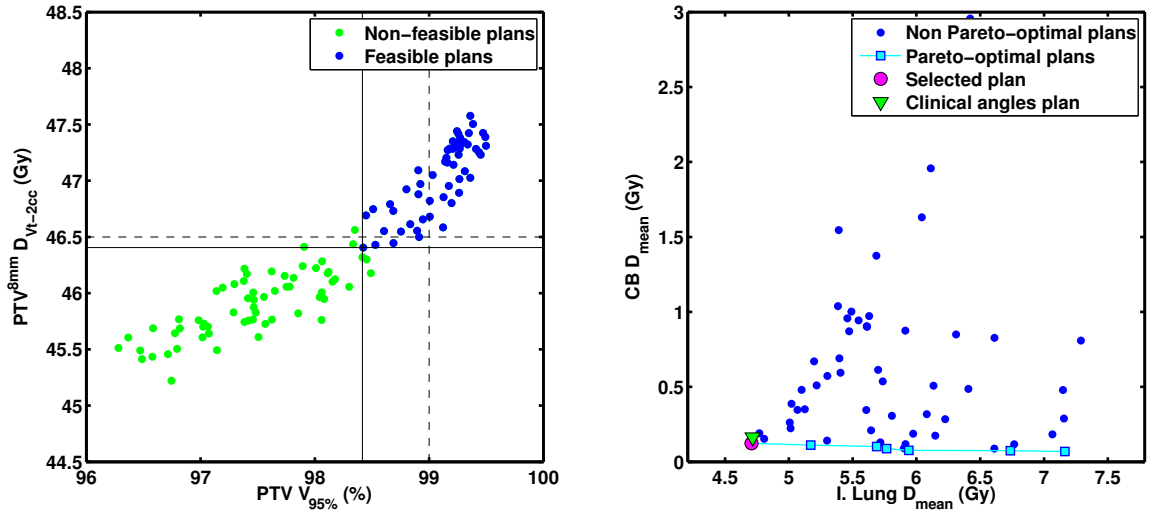

Figure B.20: *Patient right breast 05 (Ri05): feasible plans and Pareto front.*

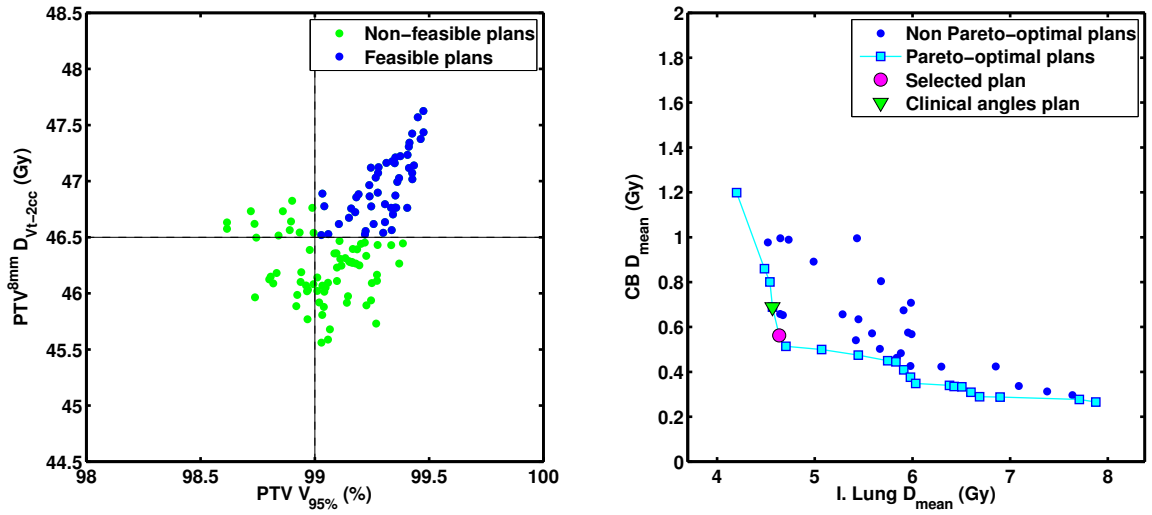

Figure B.21: *Patient right breast 06 (Ri06): feasible plans and Pareto front.*

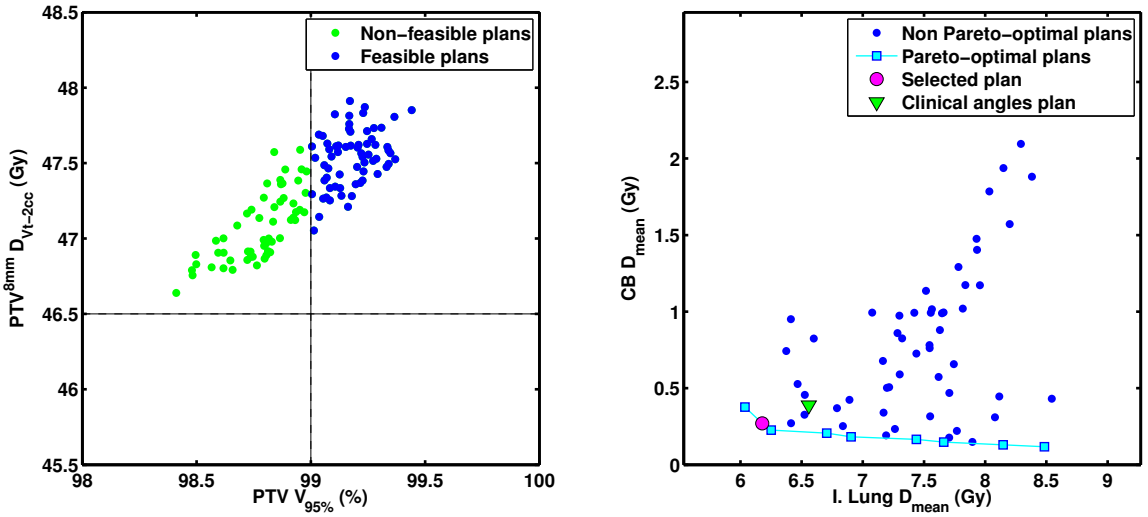

Figure B.22: *Patient right breast 07 (Ri07): feasible plans and Pareto front.*

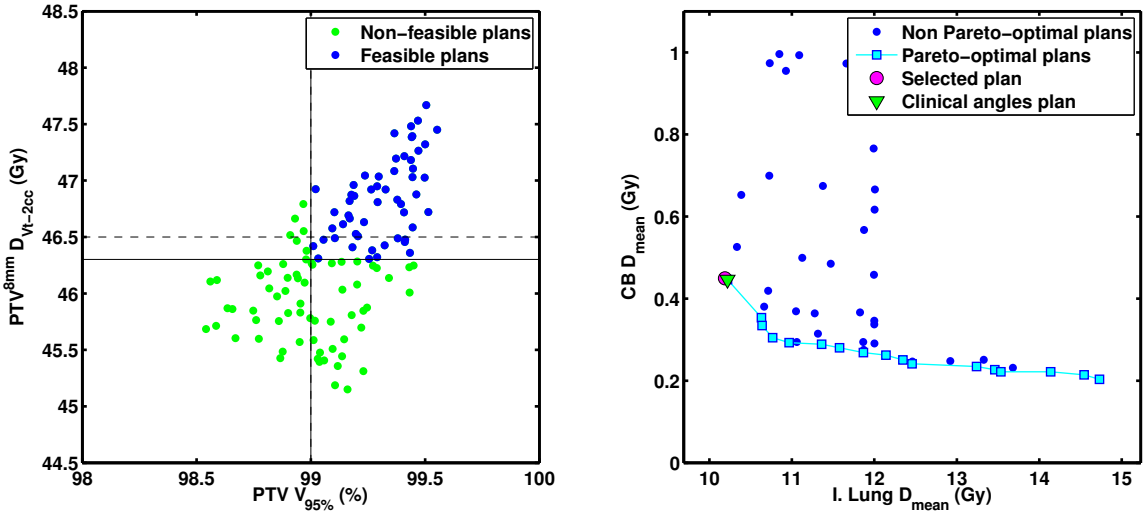

Figure B.23: *Patient right breast 08 (Ri08): feasible plans and Pareto front.*

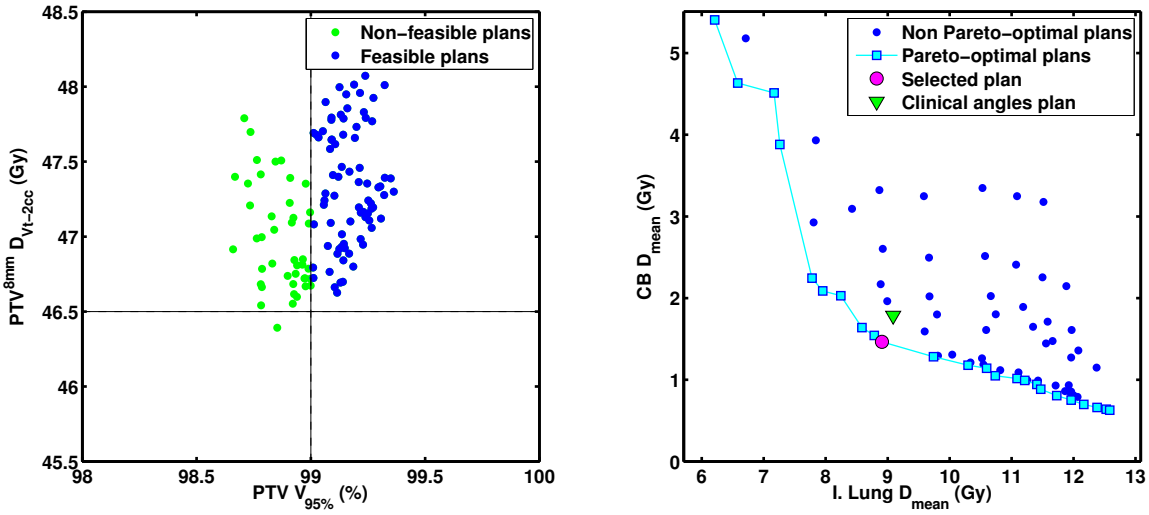

Figure B.24: *Patient right breast 09 (Ri09): feasible plans and Pareto front.*

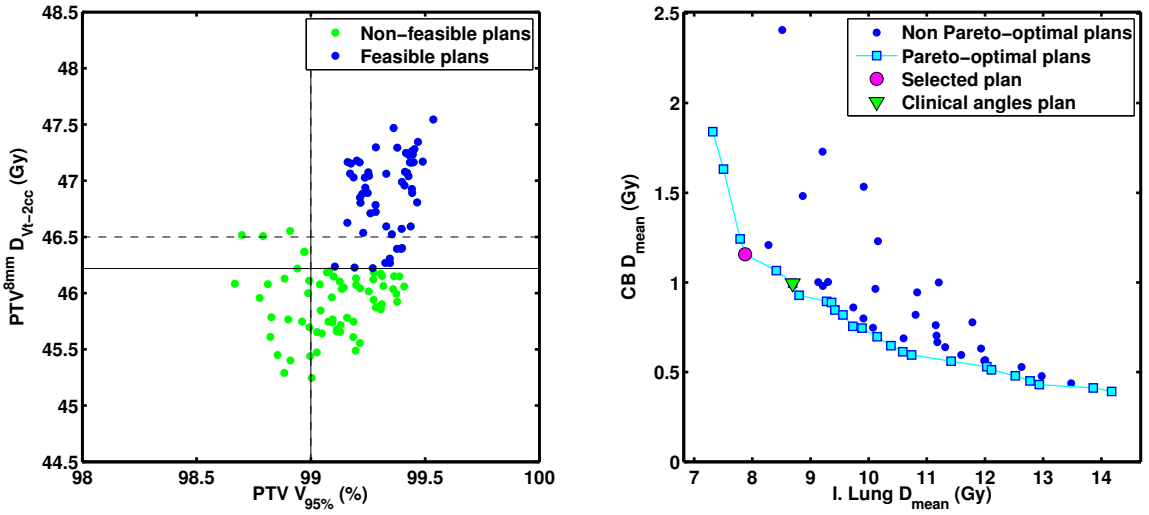

Figure B.25: *Patient right breast 10 (Ri10): feasible plans and Pareto front.*

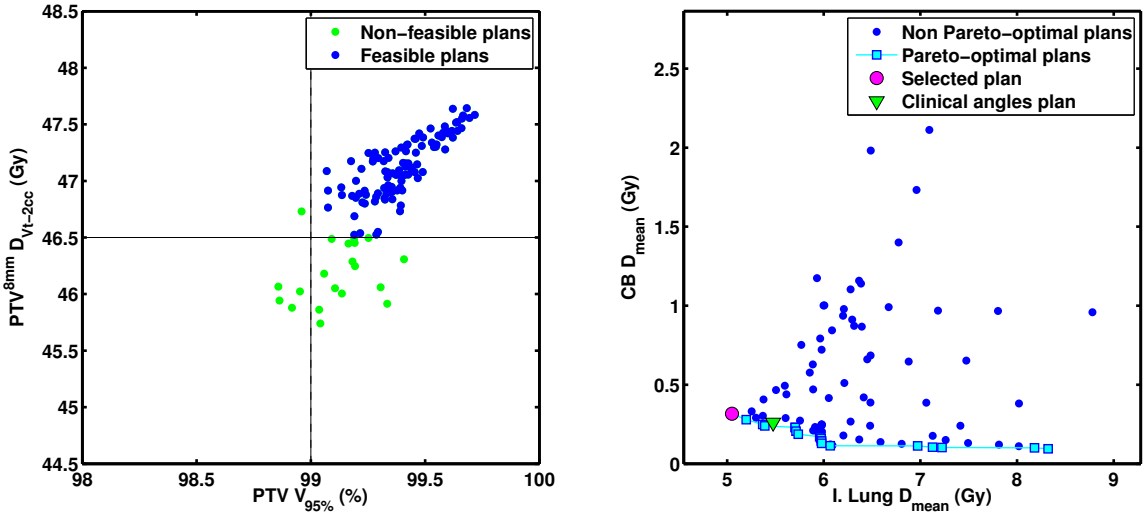

Figure B.26: *Patient right breast 11 (Ri11): feasible plans and Pareto front.*

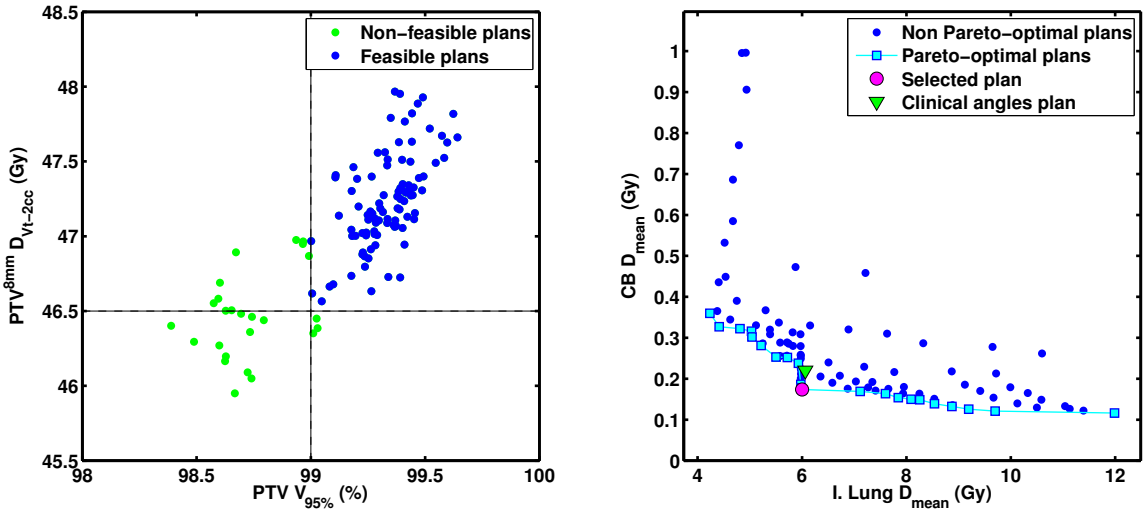

Figure B.27: *Patient right breast 12 (Ri12): feasible plans and Pareto front.*

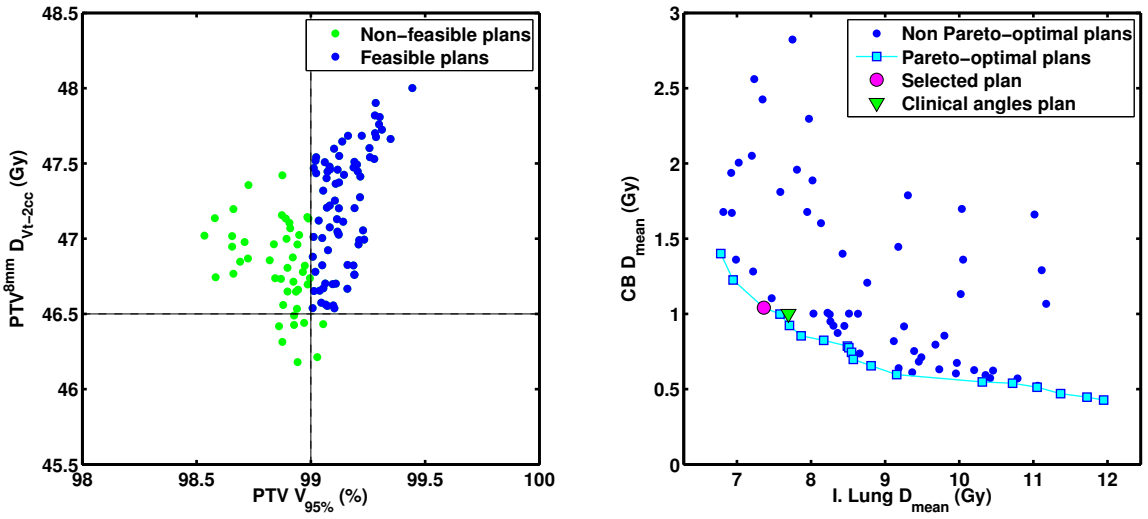

Figure B.28: *Patient right breast 13 (Ri13): feasible plans and Pareto front.*

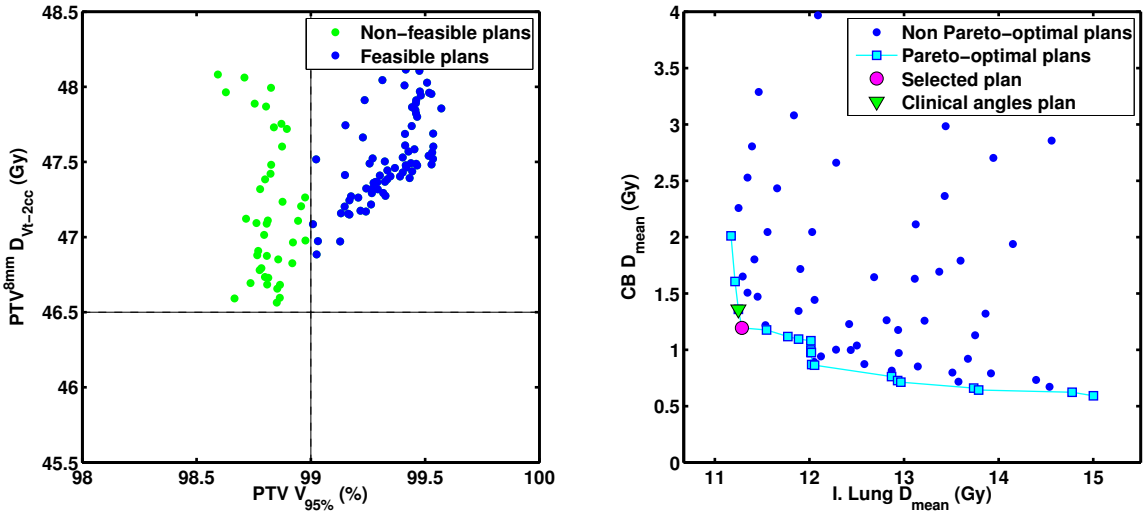

Figure B.29: *Patient right breast 14 (Ri14): feasible plans and Pareto front.*

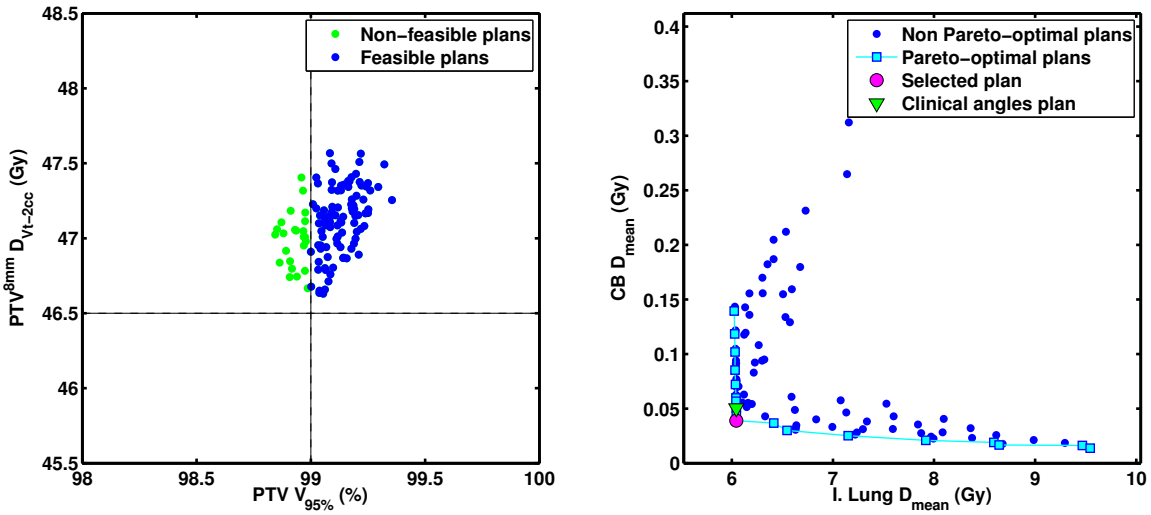

Figure B.30: *Patient right breast 15 (Ri15): feasible plans and Pareto front.*

Appendix C

Effect of the isocenter on Pareto-optimal plans

C.1 Left-sided patients

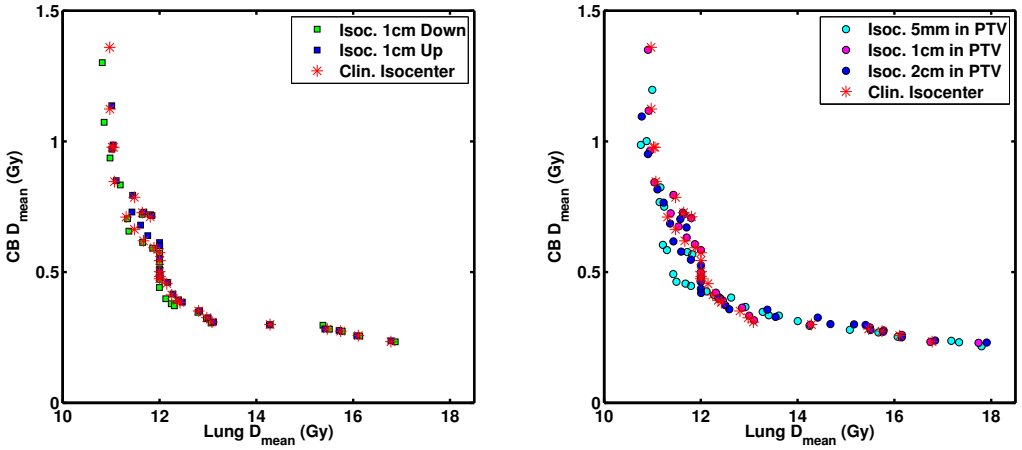

Figure C.1: *Patient left breast 01 (Le01). Pareto frontier for plans generated with the clinical isocenter and other 6 isocenter positions. Clinical isocenter position 9 mm from ipsilateral lung.*

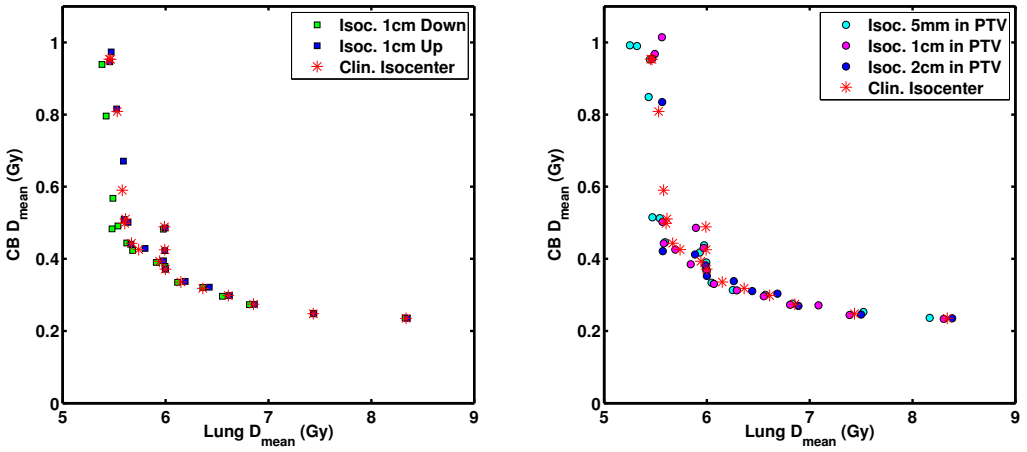

Figure C.2: *Patient left breast 02 (Le02). Pareto frontier for plans generated with the clinical isocenter and other 6 isocenter positions. Clinical isocenter position 9 mm from ipsilateral lung.*

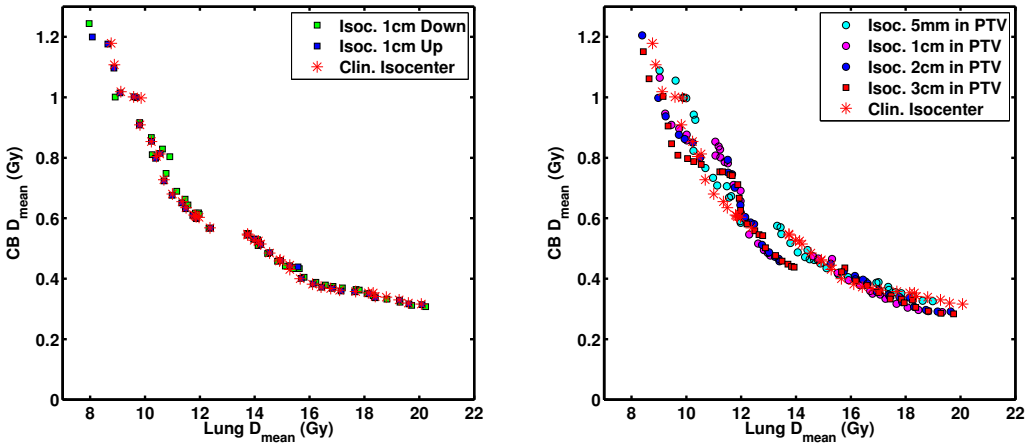

Figure C.3: *Patient left breast 03 (Le03). Pareto frontier for plans generated with the clinical isocenter and other 6 isocenter positions. Clinical isocenter position 23 mm from ipsilateral lung.*

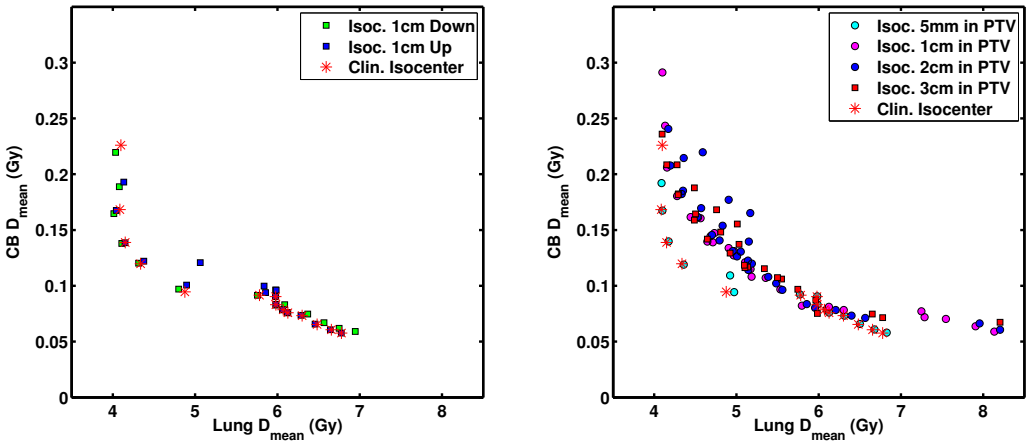

Figure C.4: *Patient left breast 04 (Le04). Pareto frontier for plans generated with the clinical isocenter and other 6 isocenter positions. Clinical isocenter position 5 mm from ipsilateral lung.*

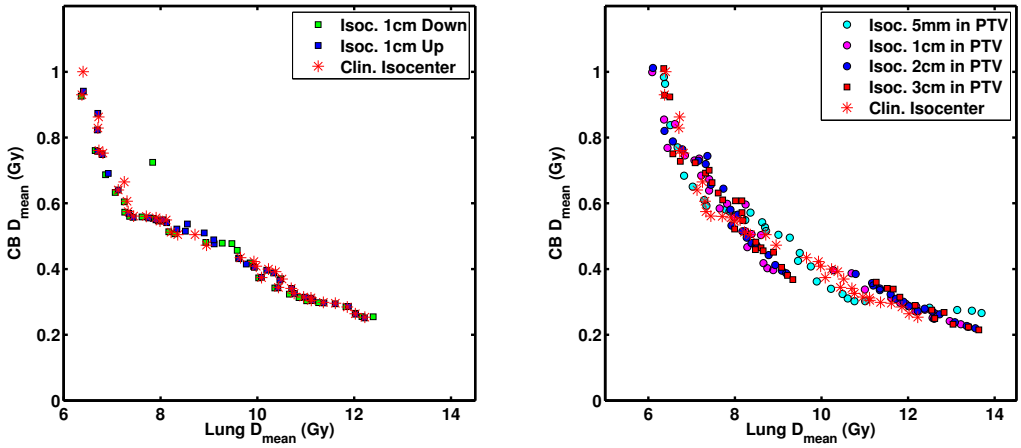

Figure C.5: *Patient left breast 05 (Le05). Pareto frontier for plans generated with the clinical isocenter and other 6 isocenter positions. Clinical isocenter position 13 mm from ipsilateral lung.*

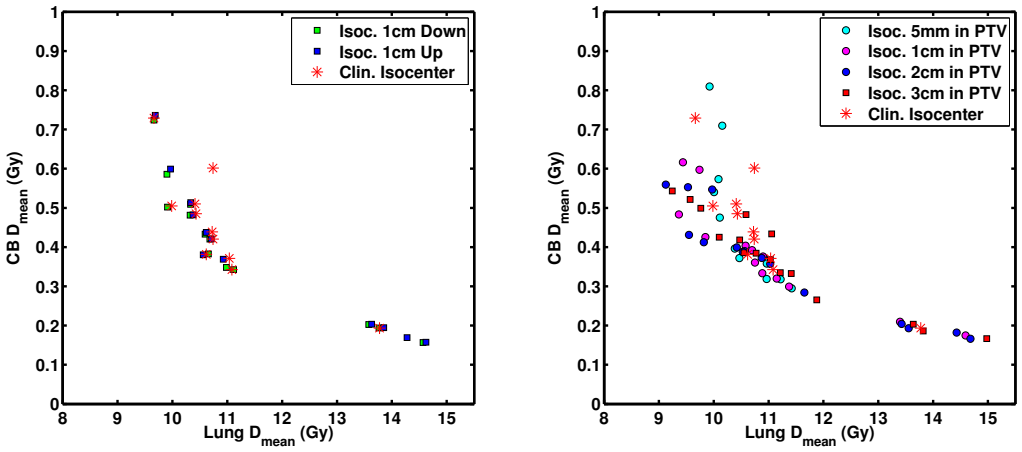

Figure C.6: *Patient left breast 06 (Le06). Pareto frontier for plans generated with the clinical isocenter and other 6 isocenter positions. Clinical isocenter position 22 mm from ipsilateral lung.*

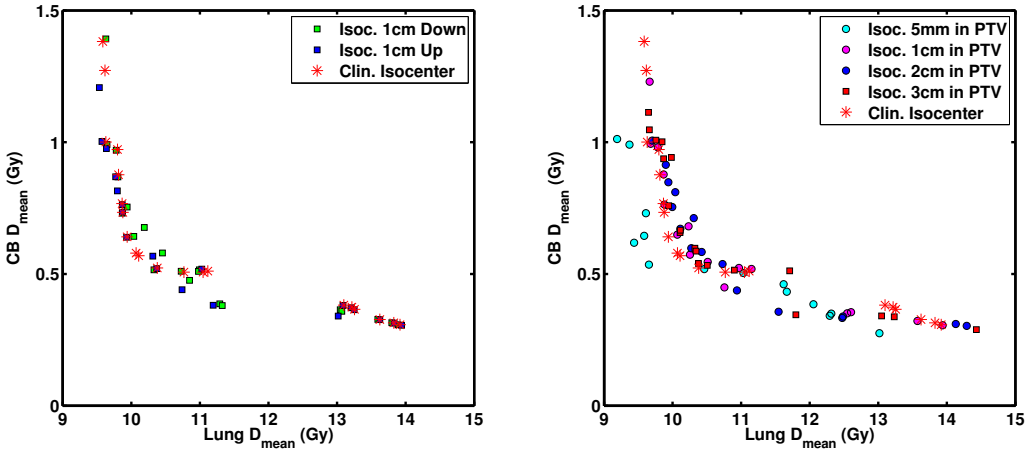

Figure C.7: *Patient left breast 07 (Le07). Pareto frontier for plans generated with the clinical isocenter and other 6 isocenter positions. Clinical isocenter position 11 mm from ipsilateral lung.*

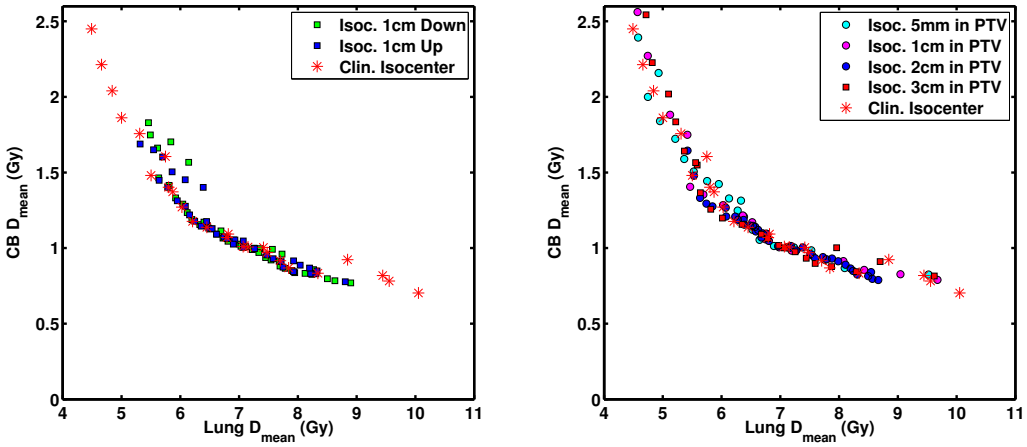

Figure C.8: *Patient left breast 08 (Le08). Pareto frontier for plans generated with the clinical isocenter and other 6 isocenter positions. Clinical isocenter position 8 mm from ipsilateral lung.*

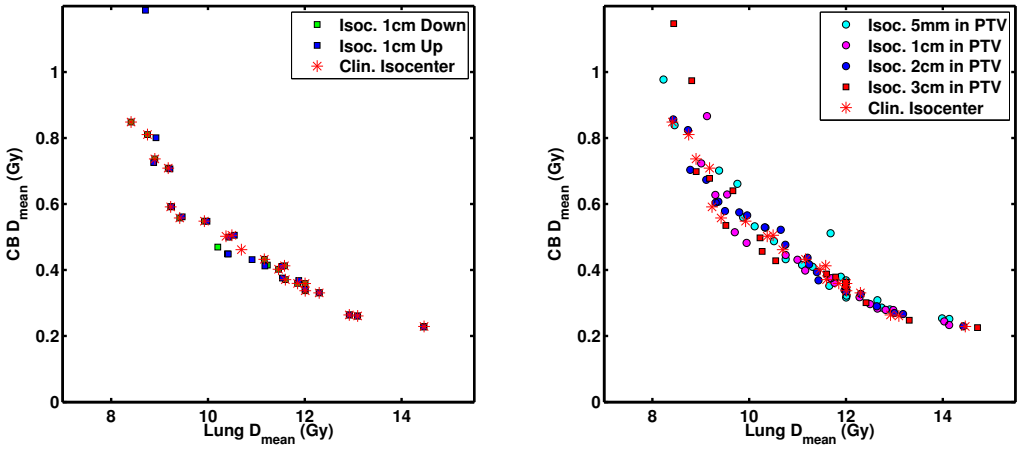

Figure C.9: *Patient left breast 09 (Le09). Pareto frontier for plans generated with the clinical isocenter and other 6 isocenter positions. Clinical isocenter position 20 mm from ipsilateral lung.*

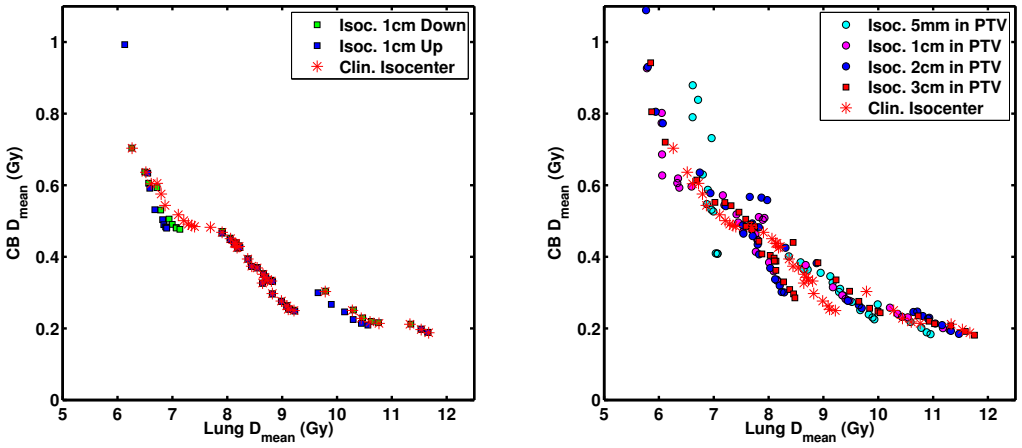

Figure C.10: *Patient left breast 10 (Le10). Pareto frontier for plans generated with the clinical isocenter and other 6 isocenter positions. Clinical isocenter position 17 mm from ipsilateral lung.*

C.2 Right-sided patients

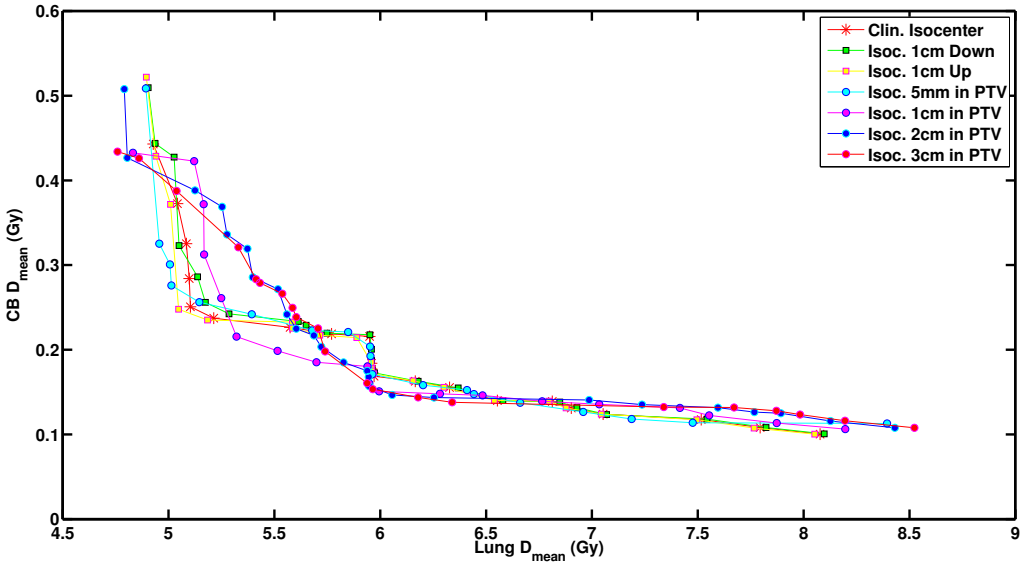

Figure C.11: *Patient right breast 01 (Ri01). Pareto frontier for plans generated with the clinical isocenter and other 6 isocenter positions. Clinical isocenter position 3 mm from ipsilateral lung.*

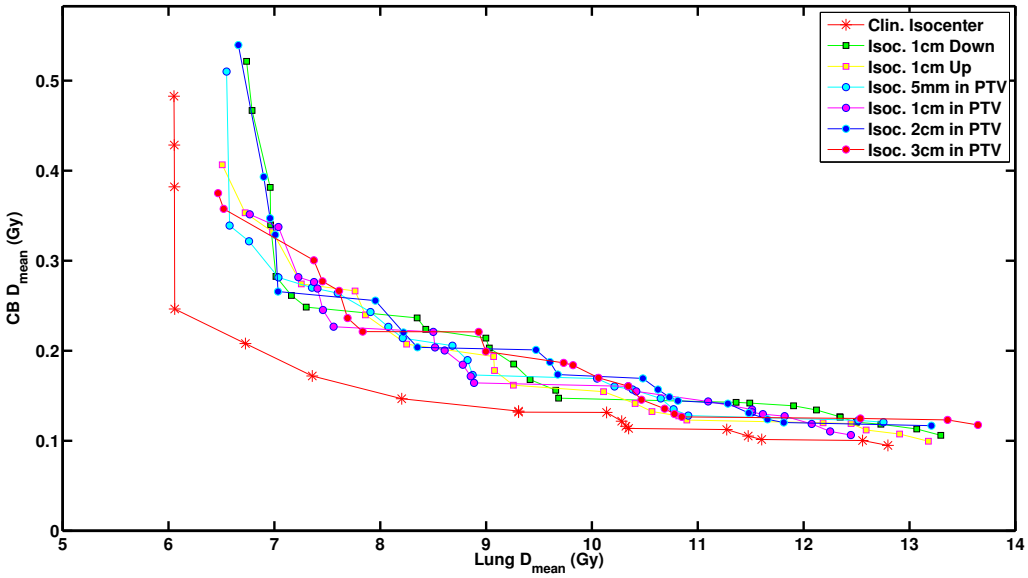

Figure C.12: *Patient right breast 02 (Ri02). Pareto frontier for plans generated with the clinical isocenter and other 6 isocenter positions. Clinical isocenter position 35 mm from ipsilateral lung.*

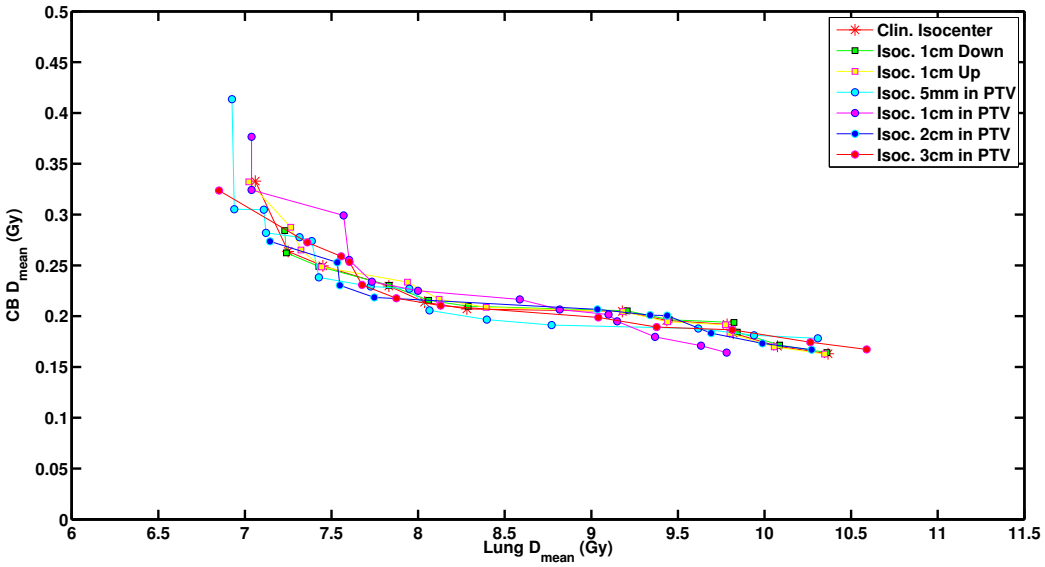

Figure C.13: *Patient right breast 03 (Ri03). Pareto frontier for plans generated with the clinical isocenter and other 6 isocenter positions. Clinical isocenter position 27 mm from ipsilateral lung.*

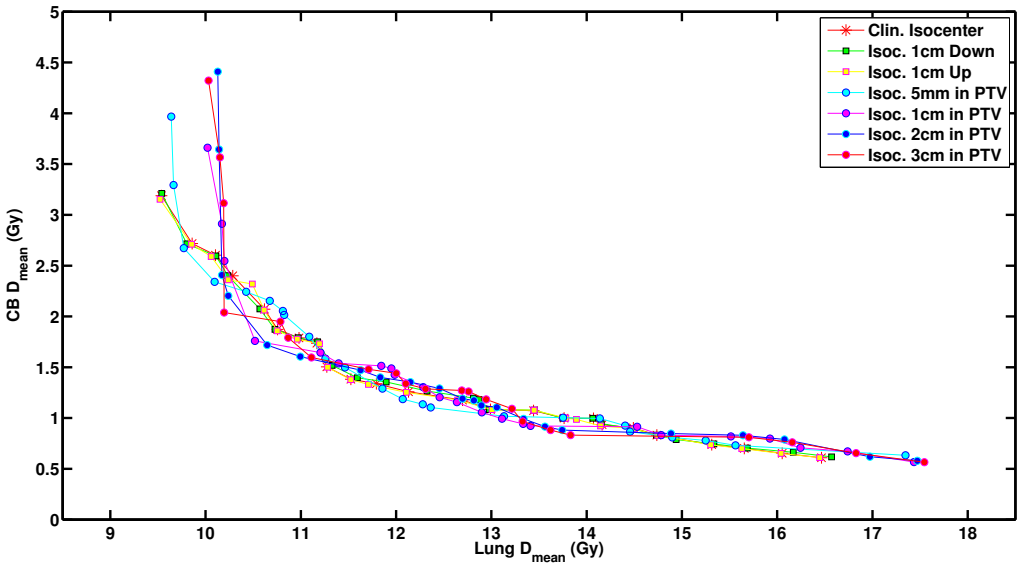

Figure C.14: *Patient right breast 04 (Ri04). Pareto frontier for plans generated with the clinical isocenter and other 6 isocenter positions. Clinical isocenter position 15 mm from ipsilateral lung.*

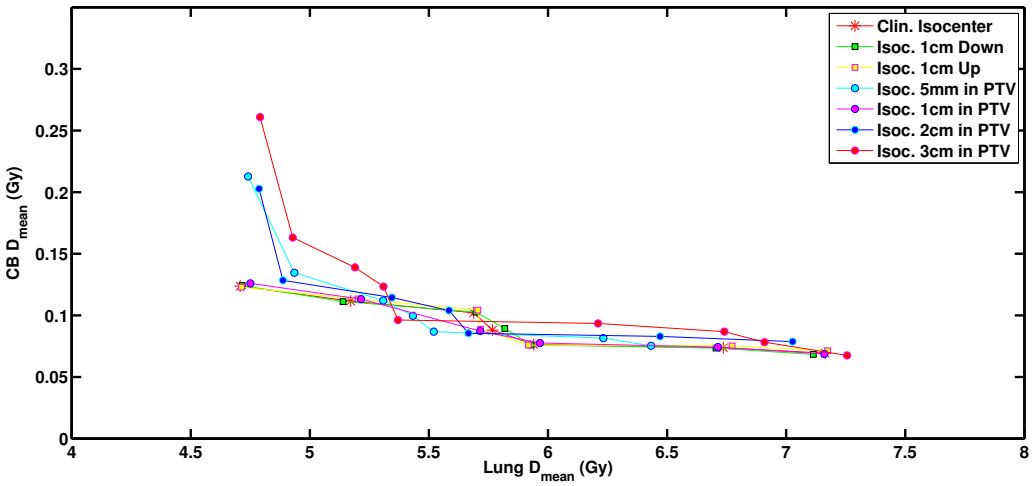

Figure C.15: *Patient right breast 05 (Ri05). Pareto frontier for plans generated with the clinical isocenter and other 6 isocenter positions. Clinical isocenter position 13 mm from ipsilateral lung.*

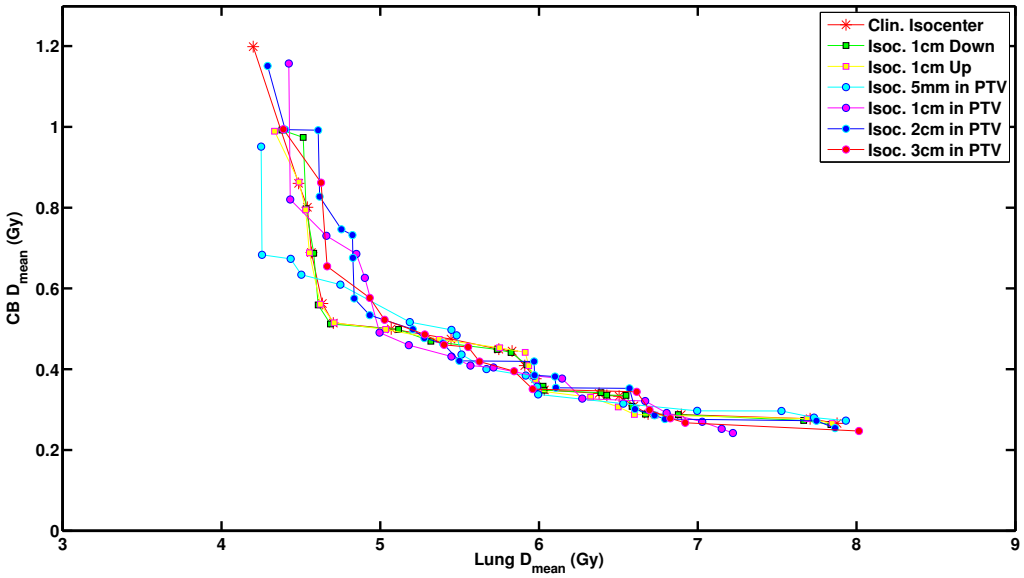

Figure C.16: *Patient right breast 06 (Ri06). Pareto frontier for plans generated with the clinical isocenter and other 6 isocenter positions. Clinical isocenter position 13 mm from ipsilateral lung.*

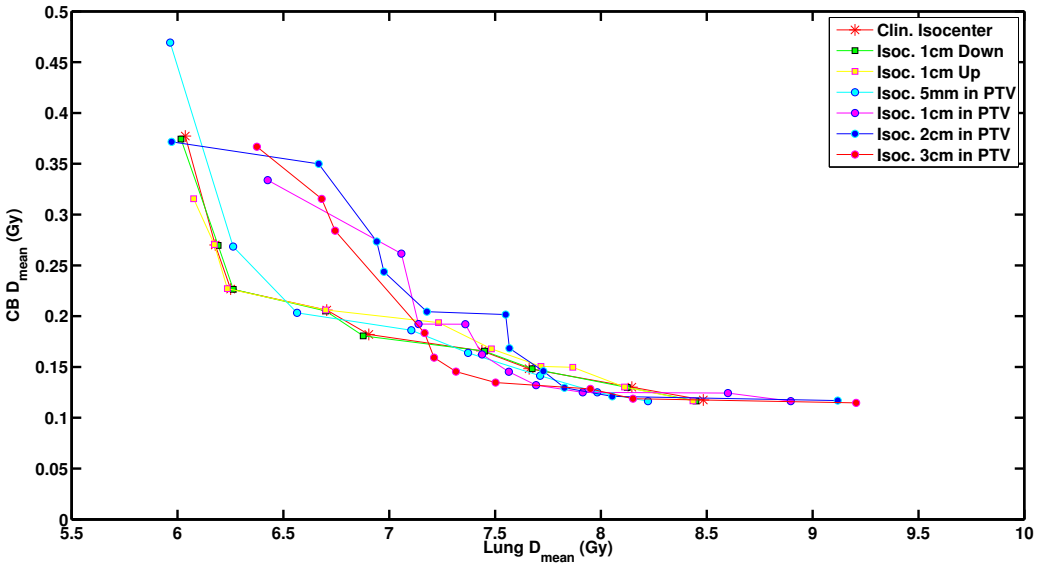

Figure C.17: *Patient right breast 07 (Ri07). Pareto frontier for plans generated with the clinical isocenter and other 6 isocenter positions. Clinical isocenter position 14 mm from ipsilateral lung.*

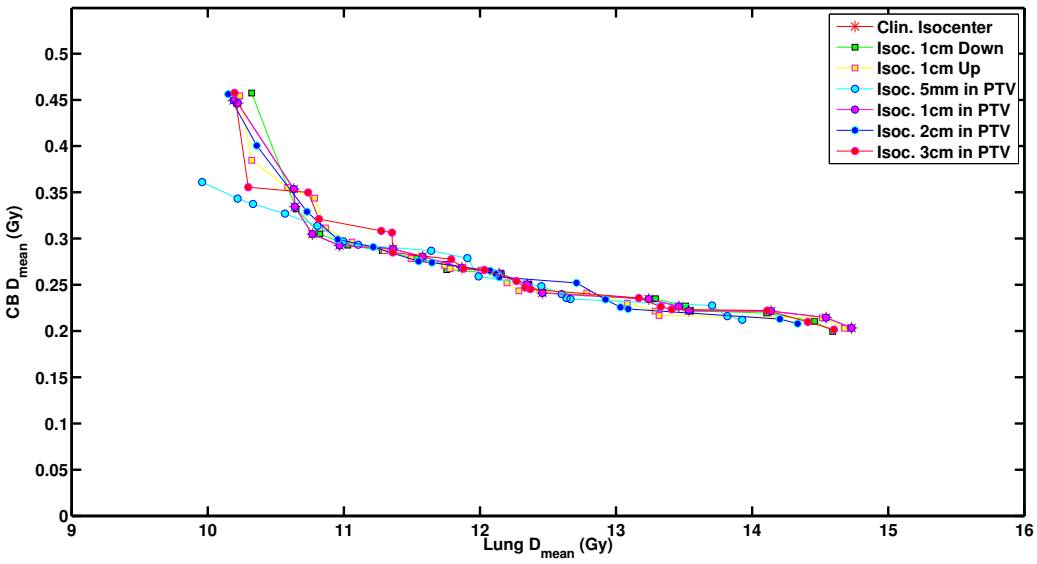

Figure C.18: *Patient right breast 08 (Ri08). Pareto frontier for plans generated with the clinical isocenter and other 6 isocenter positions. Clinical isocenter position 32 mm from ipsilateral lung.*

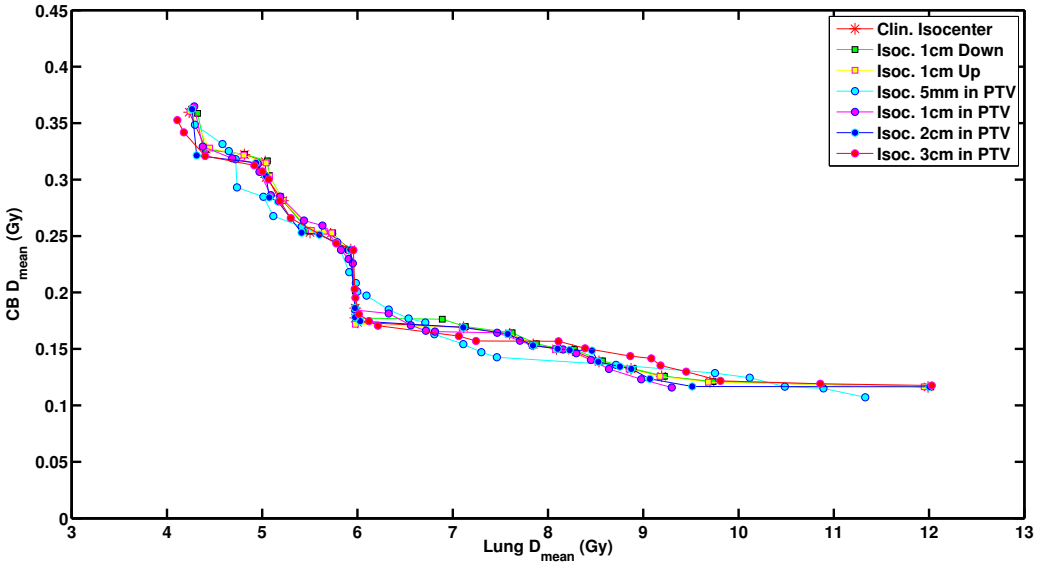

Figure C.19: *Patient right breast 09 (Ri09). Pareto frontier for plans generated with the clinical isocenter and other 6 isocenter positions. Clinical isocenter position 3 mm from ipsilateral lung.*

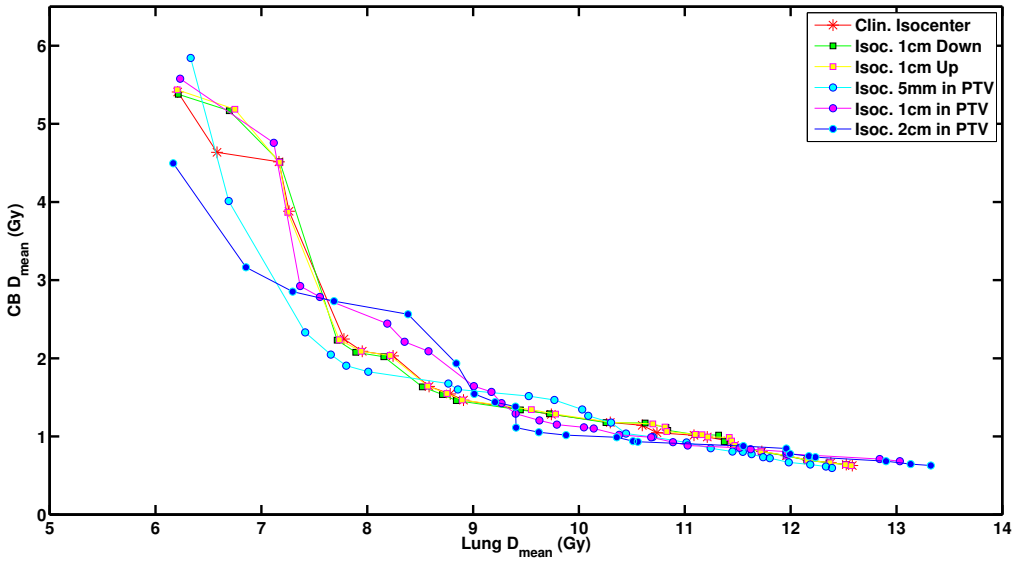

Figure C.20: *Patient right breast 10 (Ri10). Pareto frontier for plans generated with the clinical isocenter and other 6 isocenter positions. Clinical isocenter position 20 mm from ipsilateral lung.*

C.3 All patients

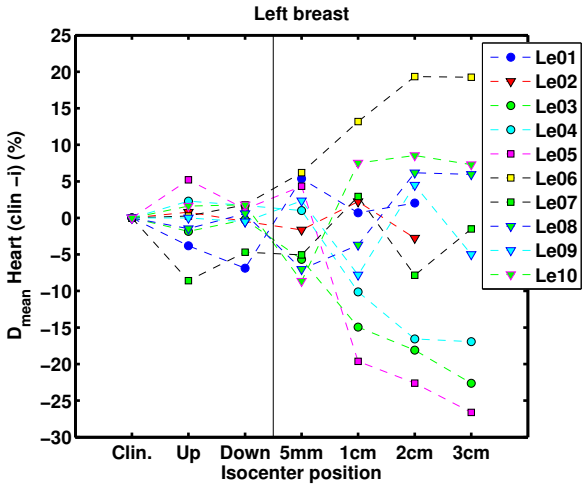

Figure C.21: *Variation in heart mean dose (%) between the value obtained for the best plan with clinical isocenter and the best plan selected with the other isocenter positions. Results for 10 left side patients.*

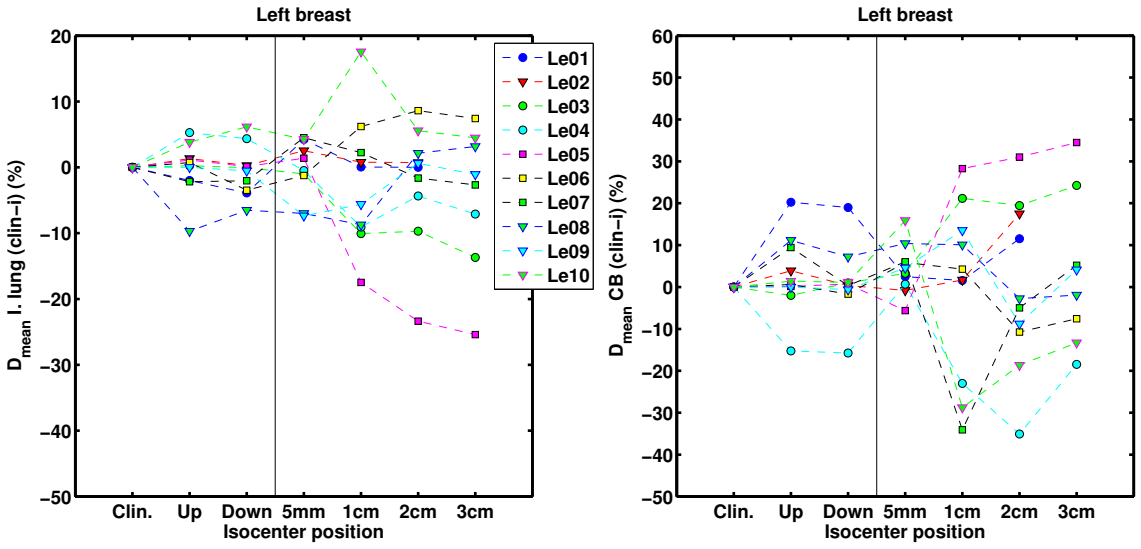

Figure C.22: *Variation in ipsilateral lung (%) and contralateral breast mean dose between the value obtained for the best plan with clinical isocenter and the best plan selected with the other isocenter positions. Results for 10 left side patients.*

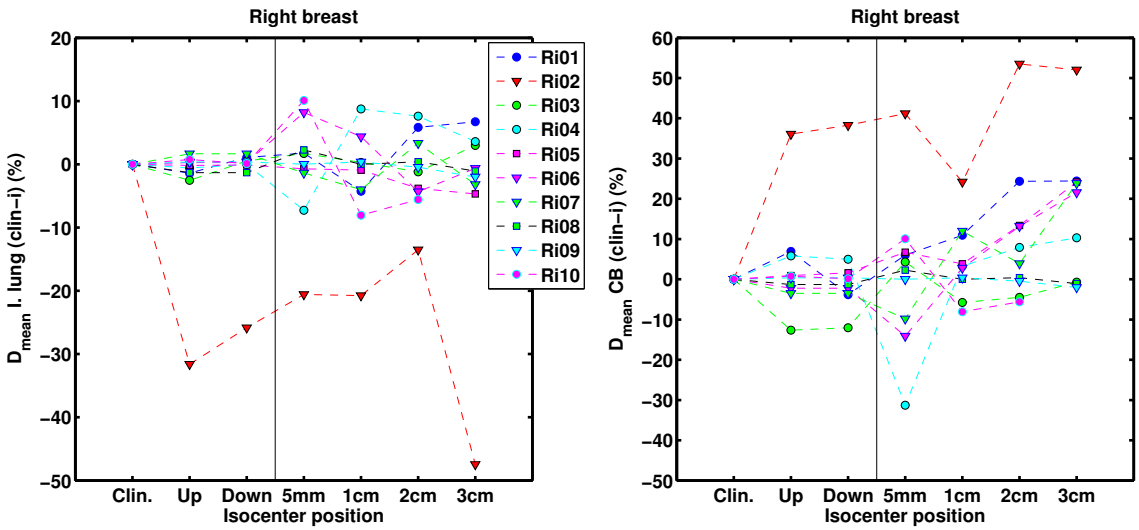

Figure C.23: *Variation in ipsilateral lung and contralateral breast mean dose (%) between the value obtained for the best plan with clinical isocenter and the best plan selected with the other isocenter positions. Results for 10 right side patients.*

Table C.1: *Wilconxon signed ranked test p-values, for left breast patients.*

	Clin. iso.	10 *mm* caudal	10 *mm* cranial	5 *mm* axial	10 *mm* axial	20 *mm* axial	30 *mm* axial
Clin. iso.	-	0.70	0.62	0.50	0.68	1.00	1.00
10 *mm* caudal		-	0.43	1.00	1.00	0.76	0.64
10 *mm* cranial			-	0.92	0.43	0.49	0.46
5 *mm* axial				-	0.92	0.84	0.84
10 *mm* axial					-	0.28	0.94
20 *mm* axial						-	0.74
30 *mm* axial							-

Table C.2: *Wilconxon signed ranked test p-values, for right breast patients.*

	Clin. iso.	10 *mm* caudal	10 *mm* cranial	5 *mm* axial	10 *mm* axial	20 *mm* axial	30 *mm* axial
Clin. iso.	-	0.85	0.49	0.76	0.16	0.49	0.21
10 *mm* caudal		-	0.84	0.62	0.43	0.38	0.10
10 *mm* cranial			-	0.43	0.13	0.28	0.14
5 *mm* axial				-	0.43	0.16	0.11
10 *mm* axila					-	0.92	0.13
20 *mm* axial						-	0.16
30 *mm* axial							-

Table C.3: *Wilconxon signed ranked test p-values, for all patients.*

	Clin. isocenter	10 mm caudal	10 mm cranial	5 mm axial	10 mm axial	20 mm axial	30 mm axial
Clin. iso.	-	0.48	0.37	0.50	0.48	0.60	0.23
10 mm caudal		-	0.40	0.71	0.55	0.30	0.12
10 mm cranial			-	0.85	0.11	0.14	0.10
5 mm axial				-	0.51	0.20	0.18
10 mm axial					-	0.41	0.20
20 mm axial						-	0.41
30 mm axial							-